

FRACTURE MECHANICS OF BLOOD CLOTS

Shiyu Liu

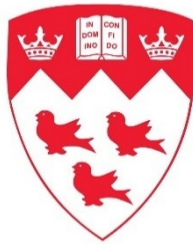
Doctor of Philosophy

Department of Mechanical Engineering

McGill University

Montreal, Quebec

December 2023



A thesis submitted to McGill University in partial fulfillment of the requirements for the degree
of Doctor of Philosophy

© Shiyu Liu 2023

Abstract

Blood clots are naturally derived bioadhesives that adhere to tissues, plug vascular defects and stop bleeding. The mechanical behaviors of blood clots are critical in both hemostasis and thrombosis, and their functions hinge on their resistance against rupture. Despite the relevance, there exist major challenges in understanding the fracture behaviors of blood clots. Challenges include the lack of proper mechanical testing methods for blood clots, limited understanding of the responses of clots under complex loading conditions and the interplay between adhesive fracture and cohesive fracture. To this end, this thesis investigates the fracture mechanics of blood clots, with a focus on developing mechanical testing methods, investigating fatigue threshold and rate-dependent fracture toughness, and evaluating the adhesive and cohesive fracture behaviors.

First, we study the fracture behavior of human whole blood clots and platelet-poor plasma clots. The fracture energies of whole blood clots and platelet-poor plasma clots are determined using a modified lap-shear method. The measured toughness is found to be independent of the specimen geometry and loading conditions. These results reveal an important contribution of blood cells to clot fracture, as well as the dissipative length scale and nonlinear elastic length scale governing clot fracture.

Next, the thesis continues with a study on the fracture properties of fibrin clots in terms of fatigue threshold and rate-dependent fracture toughness. Fibrin clot is a vital class of fibrous materials, governing the mechanical response of blood clots. We design and conduct cyclic fatigue and monotonic variable rate loading tests on fibrin clots. Furthermore, we rationalize the fatigue threshold using a semi-empirical model parameterized by 3D morphometric quantification to account for the hierarchical molecular structure of fibrin fibers. The variable loading tests reveal rate dependence of the overall fracture toughness. Our analysis with a viscoelastic fracture model suggests the viscoelastic origin of the rate-dependent fracture toughness. The toughening mechanism of fibrin clots is further compared with biological tissues and hydrogels.

The last part of the thesis proposes an integrated experimental-computational approach to evaluate the adhesive and cohesive fracture behaviors of bovine blood clots by incorporating mechanical factors including loading rate and failure modes as well as cellular components. Among biological substrates tested, the blood clot shows the largest interfacial fracture energy to the muscle and the

least adhesion to the inner arterial lining, consistent with its biological role. Both interfacial and bulk fracture energies exhibit notable rate dependency, highlighting the role of viscoelastic dissipation as a toughening mechanism. They are dependent on the contents of RBC and platelets. These findings presented in this thesis advance the fundamental knowledge of blood clot fracture, as well as mechanics of soft materials similar to clots. These insights are expected to facilitate the management of clot-related disorders and pave the way for developing innovative therapies.

Résumé

Les caillots sanguins sont des bioadhésifs d'origine naturelle qui adhèrent aux tissus, colmatent les défauts vasculaires et arrêtent les saignements. Les comportements mécaniques des caillots sanguins sont cruciaux à la fois dans l'hémostase et la thrombose, et leurs fonctions reposent sur leur résistance à la rupture. Malgré leur pertinence, des défis majeurs persistent dans la compréhension des comportements de rupture des caillots sanguins. Ces défis incluent le manque de méthodes d'essai mécanique appropriées pour les caillots sanguins, une compréhension limitée des réponses des caillots dans des conditions de chargement complexes, et l'interaction entre la rupture adhésive et la rupture cohésive. Dans cette optique, cette thèse explore la mécanique de la rupture des caillots sanguins, en mettant l'accent sur le développement de méthodes d'essai mécanique, l'étude du seuil de fatigue et de la ténacité à la rupture dépendante de la vitesse, ainsi que l'évaluation des comportements de rupture adhésive et cohésive.

Tout d'abord, nous étudions le comportement de rupture des caillots sanguins humains entiers et des caillots de plasma appauvris en plaquettes. Les énergies de rupture des caillots sanguins entiers et des caillots de plasma appauvris en plaquettes sont déterminées à l'aide d'une méthode de cisaillement en lap-joint modifiée. La ténacité mesurée s'avère indépendante de la géométrie de l'échantillon et des conditions de chargement. Ces résultats révèlent une contribution importante des cellules sanguines à la rupture du caillot, ainsi que l'échelle de longueur dissipative et l'échelle de longueur élastique non linéaire régissant la rupture du caillot.

Ensuite, la thèse se poursuit par une étude des propriétés de rupture des caillots de fibrine en termes de seuil de fatigue et de ténacité à la rupture dépendante de la vitesse. Le caillot de fibrine est une classe vitale de matériaux fibreux, régissant la réponse mécanique des caillots sanguins. Nous concevons et réalisons des essais de fatigue cyclique et de chargement variable monotone sur les caillots de fibrine. De plus, nous rationalisons le seuil de fatigue en utilisant un modèle semi-empirique paramétré par une quantification morphométrique en 3D pour tenir compte de la structure moléculaire hiérarchique des fibres de fibrine. Les essais de chargement variable révèlent une dépendance de la vitesse de la ténacité à la rupture globale. Notre analyse avec un modèle de rupture viscoélastique suggère l'origine viscoélastique de la ténacité à la rupture dépendante de la vitesse. Le mécanisme de renforcement des caillots de fibrine est ensuite comparé à celui des tissus

biologiques et des hydrogels.

La dernière partie de la thèse propose une approche expérimentale-computationnelle intégrée pour évaluer les comportements de rupture adhésive et cohésive des caillots sanguins bovins en incorporant des facteurs mécaniques tels que la vitesse de chargement et les modes de défaillance, ainsi que des composants cellulaires. Parmi les substrats biologiques testés, le caillot sanguin présente la plus grande énergie de rupture interfaciale par rapport au muscle et la moins grande adhérence à la paroi artérielle interne, ce qui est cohérent avec son rôle biologique. Les énergies de rupture interfaciale et en volume présentent une dépendance notable à la vitesse, mettant en évidence le rôle de la dissipation viscoélastique comme mécanisme de renforcement. Elles dépendent du contenu en globules rouges et en plaquettes. Les découvertes présentées dans cette thèse font progresser la connaissance fondamentale de la rupture des caillots sanguins, ainsi que la mécanique des matériaux souples similaires aux caillots. Ces connaissances devraient faciliter la gestion des troubles liés aux caillots et ouvrir la voie au développement de thérapies innovantes.

Acknowledgment

I extend my deepest appreciation to Professor Jianyu Li, my supervisor, whose unwavering support and guidance have been the cornerstone of my doctoral journey. His mentorship, characterized by excitement and enthusiasm, has significantly shaped my academic and research. I thank him for his guidance and support that encouraged me to explore new fields and pursue academic achievement. It is my honor to work with him, and this precious experience and our friendship will continue and inspire my next journey beyond academia.

A heartfelt acknowledgment is due to the excellent members of our labs. I wish to express special thanks to Aram Bahmani for the countless day-and-night efforts spent on our projects; Dr. Farshid Ghezlbash for his generous help in research design and implementation; Dr. Guangyu Bao and Dr. Zhenwei for their patience and kind support as I started my doctoral study at McGill University; Zhen Yang for his in-depth knowledge and sharing on mechanics studies; Xuan Li for her never-changing support and encouragement; Evan Johnston for his expertise in animal studies. I also thank Ran Huo, Yin Liu, Shuaibing Jiang, Tianqin Ning, Yixun Cheng, Christopher Chung, Alex Nottegar, Portia Rayner and Justin Puma from our research group. Their collective dedication, collaborative spirit, and diverse expertise have created an enriching and vibrant research environment. Each member's unique contributions have played an integral role in the success of our endeavors.

I express my gratitude to our esteemed collaborators—Professor Christian J. Kastrup and Gabriella Paige Sugerman. Their insightful contributions and collaborative efforts have not only broadened the scope of our projects but have also added depth and relevance to our research outcomes.

Lastly, heartfelt thanks to my family for their unwavering support, love, and understanding. Their encouragement has been a driving force, and I am immensely grateful for the strong foundation they provide. As I embark on the journey beyond my doctoral studies, I am filled with anticipation and gratitude for the lessons learned and the relationships forged.

Contribution to Original Knowledge

The research presented in this thesis contributed to the advancement of original knowledge in the field of fracture mechanics of blood clots in three aspects, uncovering the dissipative nature of blood clots, their fatigue threshold, and rate-dependent fracture toughness, as well as the crucial roles played by major blood constituents of fibrin, RBCs and platelets, and the biomechanics understanding could inspire biomedical applications in hemostasis and thrombosis.

An **innovative experimental methodology** was proposed for characterizing the fracture behavior of blood clots under complex loading conditions. A novel 3D-printed pure shear testing device was rationally designed to ensure reliable sample preparation and loading. I obtained the first data set of experimental results of fatigue threshold and rate-dependent fracture toughness of fibrin clots, and cohesive and adhesive fracture toughness of whole blood clots by fracture tests.

A **novel semi-empirical fibrous material model** was developed to advance the understanding of toughening mechanism of blood clots. I reconstructed the 3D geometry of the fibrin network and implemented the morphometric quantification, and fed the measured values into the semi-empirical model to estimate the fatigue threshold of fibrin clots.

A **novel fracture modality shifting model** of blood clots including cohesive fracture within the clot's bulk material the adhesive fracture at the clot-tissue interface, and the mixed mode fracture was developed through an integrated experimental-computational approach. The pivotal role of rate-dependent response, RBCs, and platelets was investigated.

The abovementioned contributions have been consolidated in the preparation or publication of the following peer-reviewed journal articles and conference proceeding:

- **Peer-reviewed articles or in preparation for submission:**

1. **Shiyu Liu**[†], Aram Bahmani[†], Farshid Ghezelbash, and Jianyu Li^{*}. Fibrin Clot Fracture under Cyclic Fatigue and Variable Rate Loading. *Acta Biomaterialia*, 177, 265-277 (2024).

[†]**These authors contribute equally.**

2. **Shiyu Liu**, Aram Bahmani, Gabriella Paige Sugerman, Zhen Yang. Manuel Rausch,

Farshid Ghezelbash*, Jianyu Li*. Blood Clot Fracture Mechanics: Adhesive and Cohesive Modalities. *Journal of the Mechanics and Physics of Solids*, preparation to submit (2023).

3. **Shiyu Liu**, Guangyu Bao, Zhenwei Ma, Christian J. Kastrup, Jianyu Li*. Fracture mechanics of blood clots: Measurements of toughness and critical length scale. *Extreme Mechanics Letters*, 48, 101444 (2021).

- **Selected conference proceeding:**

Shiyu Liu, “Fracture of blood clot: effects of loading rate, red blood cell and platelet”, North American Congress on Biomechanics (NACOB), Ottawa, Canada. Individual oral presentation, 2022.

In addition to this thesis, I have contributed to other co-first author or collaboration publications during my Ph.D. study period:

1. Aram Bahmani[†], **Shiyu Liu**[†], Evan Johnston, Weiyi Wan, Alex Nottegar, Ran Huo, Shuaibing Jiang, Jianyu Li*. Engineering Clot-like Materials with Mechanical Vibration. *PNAS*, preparation to submit (2024). **†These authors contribute equally.**
2. Xuan Li, Yin Liu, **Shiyu Liu**, Baolin Huang*, Nicole Li-Jessen, Lisbet Haglund, Jianyu Li*. Designing Regenerative Bioadhesives for Tissue Repair and Regeneration. *Advanced Therapeutics*, 2300139 (2023).
3. Xuan Li, Yin Liu, Li Li, Ran Huo, Farshid Ghezelbash, Zhenwei Ma, Guangyu Bao, **Shiyu Liu**, Zhen Yang, Michael H. Weber, Nicole Y. K. Li-Jessen, Lisbet Haglund, Jianyu Li*. Tissue-mimetic hybrid bioadhesives for intervertebral disc repair. *Materials Horizons*, 10 (5), 1705-1718 (2023).
4. Shuaibing Jiang, **Shiyu Liu**, Sum Lau, Jianyu Li*. Hemostatic biomaterials to halt non-compressible hemorrhage. *Journal of Materials Chemistry B*, 10(37), 7239-7259 (2022).
5. Farshid Ghezelbash, **Shiyu Liu**, Aboufazl Shirazi-Adl, Jianyu Li*. Blood clot behaves as a poro-visco-elastic material, *Journal of the Mechanical Behavior of Biomedical Materials*. 105101 (2022).
6. Guangyu Bao, Ran Huo, Zhenwei Ma, Mitchell Strong, Amin Valiei, Shuaibing Jiang,

Shiyu Liu, Luc Mongeau, Jianyu Li*. Ionotronic Tough Adhesives with Intrinsic Multifunctionality. *ACS Applied Materials & Interfaces* (2021).

7. Zhen Yang, Zhenwei Ma, **Shiyu Liu**, Jianyu Li*. Tissue adhesion with tough hydrogels: Experiments and modeling. *Mechanics of Materials*, 157, 103800 (2021).

Contribution of Authors

I, Shiyu Liu, clarify that the research efforts of the work presented in this thesis are led by myself. It is worth highlighting that the entirety of the work within this thesis was substantially benefitted by the invaluable insights and guidance offered by my Ph.D. mentor, Prof. Jianyu Li. We jointly conceived the concepts and co-designed the research methodology and I led the efforts to carry out the research activities for this thesis.

I, as the author of this thesis, am responsible for the conceptualization, study design, experimentation, data analysis, visualization, and writing of all the chapters in this thesis. All figures in this thesis were either created solely by me or in collaboration with Aram Bahmani. We utilized various software tools, such as OriginLab, Adobe Illustrator, and Blender, to make these figures. The completion of this thesis was made achievable through the collaborative and supportive research efforts of my colleagues and collaborators with various backgrounds, and the guidance and supervision from Prof. Jianyu Li. The detailed scientific contributions are described below.

In Chapter 3, most of the work involving conceptualization, literature survey, methodology, conducting experiments, data analysis, visualization, and writing was done by myself. Dr. Guangyu Bao assisted the author with the literature search and helped in the experiment design. Dr. Zhenwei Ma assisted the author with the preparation of reagents and testing samples. Dr. Christian J. Kastrop helped with the conceptualization of coagulation characterization and evaluation. Dr. Jianyu Li supervised the project.

In Chapter 4, most of the work involving conceptualization, literature survey, methodology, programming development, validation, data analysis, data curation, and writing was done by myself. Aram Bahmani and the author collaboratively conducted fatigue fracture experiment and contributed to cohesive zone modeling. Dr. Farshid Ghezlbash assisted the author with the design of fatigue fracture experiment. Dr. Jianyu Li supervised the project.

In Chapter 5, most of the work involving conceptualization, literature survey, methodology, programming development, validation, data analysis, data curation, and writing was done by myself. Aram Bahmani and the author collaboratively implemented fracture testing and imaging and contributed to conceptualization and modelling. Dr. Gabriella Paige Sugerman and Dr. Manuel

Rausch assisted with clot contraction study. Farshid Ghezelbash helped with conceptualization and methodology. Dr. Jianyu Li supervised the project.

Table of Contents

Abstract.....	I
Résumé.....	III
Acknowledgment.....	V
Contribution to Original Knowledge.....	VI
Contribution of Authors.....	IX
Table of Contents.....	XI
List of Figures.....	XV
List of Tables.....	XVII
Thesis organization.....	XVIII
Chapter 1 Introduction.....	20
1.1 Motivation.....	20
1.2 Literature review.....	20
1.2.1 Introduction.....	20
1.2.2 Structural fibrin network formation of blood clots.....	21
1.2.3 Blood clot cellular components.....	23
1.2.4 Blood coagulation and fibrinolysis.....	24
1.2.5 Physical interactions and covalent crosslinks.....	27
1.2.6 Mechanical properties of blood clots.....	29
1.2.7 Modeling of blood clot mechanical behaviors.....	37
1.3 Challenges in existing blood clot studies.....	38
1.4 Research rationale and objectives.....	39
1.4.1 Research rationale.....	39
1.4.2 Research objectives.....	40
Chapter 2 Materials and Methods.....	42

2.1	Material and sample preparation	42
2.1.1	Blood clotting initiation investigation	42
2.1.2	Platelet-poor plasma and recalcification solution preparation	43
2.1.3	Modified blood clots with varying cellular contents	43
2.1.4	Preparation of pure shear specimens	44
2.2	Mechanical characterization.....	45
2.2.4	Monotonic pure shear tests	46
2.2.5	Cyclic load tests.....	48
2.2.6	90° peeling adhesion tests.....	49
2.3	Image analysis	49
2.3.1	Scanning electron microscopy.....	49
2.3.2	Confocal imaging	50
2.3.3	Data-based 3D image reconstruction and morphometric quantification	50
2.4	Finite element modeling.....	51
2.5	Statistical analysis	52
Chapter 3	Fracture toughness of blood clot	53
3.1	Preface.....	53
3.2	Introduction	53
3.3	Results and discussion.....	55
3.3.1	Rheological behaviors of blood clots	55
3.3.2	Lap-shear tests of blood clots	57
3.3.3	Fracture energy measurements with varying loading.....	59
Chapter 4	Fatigue fracture and rate-dependent fracture of blood clot	61
4.1	Preface.....	61
4.2	Introduction	61
4.3	Results and discussion.....	65

4.3.1	Confocal image 3D reconstruction and data-based image analysis	65
4.3.2	Shakedown under cyclic load	66
4.3.3	Crack growth during cyclic load and fatigue threshold calculation	67
4.3.4	Theory for fibrin clot fatigue threshold	71
4.3.5	Rate-dependence overall fracture toughness	72
4.3.6	Theory for the overall fracture toughness of fibrin clots	74
Chapter 5 Adhesive and cohesive fracture modalities		77
5.1	Preface	77
5.2	Introduction	77
5.3	Results and discussion	80
5.3.1	Interfacial fracture energy	80
5.3.2	Bulk fracture energy	81
5.3.3	Effects of RBC and platelet	82
5.3.4	Finite element model	84
Chapter 6 Discussion and future work		87
6.1	Discussion	87
6.1.1	Pure shear configuration	87
6.1.2	Fracture toughness of blood clots	88
6.1.3	Critical length scales during clot fracture	88
6.1.4	Toughening mechanism of fibrin clots	91
6.1.5	Adhesive fracture and cohesive fracture	93
6.1.6	Rate dependency of clot fracture	94
6.1.7	Cell inclusions	95
6.1.8	Clinical relevance	96
6.1.9	Limitations	97
6.2	Future work	98

Chapter 7 Concluding remarks.....	100
Bibliography	103

List of Figures

Figure 1-1 Schematic diagram of fibrin formation.	22
Figure 1-2 Mechanisms of primary and secondary hemostasis, and fibrinolysis.	26
Figure 2-1 3D-printed pure-shear specimen frames..	44
Figure 2-2 Pure shear fracture test specimen, monotonic and cyclic loading.....	47
Figure 2-3 Cyclic fatigue test setup.....	48
Figure 3-1 Clot formation and failure at a wound of a blood vessel	55
Figure 3-2 Rheological measurements of blood clots	56
Figure 3-3 Fracture energy of blood clots measured by lap shear test were size independent	58
Figure 3-4 Lap shear test results were compared with double cantilever beam tests	59
Figure 4-1 Structure and mechanical responses of blood clots under complex loading	63
Figure 4-2 Microstructure of fibrin clots	65
Figure 4-3 Histograms of fiber segment diameter and length	66
Figure 4-4 Mechanical responses of fibrin clots under cyclic load	68
Figure 4-5 Fatigue threshold experimental and theoretical estimation.	69
Figure 4-6 Micro-deflection mechanisms of fatigue crack growth.	70
Figure 4-7 Crack propagation rates of fibrin clots increase with loading rates or strain rates.	73
Figure 4-8 Mechanical responses of fibrin clots under variable rate loading	74
Figure 4-9 Semi-empirical prediction of overall fracture toughness.....	76
Figure 5-1 Adhesive and cohesive fracture of blood.....	78
Figure 5-2 Characterization of interfacial fracture energy	80
Figure 5-3 Characterization of bulk fracture energy	81
Figure 5-4 Effects of RBC on mechanical properties of the blood clot	82
Figure 5-5 SEM images of blood clots for different red blood cell content	83

Figure 5-6 Effects of PLT content on mechanical properties of the blood clot	83
Figure 5-7 SEM images of blood clots for different platelet content	84
Figure 5-8 Rate independent model of the blood clot.....	85
Figure 5-9 Comparison between measured and estimated force-displacement responses.....	86
Figure 6-1 Variation of height, width, and volume of unnotched pure shear sample	87
Figure 6-2 Dissipative and nonlinear elastic length scales of a variety of materials	91
Figure 6-3 Toughness enhancement comparison	92

List of Tables

Table 2-1 Mechanical properties of blood clots.....	30
Table 6-1 Critical length scales.....	90

Thesis organization

This thesis is written in a traditional monograph style, structured into seven chapters for clarity and coherence.

Chapter 1 begins by outlining the structure of the paper and the arrangement of chapters. It then delves into the background and outlines the challenges of interest, providing a comprehensive review of relevant literature in the field of coagulation and blood clot composition, and their emerging progress in biomechanics. Existing mechanical studies and characterization on blood clot related materials are summarized. Their limitations and challenges are identified. Future directions for advancing structural and biomechanical understanding of blood clots are proposed. Following this, the rationale for tackling the aforementioned issues is underscored, and the objectives and hypotheses of the thesis are described.

Chapter 2 describes the experimental methods and materials used in the thesis. The experimental methods cover blood clot initiation, sample preparation, mechanical and structural characterization, image analysis, and finite element modeling. The chapter also includes information on ethics statements and statistical analysis.

Chapter 3 proposes our first result on fracture behavior of human whole blood clots and platelet-poor, focusing on the investigation on fracture mechanics characterization. Their fracture energy is determined using a modified lap-shear method, demonstrating that the measured toughness is independent of the specimen geometry and loading conditions. These results also reveal an important contribution of blood cells to the clot fracture, as well as the dissipative length scale and nonlinear elastic length scale governing clot fracture.

Chapter 4 proposes a method to investigate the toughening mechanism of fibrin clots. Here we conduct cyclic fatigue and monotonic variable rate loading tests on fibrin clots to characterize their fracture properties in terms of fatigue threshold and rate-dependent fracture toughness. We demonstrate that the fracture behavior of fibrin clots is sensitive to the amplitude of cyclic load and the loading rate. Furthermore, we rationalize the fatigue threshold using a semi-empirical model parameterized by 3D morphometric quantification to account for the hierarchical molecular structure of fibrin fibers. The variable loading tests reveal rate dependence of the overall fracture toughness of fibrin clots. Our analysis with a viscoelastic fracture model suggests the viscoelastic

origin of the rate-dependent fracture toughness.

Chapter 5 proposes an integrated experimental-computational approach to evaluate the adhesive and cohesive fracture behavior of bovine blood clots by incorporating mechanical factors (e.g., loading rate, failure modes) as well as cellular components, such as red blood cells (RBCs) and platelets. Among biological substrates, the blood clot showed the largest interfacial fracture energy to the muscle and the least adhesion to the inner arterial lining, consistent with its biological role. Both interfacial and bulk fracture energy exhibited notable rate dependency, highlighting the role of dissipation as a toughening mechanism. An elevation in RBC content increased interfacial/bulk fracture energy, without influencing the clot's hysteresis, and this phenomenon – as substantiated by our finite element model – was due to an increase in intrinsic toughness. Increasing the platelet content enhances interfacial fracture energy to a level where the failure mode in the peeling tests shifted from adhesive to mixed-mode fracture, underscoring the crucial role platelets of in adhesion.

Chapter 6 provides a comprehensive discussion of all the findings, limitations of the reported technologies and future opportunities for improvement.

Finally, Chapter 7 provides a conclusion and remarks, comprising a conclusion encompassing all research findings of this thesis and recommendations for future work. This thesis aims to develop an interdisciplinary understanding of clot mechanics by exploring the fracture mechanics of blood clots. It describes the fracture properties and underlying mechanisms of blood clots and fibrin clots, acknowledging the significant impact of RBCs and platelets. The outcomes can inform strategies for managing clot-related disorders and inspire innovative therapeutic approaches.

Chapter 1 Introduction

1.1 Motivation

Blood clots are complex bioadhesives formed naturally within the body to halt bleeding and facilitate tissue healing. They consist of primarily fibrin, intertwined with platelets, red blood cells (RBCs), and other cellular components. These clots play a pivotal role in the body's hemostasis, preventing bleeding from wounded blood vessels. However, they also present a potential hazard when pathological clots form within intact vessels, leading to thrombosis, a condition that can have life-threatening consequences.

Understanding the mechanics of clot fracture is essential, as it holds significant implications for human health. A fracture within a clot can lead to rebleeding at wound sites or, in the case of intravascular clots, can result in thromboembolism, potentially causing severe conditions like pulmonary embolism, heart attacks, or strokes. The relevance of this understanding becomes particularly evident in the context of various diseases, such as COVID-19, where thrombotic complications are a significant concern.

1.2 Literature review

1.2.1 Introduction

Loss of blood is associated with a variety of pathologic scenarios that can lead to tissue morbidities and mortalities. In traumatic injuries, significant blood loss can result in significant prehospital mortalities stemming from hypothermia, coagulopathy, infection, acidosis, and multiple organ failure¹. Worldwide, severe trauma results in the death of over 5 million persons annually and is projected to surpass 8 million annually by the year 2020². Hemorrhage accounts for approximately 35% of the mortality from these traumatic injuries³. Therefore, hemostasis is of clinical significance in prophylactic, surgical, and emergency scenarios, attracting intense research interest⁴.

Whole blood generates a natural, *in vivo* biomaterial that not only decreases bleeding but also offers solid bioadhesives for the repair of wounded tissues via the processes of primary, secondary hemostasis^{5,6}. Blood clot needs to be mechanically tough and resistant to fracture, as it should

withstand forces of blood flow and dynamic pressure of extravascular contraction, pulsations of blood vessel walls, and tensile forces generated by the contracting platelets. Mechanical properties of blood clots have been studied for decades and various clots from whole blood, platelet-rich, and platelet-poor plasma and purified fibrinogen have been characterized⁷. Some of the fundamental mechanical properties of fibrin clots are used in several commercial tools used in clinical practice for characterizing coagulation rates and clot elasticity, determining the gelation point and estimating clot stiffness to provide useful information in a large range of clinical cases, including bleeding, directing procoagulant and anticoagulant therapies, and so on⁸. While many studies have investigated the fundamental mechanical behavior of blood clots, these characteristics alone do not illustrate how blood clot is ruptured or detached under multiple intravital forces.

In this literature view, a brief introduction of the blood clot formation process and major components is provided from a perspective that views blood clots as natural-derived hydrogels. The molecular biochemical formation mechanisms of fibrin network are introduced. The coagulation mechanisms, fibrinolysis, and the corresponding fiber interactions and crosslinks formed during coagulation.

A state-of-the-art summary of the progress in characterizing the mechanical properties of blood clots was then given, followed by several advances in constitutive and computational modeling methods.

1.2.2 Structural fibrin network formation of blood clots

Fibrinogen, which is also known as Factor I, is essentially a glycoprotein complex that spreads in the blood of mammals. At the time of tissue and vessel injury, it is transformed enzymatically by thrombin into fibrin and then into a fibrin-based blood clot. Fibrin is essentially a hydrogel made from a polymeric proteinaceous network that self-assembles during blood clotting to form porous 3D filamentous networks with mechanical properties substantially different from synthetic polymers⁹. Fibrin naturally acts as the scaffold of hemostatic blood clots and obstructive thrombi. Fibrin clots perform mainly to occlude vessels to stop blood loss. Fibrin also mediates platelet and endothelial cell spreading, tissue fibroblast spreading, capillary tube formation, and angiogenesis and thereby supports revascularization and wound healing¹⁰. Besides, fibrin glues or sealants are extensively applied in surgical treatment to prevent blood loss from injuries of various origins¹¹.

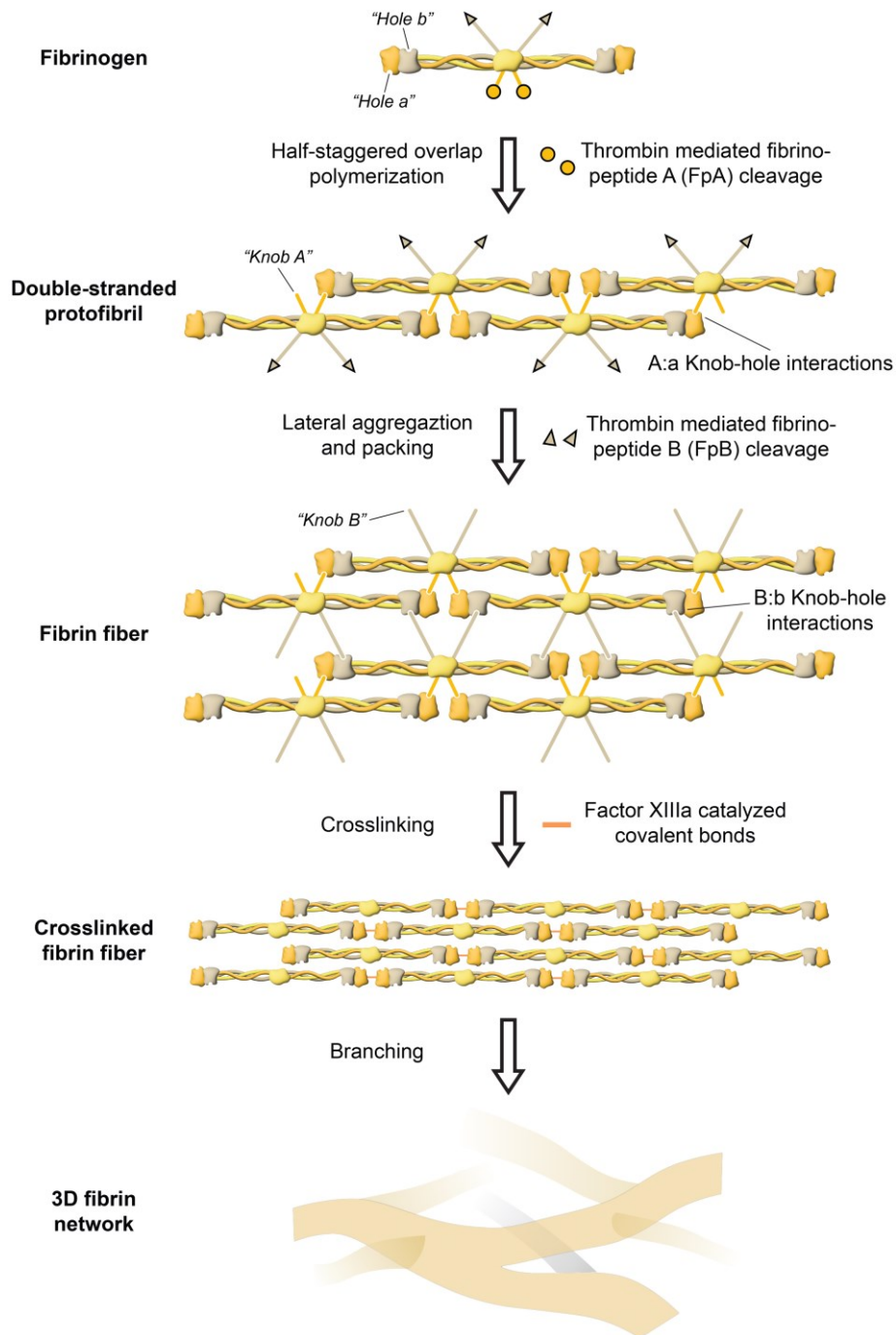


Figure 1-1 Schematic diagram of fibrin formation. Fibrinogen has two complementary protein structures: the “knobs” in the central nodule that are covered by fibrinopeptides, and the “hole” at the ends of the protein. Once the fibrinopeptides are removed by thrombin, the “knobs” are exposed and corresponding knob-hole interactions occur, resulting in the formation of double-stranded protofibril. As the protofibrils elongate, they aggregate laterally and pack into fibrin fibers. Crosslinking mediated by Factor XIIIa further produces covalent bonds between fibrin monomers and results in stabilized crosslinked fibrin fibers. During the polymerization, a split of protofibril strands creates branch points, and the branching of fibers results in the formation of three-dimensional structure of fibrin network.

The arrangement of individual fibrin fibers, which are crosslinked to form a complex fibrin network, determines the overall structure of a blood clot. Thrombin cleaves fibrinogen, a 340-kDa soluble glycoprotein, into an insoluble fibrin polymer during the clotting process, leading to the release of fibrinopeptides FpA and FpB¹² (Fig. 1-1). These fibrin monomers then polymerize into half-staggered oligomers upon the release of FpB, aggregating to produce protofibrils, the structural building blocks of the clot's fibrin network¹³. As the protofibrils grow to a critical length, they bind together laterally and produce thicker fibrin fibers via staggered half-molecule overlaps¹⁴. The interaction of fiber branching and lateral aggregation creates a three-dimensional structure that determines the mechanical and structural properties of a clot¹⁵.

Even though the abovementioned molecular model for clot formation has been thoroughly investigated and widely accepted¹⁶, the underlying mechanisms of structural evolution of fibrin networks originating from protofibrils are not yet fully understood. Evidence was shown that increased lateral association during blood clot formation produced clots with larger fiber diameters and less branches, whereas decreased lateral association produced clots with thinner fibers and more branches¹⁷. Fibrinogen, because of its autologous origin, offers a natural scaffolding for clots meant to be used as biomaterials. Investigating the underlying mechanisms behind fibrin formation could yield significant insight for developing innovative clinical methods with clot-related biomaterials and hemostasis technologies.

The structure of blood clots varies depending on the composition of a clot. Although an extensive amount of research has been conducted on plasma clots, only limited studies have been done to investigate how red blood cells affect the structural properties of a clot. It has been shown that the presence of red blood cells in the clot produced from whole blood increases the fibrin fiber thickness and promotes an enhanced alignment of the network¹⁸. During platelet-driven contraction process of clots, RBCs are forced to form a densely packed array of polyhedral erythrocytes which creates a nearly impermeable barrier that plays a crucial role in hemostasis and wound healing¹⁹. In addition, whole blood clots are more resistant to lysis than plasma clots²⁰. These results underscore the significance of taking red blood cells' role in clot structure into account and urge for further study.

1.2.3 Blood clot cellular components

1.2.3.1 Red blood cells

In contrast to the outdated belief that red blood cells (RBCs), also known as erythrocytes, play a negative and insignificant role in hemostasis and thrombosis, there has been increasing evidence in recent years that RBCs have biologically and clinically important functions in blood clot formation and its diseases. Recently, the potential of stored and pathologically changed RBCs to generate thrombin via direct phosphatidylserine exposure has been demonstrated²¹. In addition to the prothrombotic effects of free hemoglobin^{22,23}, the procoagulant and prothrombotic capabilities of RBC-derived microparticles transfused with stored RBCs^{24,25} or developed in various pathological circumstances associated with hemolysis have been elucidated. Fibrinogen or fibrin attachment to RBCs may influence their effect on fibrin network structure, clot mechanical properties, and fibrinolytic resistance^{20,26}. Current research on platelet-driven clot contraction shows that RBCs squeezed by platelets pulling on fibrin form a tightly bundled array of polyhedral RBCs that create an almost impermeable barrier needed for hemostasis and wound healing²⁷. RBCs may have dual roles, helping in the prevention of bleeding while also contributing to thrombosis in a number of ways.

1.2.3.2 Platelets

Nascent fibrin offers the structure of blood clots and strengthens the forming clot, while platelets can be considered the actuators of coagulation, which can sense and apply force to equilibrate the local microenvironment. Sensing happens biochemically on the platelet surface via a range of receptors, like integrins, that can sense thrombin, ADP, adrenaline, collagen, vWF, and fibrinogen²⁸. Platelets can respond to mechanical and biophysical stimulations²⁹⁻³². Notably, platelet mechanosensing is mediated by different approaches, depending on whether the platelet is experiencing initial adhesion or if it is actively spreading³³. Application of force by platelets is a mechanosensitive procedure, and the force increases with increasing substrate stiffness^{27,34}; however, biochemical and mechanical conditions synergize to maximize platelet forces³⁴⁻³⁶.

1.2.4 Blood coagulation and fibrinolysis

1.2.4.1 Primary and secondary hemostasis

Hemostasis is an intricate process leading to the formation of a blood clot at the site of vascular damage. In healthy and intact blood vessels, the endothelium acts as a barrier preventing blood clotting by inhibiting the adsorption of coagulation factors and releasing various bioactive

molecules, including heparin-like molecules, thrombomodulin, nitric oxide, and prostacyclin³⁷. Upon endothelial injury, blood coagulation is initiated, involving a series of coagulation cascades influenced by the components and tissue microenvironment of blood. This process comprises two distinct mechanisms: (a) primary hemostasis, defined as the formation of the primary platelet plug (Fig. 1-2a), and (b) secondary hemostasis, defined as the formation of fibrin by coagulation factors^{37,38} (Fig. 1-2b). Platelets and fibrinogen play pivotal roles in primary and secondary hemostasis, respectively. Notably, secondary hemostasis is usually initiated simultaneously with primary hemostasis, and the outcomes of these two hemostasis mechanisms interact with each other and achieve enhanced final hemostasis seals.

In the primary hemostasis, subendothelial collagen is exposed following blood vessel injuries and vasoconstriction, which encourages platelet adhesion, activation, and aggregation to form a platelet plug covering the damaged surface (Fig. 1-2a). The process begins with platelet adhesion facilitated by specific interactions between platelet membrane receptors and plasma proteins, including receptor glycoprotein (GP) Ib-IX binding with von Willebrand Factor (vWF), a blood glycoprotein acting as an adhesive protein, and receptor GP Ia-IIa binding with collagen^{39,40}. Adhered platelets undergo activation triggered by various stimuli, releasing cytoplasmic granules containing serotonin, platelet-activating factors, and adenosine diphosphate (ADP). The ADP receptors (P2Y1 and P2Y12) are stimulated and play a significant role in promoting initial shape changes and aggregation. The activated platelets change shape into a pseudopodal form, activating receptors GP IIb-IIIa through a calcium-dependent association. They bind with fibrinogen and initiate platelet aggregation involving extensions of pseudopods, clumping, and aggregation. The aggregation is further heightened by thrombin generation and resulting in the formation of primary platelet plugs.

Secondary hemostasis refers to the process of fibrin formation through the coagulation cascade, traditionally categorized into three pathways: intrinsic, extrinsic, and common pathways (Fig. 1-2b). This process unfolds in three key steps: a complex cascade triggering chemical reactions mediated by coagulation factors; the conversion of prothrombin (PT) to thrombin catalyzed by the PT activator; and the conversion of fibrinogen (Fib) into fibrin, enmeshing plasma, platelets, and blood cells to form a firmer clot^{41,42}. The intrinsic pathway can be initiated by negatively charged surfaces such as the high-molecular-weight kininogen (HMWK) on subendothelial collagen and kallikrein (KLK). They trigger the cascade activation of factors XII, XI, IX, and VIII. Factor VIII

serves as a cofactor for factor IXa-mediated activation of factor X. The extrinsic pathway starts from the release of tissue factor (TF) from hemorrhagic trauma tissue, which further binds to factor VII. The activated complex TF-VIIa mediates the conversion from factor X to factor Xa. Both pathways contribute to the generation of factor Xa, which forms the prothrombinase complex by binding with factor Va and II on the platelet plug surfaces. This FXa-FVa-FII complex further amplifies the conversion from PT to thrombin (FIIa), subsequently converting fibrinogen into fibrin.⁴³ Thrombin also activates factor XIII which leads to the crosslinking of fibrin to achieve a stabilized fibrin network.

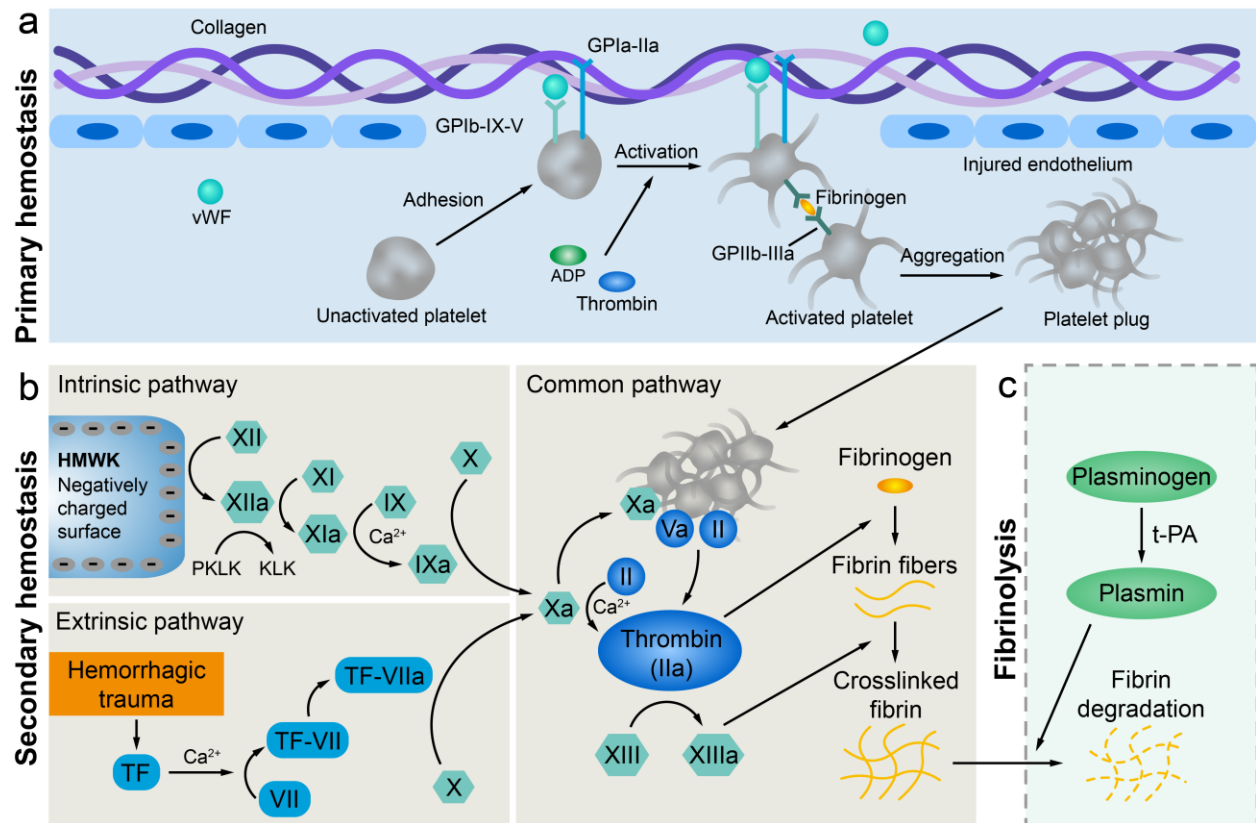


Figure 1-2 Mechanisms of primary and secondary hemostasis, and fibrinolysis. (a) Injuries expose subendothelial collagen and von Willebrand factor (vWF), as well as tissue factor (TF) bearing cells at wound sites. Platelets adhere to the bleeding sites through collagen and vWF, then undergo activation and aggregation via fibrinogen-mediated bridging, and eventually form a platelet plug (primary hemostasis). (b) The intrinsic pathway is activated when blood contacts negatively charged surfaces. The exposed TF triggers the extrinsic coagulation pathway and generates thrombin (IIa). Two pathways converge into a common pathway where the prothrombinase complex (FVa + FXa + FII) is formed on platelet surface, further promoting the production of thrombin for converting fibrinogen into fibrin. Fibrin polymerizes and assembles into a fibrous network that is crosslinked by FXIII (secondary hemostasis). (c) Fibrin is subject to the fibrinolysis, leading to the degradation of blood clots.

1.2.4.2 Fibrinolysis

After a clot has formed in the body and achieved its hemostatic role, it is normally dissolved by the fibrinolytic system in order to restore impeded blood flow (Fig. 1-2c)⁴⁴. Fibrinolysis is a part of a complex system of metabolic processes. The key enzyme involved is plasmin (Pn), a serine protease that is activated from its inactive precursor, plasminogen (Plg). Fibrinolysis begins with the activation of Plg by a Plg activator and is followed by fibrin breakdown mediated by Pn (Fig. 1-2c). Common Plg activators include serine proteases such as tissue-type plasminogen activator (t-PA) or urokinase-type plasminogen activator¹⁶. Inhibitors that promptly inactivate any Pn that dissociates from fibrin include plasminogen activator inhibitor (PAI) and α 2-antiplasmin⁴⁵.

1.2.4.3 Clotting time

The clotting duration required to form solid clots out of liquid blood is critical for hemostasis. Faster clotting is prone to shorten the bleeding duration and the amount of blood loss. The clotting duration depends on not only the native coagulation cascades (varies pathologically), but also exogenous factors that intervene in the coagulation process. A variety of assays are applied to measure clotting time. In clinical, prothrombin time (PT) and activated partial thromboplastin time (aPTT) are measured with plasma, while activated clotting time (ACT) test is performed on whole blood. These are widely used to analyze the functions of coagulation factors and anticoagulants. Simple tests like vial inversion can be used to roughly determine the clotting time. Thromboelastography (TEG) and rheology measurements are much more quantitative to monitor the whole kinetics of the clotting process. Also, the TEG can generate parameters that reflect clot strength and fibrinolysis, while the rheometer can output the shear modulus-time profiles. Due to the complexity of coagulation cascade and its sensitivity to testing conditions, a range of clotting duration is reported in literature. For TEG assay without addition of activators, a clotting time of human whole blood is reported as 630 seconds⁴⁶. According to rheological measurements, normal whole blood clotting generally reaches gel point within 240 seconds, which can be shortened to 10 seconds with the administration of thrombin^{46,47}; extreme cases such as severe hemophilia even lead to no clotting.

1.2.5 Physical interactions and covalent crosslinks

1.2.5.1 Physical interactions during fibrin self-assembling

Formation of fibrin network from fibrinogen is essential for hemostasis, thrombosis, and wound healing^{48,49}. Fibrin network formation is initiated by thrombin-catalyzed cleavage of the fibrinopeptides of fibrinogen to form the fibrin monomer, followed by the non-enzymatic polymerization of fibrin which is found to be driven by non-covalent bonds, or physical interactions. At the non-enzymatic stage, the fibrin monomers self-assemble spontaneously into fibrin oligomers which further lengthen to make two-stranded half staggered rod-like protofibrils. Then lateral and longitudinal aggregation of protofibrils results in the formation of thicker fibrils that branch to yield a 3D clot network, which is referred to as an immature clot^{14,16,50-52}. It is demonstrated that protofibril formation is motivated by the intermolecular A:a knob-hole interactions, while B:b knob-hole interactions are involved in the lateral aggregation of protofibrils⁵³. Although the mechanisms, structural motifs, and driving forces of the protofibril aggregation remain largely unknown¹⁶, some recent studies argue that their results from laser tweezer tests⁵² and molecular dynamics simulations⁵³ suggest that electrostatic contacts and hydrogen bonds are the driving forces of the physical knob-hole interactions.

1.2.5.2 Factor XIIIa mediated covalent crosslink

To strengthen the immature clot against proteolytic and mechanical impacts, fibrin is covalently cross-linked by the plasma transglutaminase, Factor XIIIa, an active form of Factor XIII zymogen activated by thrombin in the presence of calcium chloride⁵⁴. The C-terminal ends of the γ chains of fibrin have amino acid residues comprising a crosslinking region for 2 end-to-end interacting molecules that form covalent isopeptide bonds between molecules. There has been an argument about longitudinal γ - γ -crosslinking within a filament of a protofibril versus transverse γ - γ -crosslinking between fibers⁵⁵, but later evidence has been offered for the longitudinal orientation of these bonds⁵⁶. The development of the same isopeptide bonds is catalyzed at a lower rate between the α C regions to stabilize long α C polymers⁵⁷. Crosslinking also happens between α and γ chains followed by the formation of α - γ -heterodimers⁵⁸. Before crosslinking, fibrin polymerization is reversible, with fibrin being an equilibrium polymer⁵⁹. After crosslinking within and between protofibrils, polymerization becomes irreversible, and the clot is more stable, mechanically strong, and resistant to fibrinolysis. The crosslinked fibrin can be dissolved either by the reduction of disulfide bonds that hold polypeptide chains together or by chemical hydrolysis of peptide bonds. A normal genetic variant of Factor XIII forms either porous permeable mesh or

dense meshes with reduced permeability at different fibrinogen levels⁶⁰.

1.2.5.3 Fiber-fiber cohesive contacts

In addition to the well-known fiber alignments along the direction of strain, the formation of fiber-fiber cohesive contacts is another structural change, also known as the fiber crisscrossing and fiber densification. The fiber-fiber cohesive contacts contribute to the overall stiffness of stretched fibrin network by fibrin fiber shortening and partial bending, changing fibrin fiber stiffness, fiber alignment and increasing network density⁶¹. Although the molecular mechanism of fiber-fiber cohesive bond formation is not understood, it is reported that inhibiting Factor XIIIa does not alter the interaction force between fibrin fibers, indicating the irrelevance between Factor XIIIa mediated covalent bonding with fiber-fiber cohesive contacts⁶². On the other hand, a recent study that estimated the force between interacting fibers supports the assumption that the contact between fibers was formed by irreversible bonds of non-covalent interactions⁶³.

1.2.6 Mechanical properties of blood clots

Regarding studies in the biomechanics of blood clots, researchers were focusing on associating the mechanical properties with diseases⁶⁴. Although a variety of experimental approaches of determining mechanical properties of blood clots have been proposed⁶⁵, the fracture properties of blood clots remain largely unexplored.

1.2.6.1 Summary

The coagulation cascades yield blood clots, serving as plugs to stop bleeding and seal injury sites. This purpose of hemostasis is mechanical in nature. The mechanics of blood clots are essential to the hemostatic function, as well as the downstream consequences such as wound healing and tissue regeneration. Clot mechanics studied by TEG indicates decreased clot stiffness is associated with bleeding disorders in some patients who have hemophilia and von Willebrand disease⁵. Despite the appreciation of clot mechanics on hemostasis, the exact link demonstrated in vivo is missing. The gap was filled recently with a rodent study, showing that both adhesive and cohesive fracture of blood clots lead to rebleeding and decrease survival from hemorrhage in vivo⁶⁶. Substantiating the direct link between clot mechanics and hemostasis requires further investigation.

The mechanical properties of blood clots include stiffness (i.e., elastic modulus or shear modulus), strength, viscoelasticity, poroelasticity, and fracture toughness. The representative values are

summarized and listed in Table 1-1; some of the testing methods and apparatus have been reviewed elsewhere^{5,64}. Attention is called on the difference between toughness and fracture toughness; toughness quantifies the energy dissipation capacity of an unnotched sample in a unit of J m^{-3} , while the fracture toughness in a unit of J m^{-2} reflects the resistance against crack propagation⁶⁷. It should be noted that the list is by no means exhaustive.

Table 1-1: Mechanical properties of blood clots.

Properties	Value	Material
Young's modulus	4.4 kPa	Human whole blood clot ⁶⁸
Shear modulus	5 kPa	Bovine whole blood clot ⁶⁹
Permeability	$(3.5 \pm 0.9) \times 10^{-2} \mu\text{m}^2$	Human whole blood ⁷⁰
Fracture toughness	$7.6 \pm 0.45 \text{ J/m}^2$	Human blood plasma-derived fibrin clot ⁷¹
Adhesive strength	$1.1 \pm 0.2 \text{ kPa}$	Human platelet-rich plasma clot ⁶⁶

As can be seen from the above table, blood clots are mechanically inferior to other biological materials such as blood vessels and skin. Considering fracture resistance, the fracture toughness of blood clots is measured at $\sim 1 \text{ J m}^{-2}$, which is two and three orders of magnitude lower than that of blood vessels and skin, respectively. The mechanical mismatch is concerning as the clot can neither survive the force from the surrounding tissues, nor restore the biomechanics of the injured tissues. A downstream consequence is the mechanical failure of clots, causing rebleeding and hemorrhage. This issue necessitates strategies to augment the clot mechanics, one of the main focuses of the existing invention technologies.

1.2.6.2 Tensile properties

Tensile testing of blood clots both *in vivo* and *in vitro* has been extensively applied to determine their tensile strength and elastic modulus.

Blood clots are soft *in vivo*, therefore they could be highly challenging to be gripped for testing.

Various approaches to solve the slipping issue of the samples during testing have been developed. Uniaxial tensile tests were conducted on aortic blood clot specimens that were removed from six male patients undertaking elective resection of abdominal aortic aneurysm (AAA)⁷². The results from this research revealed a linear load-displacement relationship for each of the samples. Similar results were obtained through tensile testing on intraluminal blood clots (ILT) also collected from AAA patients⁷³. Their purpose was to determine the maximum tensile strength and fatigue. The results further demonstrated that the ILT material displayed a nearly linear response under biaxial tensile force⁷⁴. However, recent studies have revealed that the material exhibits nonlinear elastic behavior and high deformability^{73,75-77}.

Studies involving blood clots in vitro from human sources can often be costly and especially regulated, making blood clot related samples challenging to obtain. Thus, clot analogs have been developed as a more available option for testing⁷⁸, which are synthetic clots that are developed in vitro from human or animal blood products to have a comparable chemical structure to natural clots. There are many existing protocols for the manufacture of clot analogs, and typical variables include the donor species, the concentration of thrombin⁷⁹⁻⁸¹. The mechanical properties of these products, including elastic modulus, permeability, and strength, can also be manipulated by varying the concentrations of fibrinogen, thrombin, factor XIII, fibronectin, platelets, and calcium^{82, 83}. Previous results demonstrated that existing analog products have been successful at simulating different clot types. A tensile test was carried out on clot analogs, generated in vitro from porcine and human whole blood⁸⁴. Its results demonstrated that the material reached stress of around 10 kPa, and a strain of 300% before rupture, suggesting that the material is highly elastic. Additionally, results from a tensile experiment on fibrin clots made from purified human fibrinogen showed that the clots had a non-linear stress-strain relationship in which the samples could be stretched to three times their relaxed size prior to failure⁵⁴. The tension of human whole blood clots under stretch is measured using a self-designed microtensometer and Young's modulus was estimated to be 4.4 kPa. In contrast, the clots with no platelets showed a decreased Young's modulus of 2.5 kPa⁶⁸

1.2.6.3 Compressive properties

Blood clots can be exposed to compressive stress/strain resulted from blood flow, vasoconstriction, and clot retraction. Therefore, it is necessary to characterize the compressive behavior of blood

clots⁸⁵. Such properties have been investigated with *in vivo* and *in vitro* setups.

As for blood clots formed *in vivo*, a customized measurement device was developed to determine the compressive properties of blood clots formed on rodent inferior vena cava (IVC)⁸⁶. The device measured the force and displacement of the blood clot as a cylindrical specimen when compressed by a rectangular stamp. The purpose of this study was to determine Young's modulus of the blood clots. The results indicated that the stress had a nonlinear relationship with the strain. Then, similar results⁸⁷ illustrated that the human blood clots displayed a small increase in stress at low strains and a large increase in stress when strains reached above approximately 80%, which is the typical soft-tissue behavior. It was also discovered that the aged blood clots had a reduced elasticity compared to the soft, highly elastic fresh red clots. The red clots were as well less likely to fragment compared to the aged samples.

Mechanical properties of fibrin clots under compression were investigated. The fibrin clots were formed *in vitro* by mixing diluted human citrated platelet-poor plasma with calcium chloride and human thrombin⁸⁸. The results from these tests illustrated that the compressive stress-strain curve was dependent on the initial clot stiffness as well as on the loading rate of compression. Additionally, the structural transitions of the networks under compression were studied after reconstructing the 3D structure of the fibrin networks obtained using a rheometer-coupled fluorescent confocal microscope⁸⁸. An unconfined compression test of blood clots was performed on blood clot analogs prepared *in vitro*⁸⁴. There was a linear stress-strain relationship up to strain values of roughly 70% and at higher strain magnitudes the stress values increased notably at a significantly larger rate. Such results were validated by similar tests on *in vitro* clot analogs, produced using bovine, porcine, and human whole blood^{87,89}.

1.2.6.4 Stress relaxation

Stress-relaxation is a time-dependent behavior that exhibits stress decrease under constant strain. The stress-relaxation behavior of clots has been confirmed in several studies^{83,90,91}. A relaxation time value of 2 to 52 seconds was reported, characterized by stress-relaxation tests on single fibrin fibers⁹². Moreover, the non-surface-creating dissipative mechanisms were recently identified and quantified by investigating their dissipative mechanics under simple uniaxial extension, cyclic loading, and stress-relaxation. And the experimental results indicated that whole blood clots exhibit Mullins-like effect, hysteresis, permanent set, strain-rate dependence, and nonlinear stress-

relaxation⁹¹.

1.2.6.5 Viscoelasticity

The major component of blood clots, fibrin, exhibits various levels of elasticity and viscosity. Over the past few decades, an extensive amount of study has been conducted on the viscoelastic characteristics of blood clots⁹³. Understanding these mechanical properties is critical because of their important implications for biological and clinical applications. The elastic properties of the fibrin polymer contributes to the overall stiffness, while its inelastic behaviors are described by its irreversible viscosity⁴⁸. The viscoelastic properties of blood clots are determined by their structural composition. RBCs' participation, for example, alters the fibrin network structure, the properties of individual fibers, and the overall viscoelasticity of the clot^{18,94}. Therefore, extensive research has employed compression, deformation, and tension experiments to describe the viscoelastic behaviors of blood clots⁹¹.

As for clinical use, thrombo-elastography is widely used to quantify dynamic changes in the viscoelastic properties of a blood sample during clotting under low shear stress, and clinically evaluate the coagulation status of patients⁵. It can also provide information about the development of physical characteristics of the clot, including thrombin time, PT, and PTT, which can be much useful clinically⁴⁸. Furthermore, the mechanical properties measured by thrombo-elastography, the strength, and integrity of the clot, are what matters most in effective hemostasis⁹⁵. However, many of the parameters measured by thromboelastography have not been related to normal viscoelastic mechanical properties and have no physical meaning except in comparison with other such thrombo-elastography measurements.

Rheometry is another technique that has been extensively adopted by researchers⁹⁶. A shear rheometry test utilizing a parallel plate rheometer to determine the storage and loss modulus of blood clot samples taken from individuals undertaking AAA repair was successfully conducted⁹⁷. Also, results from a compression stress-relaxation test on blood clots from patients and clot analogs formed *in vitro* from bovine fibrinogen, thrombin, and calcium chloride indicated that the clots exhibit obvious viscoelastic behaviors⁸³. Nonlinear viscoelastic properties of blood clots have also been investigated utilizing large amplitude oscillatory shear (LAOS) on clots developed from porcine whole blood, platelet-rich plasma and platelet-poor plasma *in vitro* to investigate the effect of RBCs, platelets, and fibrin, respectively⁹⁸. The rheological results obtained were then applied

to develop a series of constitutive equations for blood clot formation and the linear and nonlinear viscoelastic properties of the mature blood clots. Furthermore, a dynamic ultrasound elastography method was implemented to evaluate the storage and loss modulus of clot analogs formed *in vitro* from porcine entire blood⁹⁹. Finally, nanoindentation has also been utilized to capture the mechanical property of rodent clots prepared from platelet-rich plasma *in vitro*¹⁰⁰. This testing approach has several advantages over other techniques, including a small scale of measurements, customized indenter tips, and high resolution for both load and displacement measurements.

1.2.6.6 Poroelasticity

Mechanical behavior of blood clots is critical in both hemostasis (i.e., stoppage of bleeding) and thrombosis (i.e., blocking of arteries/veins), and thus attract significant amounts of interest, however the poroelastic behavior of clots is still a topic that needs further investigation. The time-dependent deformation of the blood clot is commonly attributed to its viscoelasticity^{94,101,102}, and various studies have characterized the viscoelastic behavior of the blood clot with rheology^{103,104}, compression^{88,94,105} and uniaxial tension tests^{91,101}. However, poroelasticity is recognized, in addition to the viscoelasticity, to contribute to the time-dependent responses of biological tissues¹⁰⁶. Although some hallmark features of poroelasticity (e.g., permeability¹⁰⁷ and fluid transport⁵⁴) have been observed in the blood clot, little study has yet comprehensively investigated its poroelasticity¹⁰⁸⁻¹¹⁰.

Despite distinct microscopic mechanisms underlying, both poroelastic and viscoelastic processes manifest the time-dependent mechanical responses¹¹¹. The poroelasticity is caused by long-range fluid transports in a porous medium, whereas the viscoelasticity is related to localized processes such as sliding and reconfiguration of polymer chains as well as the rearrangement of reversible crosslinks^{112,113}. Such microscale differences lead to distinct behaviours at the macroscale. While the transient response of a viscoelastic material is independent of the macroscopic characteristic dimension (or sample geometry); the sample geometry influences substantially temporal and spatial variations in the mechanical response of a poroelastic material (e.g., stress relaxation with time)¹¹⁴. In the absence of solid evidence on the underlying mechanisms of the time-dependent behaviour (poroelasticity, viscoelasticity or both) of the blood clot, foregoing theories might be misused, potentially leading to erroneous interpretations.

Blood clots can exhibit both viscoelasticity and poroelasticity at the same time¹⁸. Blood clots have

been found to possess behaviors associated with poroelasticity, such as fluid transport and permeability, highlighting their poroelastic nature¹⁰⁶. Further proof of blood clots' poro-viscoelastic nature has been provided by a recent study through the co-existing evidence of size-dependent stress relaxation and mass loss (fluid migration through porous matrix) under compression due to poroelasticity as well as substantial stress relaxation under shear deformation due to viscoelasticity¹¹¹. The specific contributions of viscoelasticity and poroelasticity to the blood clots' function as a natural-derived bioadhesive remain largely unexplored. Investigating the role of poroelastic behavior in hemostasis and thrombosis biomaterials could be insightful given the coexistence of poroelasticity and viscoelasticity.

The poroviscoelasticity of the blood clot is due to time-dependent responses of its constituents as well as their interactions. Fluid transport inside the porous matrix (i.e., red blood cells embedded in the fibrin network) appears to be the major mechanism for the poroelasticity of the blood clot. An individual red blood cell has shown poroelastic/viscoelastic behaviour at $t < 0.5$ s^{115,116}; however, because of the duration of the ramp loads in relaxation tests, such fast responses in our experiments are not captured in this study. Regarding viscoelasticity, micromechanical tests have shown that a single fibrin fiber is viscoelastic⁹³; interestingly, relaxation time constants of a fibrin fiber ($\tau \sim 3$ s and 50 s) matches those of the blood clot⁹². In the fibrin network, the breakage of crosslinks and other conformational change of fibrin such as sliding and disentanglement also contribute to the viscoelastic response of the blood clot^{59,117}.

Recent investigations on the clot poroelasticity reveal clinically relevant insights. The blood clot derived from patients with thromboembolism and/or vascular disorders have significantly lower hydraulic permeability¹¹⁸⁻¹²³, which substantially alters temporal and special responses of the blood clot under mechanical loads. The permeability values are largely determined by the compositions of the blood clots⁷⁰. It is showed that for platelet rich plasma with volume fractions of platelet increases from 1% to 61% can contract to alter permeability of the platelet-rich clot from $1.1 \times 10^{-2} \text{ m}^2$ to $1.5 \times 10^{-5} \text{ m}^2$ ¹²⁴.

1.2.6.7 Fracture toughness

Blood clots, whether functioning as a hemostasis sealant or a thrombotic embolism, fail either by cohesive fracture occurring at the bulk material of clot or by adhesive fracture at the interfaces to adherent. Fracture toughness is a metric broadly used to describe the material's ability to crack

growth resistance. Although in linear elastic fracture mechanics (LEFM), toughness can refer to both of the critical stress intensity factor upon the onset of crack growth and the critical energy required to extend a unit area of crack, the latter concept of fracture toughness, or known as the fracture energy, is more appropriate for soft materials because it is difficult to define stress intensity factor for cracks under large deformation¹²⁵.

The major polymer scaffold of clot, fibrin, is a highly ductile and soft material. Mature fibrin clots could be stretched to over three times their original length before breaking with an average stretch of 270%⁵⁴. Under hydraulic tension, plasma clots were reported to be elongated more than 200% before rupture that happened at average rupture stress of 550 mN/mm²¹²⁶. The fracture strain of a clot was also found to be highly dependent on the volume fraction of RBCs¹²⁷.

In recent years, there has been a growing focus on the study of fracture toughness of clots, and notable progress has been achieved. The fracture toughness of fibrin gel was calculated directly from experimental data on single edge notched tension specimens⁷¹. An independent finite element simulation using fibrin material models that account for forced protein unfolding was conducted and it supported the measured value of fracture toughness and showed that breaking of fibers ahead the crack at a critical stretch is the mechanism of rupture of blood clots, including thrombotic embolization. Recently, the toughness of plasma clots was determined as a function of fibrin content and was correlated with fibrin network structure measured by confocal and scanning electron microscopy¹²⁸. The challenge of experimental characterizing of clot fracture toughness was met using an experiment-simulation combined method. First, a single edge notched tension test was performed to capture the force-stretch response for cracked samples with various fibrinogen concentrations of varying crack length, and a material model was fit to the experimental results by finite element simulation. Then the critical energy release rate was computed as J-integral using finite element simulations given the experimental data of critical displacement related to the onset of crack propagation.

1.2.6.8 Adhesion properties

In order to achieve hemostasis and close damaged vasculature, blood clots are required to adhere to wounded tissues¹²⁹. On the other hand, the clot delamination inside the vessels can lead to the blocking of veins or arteries and cause thrombosis¹³⁰.

The adhesion of blood clots was investigated by characterizing adhesive strength using lap shear test⁶⁶. It is found that Factor XIII plays a vital role in clot adhesion and the clot adhesive strength to collagen increased 2-times at a physiological concentration of Factor XIII compared to Factor XIII poor plasma. Notably, no significant difference in clot adhesive strength was observed comparing clots with and without red blood cells added, whereas platelet-rich plasma with a high platelet concentration (2-times of physiological concentration) displayed 52% higher adhesive strength than platelet-poor plasma. Adhesion energy characterization of blood clots could provide further insights into the energy dissipative mechanism yet remains largely unexplored.

1.2.7 Modeling of blood clot mechanical behaviors

Several theoretical and computational methods have been recently proposed for modeling fibrin structural mechanics at different spatial scales varying from molecular scale to macroscale.

Constitutive models are important for the numerical simulation of blood clot behavior and deformation *in vivo*^{99,100 102}. A variety of models have been developed to illustrate the mechanical properties of the components of the blood clot¹³¹. These models emphasize the clot formation, coagulation, and dissolution in flowing blood or the formation of the fibrin network^{81,98,132}. The linear viscoelastic properties of the clot have additionally been modeled employing ultrasound techniques and the results were fitted to linear viscoelastic models⁹⁹.

Several linear models have been developed in recent years¹³³. A study described the linear viscoelastic properties of clots through a multi-mode Maxwell model. This model was calibrated via the shear test data and the material was presumed to be isotropic and incompressible⁹⁷. Similarly, a model was developed to capture the stress-strain behavior of the structures⁵⁴. Blood clots were modeled as random networks of folded proteins that utilize a system of linked fibers, which can relate the response of the network to its fibers that behave as linear springs.

However, the linear models described were merely applicable for small strains up to 5% as the materials only behaved linearly at small strains. Therefore, a non-linear viscoelastic model was later proposed to capture the material behavior at larger strains more precisely⁹⁰. The constitutive model described was built on a model created to illustrate the material properties of animal brain tissue¹³⁴. Furthermore, a comparable model was proposed inspired by earlier developed models^{90,135,136}. This model is similarly based upon a generalized multi-arm Maxwell model, which

is modeled by an elastic spring, a viscous dashpot, and several Maxwell modes assembled in parallel¹⁰².

In addition, many computational modeling studies have been emphasized on the mechanisms of blood clot formation via computational fluid dynamics¹³⁷. However, only a few studies delved into the microstructural behavior of blood clots. One of the early investigations studied the mechanical properties of blood clots under compression using finite element modeling. The sample was modeled as elastic, linear, isotropic, and quasi-incompressible⁸⁶. Besides, an elastic 2D plane stress finite element computational model was used to validate tensile experimental data. The incompressible mechanical properties were modeled by a one-parameter Ogden strain energy function which can predict a near-linear force-displacement behavior⁷³. Then, a 2D axisymmetric poroviscoelastic finite element model was developed, which replicated the blood clot sample and the flat punch indenter tip throughout a nanoindentation experiment¹⁰⁰. The blood clot was modeled as a biphasic material consisting of a porous solid and a fluid¹³⁸. In this model, the solid phase of the blood clot is viscoelastic, and the model utilized a standard linear solid model, comprising of a linear spring in parallel with a Maxwell element. Similarly, high strain poroelastic and poroviscoelastic biphasic models were implemented into a finite element model of a fibrin network¹³⁹. However, this macroscale strategy does not involve the deformation mechanics of the single fibers which rule the structural source of clot rheology.

Some multiscale methods of modeling have recently been proposed. A multiscale model of platelet aggregation combining cellular scale and subcellular scale was established¹⁴⁰. A 3D platelet aggregation model was proposed which modeled the platelets as circular instances¹⁴¹. Recently, a 3D fibrin fiber network was reconstructed based on 2D microscopy image analysis. Each network was modeled adopting nonlinear or linear mass-spring models¹³³. The network's response to uniaxial tensile and shear stresses was investigated to determine the mechanical properties. The elasticity of the fiber network predicted by the model agreed well with the previous test result¹³³. These 3D and multiscale computational designs are incredibly computationally expensive. Hence, further effective computational methods and improved equipment are needed to achieve the efficiency needed for these comprehensive computational studies of blood clot dynamics¹⁴².

1.3 Challenges in existing blood clot studies

Despite the critical importance of comprehending the fracture mechanics of blood clots, it remains

a complex and relatively unexplored field compared to the study of hydrogels and other soft materials. Previous research has primarily focused on the nonlinear behavior of blood clots, examining their mechanical properties like stiffness, strength, and viscoelasticity. However, the specific investigation of clot toughness, particularly in whole blood clots that incorporate a substantial volume of RBCs and platelets, has been limited.

Characterizing the fracture properties of blood clots presents distinct challenges due to their soft, deformable nature. Conventional fracture testing methods designed for rigid materials are unsuitable for these delicate structures. The wet and fragile characteristics of blood clots further complicate testing. These biological materials possess a limited operational window due to their dynamic biochemical and mechanical properties, making specimen preparation and testing time-sensitive.

The mechanical, physical, and biochemical processes involved in clot fracture are intricate, given the structural complexity of blood clots. Understanding the crack tip region, with its complex stress and strain fields, is vital to unraveling the clot's fracture. This area is associated with parameters such as the dissipative length scale, reflecting the critical flaw size, and the nonlinear length scale, characterizing nonlinear deformation. These essential length scales are crucial for deciphering the mechanics of clot rupture.

1.4 Research rationale and objectives

1.4.1 Research rationale

This thesis addresses the above-mentioned challenges by developing characterization methods and fracture mechanics of blood clots.

The challenge posed by the fracture of blood clots in hemostasis and thrombosis treatment calls for innovative solutions to enhance medical outcomes and patient well-being. Existing understanding in this field faces limitations, prompting the necessity for a paradigm shift in biomechanics study and application. The research work of this thesis is dedicated to overcoming these limitations through an exploration of blood clot fracture behaviors. The emphasis on fracture toughness characterization, intrinsic and rate-dependent toughness, and cohesive and adhesive fracture represents a pioneering and comprehensive understanding of blood clot fracture. The implications of this study have the potential to significantly improve the quality of life for patients

facing the threat of hemorrhage and thrombosis.

1.4.2 Research objectives

The research objectives of this thesis are categorized into the following three areas.

Objective 1: Investigating fracture toughness measurement for blood clots

This objective involves the investigation into the fracture behavior of human whole blood clots and platelet-poor plasma clots and the fracture toughness measurement. The fracture energy of whole blood clots and platelet-poor plasma clots will be determined using modified lap-shear method. The measured toughness will be investigated whether to be independent of the specimen geometry and loading conditions. We will evaluate the importance of blood cells in the clot fracture. The dissipative length scale and nonlinear elastic length scale governing clot fracture will be calculated and discussed. Overall, this proposed study will motivate the investigation on blood clot fracture and inspire the development of clot-mimicking bioadhesives.

Objective 2: Exploring the multifaceted toughening mechanisms of fibrin network under complex loading conditions.

In this objective, cyclic fatigue and monotonic variable rate loading tests will be conducted on fibrin clots to characterize their fracture properties in terms of fatigue threshold and rate-dependent fracture toughness. The fracture behavior of fibrin clots will be evaluated whether to be sensitive to the amplitude of cyclic load and the loading rate. The intrinsic toughness can be revealed by fatigue tests, and the rate dependence of overall fracture toughness will be explained by the variable loading tests. Next, a semi-empirical model parameterized by 3D morphometric quantification will be developed to rationalize the fatigue threshold and account for the hierarchical molecular structure of fibrin fibers. Besides, a viscoelastic fracture model will be proposed to understand the viscoelastic origin of the rate-dependent fracture toughness. The toughening mechanism of fibrin clots will be investigated with confocal image analysis and further compared with biological tissues and hydrogels.

Objective 3: Assessing adhesive and cohesive fracture of blood clots

In this objective, the fracture modalities of blood clots including cohesive fracture within the clot's bulk material the adhesive fracture at the clot-tissue interface, and the mixed mode fracture will be evaluated through an integrated experimental-computational approach. We will investigate the

adhesive and cohesive fracture behavior of bovine blood clots by incorporating mechanical factors, like loading rate and failure modes, as well as cellular components, such as red blood cells and platelets. The adhesive fracture will be assessed on multiple biological related substrates. The rate dependency of both interfacial and bulk fracture energy will be studied to understand the toughening mechanism. Finite element models will be developed to further evaluate the role of red blood cells and platelets on interfacial/bulk fracture energy.

Chapter 2 Materials and Methods

Human whole blood clots, bovine whole blood clots and platelet-poor plasma clots were used in the experiments. Platelet-poor plasma clots serve as a model for fibrin clots given that fibrin is their primary constituent. These experiments include mechanical testing, structural characterization, and imaging analysis. The materials and testing methods are detailed as follows.

2.1 Material and sample preparation

2.1.1 Blood clotting initiation investigation

The human ethics protocol for this study has been approved by the Research Ethics Board at McGill University. Human whole blood (WB) and platelet-poor plasma (PPP) were purchased from ELEVATING SCIENCE®, BioIVT; the donors were unidentified. They were both pooled, drawn in citrate phosphate dextrose adenine (CPD-A) anticoagulant, and preserved in 1 mL aliquots. The human WB was kept at 4 °C and the PPP was frozen at -80°C. They were thawed at room temperature before use. Tissue factor was a recombinant thromboplastin reagent (Dade® Innovin® Reagent). Sample molds and cantilever beams were made of acrylic sheets after laser cutting. The acrylic and polyester backing films were from McMaster-Carr. Sodium chloride and calcium chloride dihydrate for preparing the recalcification solution were purchased from Sigma Aldrich.

The human blood clots were formed following a reported protocol¹⁴³. To initiate the clotting cascade, the recalcification solution containing NaCl and CaCl₂ was mixed with the tissue factor at a volume ratio of 249:1. The mixture was then added into the blood samples (either WB or PPP), with a final volume ratio of the blood to the recalcification mixture solution at 3:1. While NaCl was fixed at 22.5 mM, the final concentration of CaCl₂ was varied between 10 mM and 40 mM. Consequently, coagulation occurred as the clotting factors were activated and then cleaved and polymerized fibrinogen into a fibrin network. Immediately after recalcification, the blood clot was kept in a sealed Ziploc bag with saturated humidity inside to maintain hydration, and the samples were incubated at 37 °C for 2 hours to allow complete coagulation and crosslinking prior to testing; the duration is sufficient according to the rheological measurement results shown in section 3.4.1.

2.1.2 Platelet-poor plasma and recalcification solution preparation

Gender-unspecified bovine whole blood was collected in citrate-phosphate-dextrose anticoagulant (Lampire Inc.) and processed into the platelet-poor plasma using the following protocol: The bovine whole blood was centrifuged at 1500 g for 15 minutes at room temperature to separate platelet-rich plasma and erythrocytes. The platelet-rich plasma was carefully collected with a dispo-pipette, leaving approximately 0.5 cm above the buffy coat, and further centrifuged at 1500 g for 15 minutes at room temperature to obtain plasma¹⁴⁴. In addition, the recalcification solution was prepared using sodium chloride (90 mM, Sigma Aldrich) and calcium chloride dihydrate (300 mM, Sigma Aldrich) for initiating clotting.

2.1.3 Modified blood clots with varying cellular contents

Bovine whole blood (CPDA-1 anti-coagulant; sourced from McGill Veterinary Services, or Lampire Biological Laboratories, USA) was utilized. Clots were formed through the addition of a calcification solution (10:1 volumetric ratio), resulting in a final concentration of 22.5 mM NaCl and 30 mM CaCl₂. Due to the time-sensitivity of platelets, for tests involving platelet content variations, a local source (McGill Veterinary Services) was used, and clotting was performed within 4 h of the blood collection. The remaining tests were completed in less than 72 hours from collection to minimize blood aging and maintain mechanical property consistency^{69,145}.

We modified the RBC content of blood (while keeping fibrinogen and platelet content constant) by centrifuging the whole blood at 1500 g for 15 min to separate platelet-rich plasma (PRP) and erythrocytes. By leaving a buffer of 0.5 cm above the buffy coat, the PRP was carefully pipetted and placed in a 37 °C incubator to evaporate 40% of the water and obtain a concentrated PRP. RBCs were re-suspended in concentrated PRP (7:3 v:v) to achieve 70% volume ratio of RBC content blood samples. To reach 30% volume ratio RBC content, we mixed RBCs in unprocessed PRP and normal saline (NS; 0.9% w/v of NaCl) at a volume ratio of 3:5:2 (RBC:PRP:NS)¹⁴⁶.

To alter platelet content, the bovine whole blood was centrifuged at 1500 g for 15 min at room temperature to separate PRP and erythrocytes¹⁴⁴. The PRP was further centrifuged under the same conditions to yield platelet-poor plasma (PPP) and a platelet pellet. RBCs were then re-suspended in PPP (1:1 v:v) to create a blood sample devoid of platelets, using the same volume of native whole blood for RBC and PPP. A blood sample with triple platelet content was then prepared by

mixing the platelet pellet into the zero-platelet blood sample¹⁴⁷.

2.1.4 Preparation of pure shear specimens

The specimens were prepared in pure-shear configuration. The pure shear test, originally proposed by Rivlin and Thomas¹⁴⁸ for measuring the fracture energy of rubbers, has been widely used to characterize gel fracture¹²⁵. This testing method involves unnotched and notched samples sharing identical geometry: the sample width L and the initial crack length c are both far greater than the sample height H . This configuration ensures that the stretch state of incompressible materials like rubber under tension is equivalent to a pure shear state; hence, we conventionally call our samples pure shear specimens since they are long thin strips. The configuration also facilitates the determination of the strain energy density function $W(\lambda)$. Given translational invariance of the stress and strain fields during the crack propagation, the strain energy density function $W(\lambda)$ at the bulk material point far ahead of the crack tip in the notched sample is experimentally determined using the stress-stretch curves from unnotched samples. It should be noted that this approach is applicable to compressible materials.

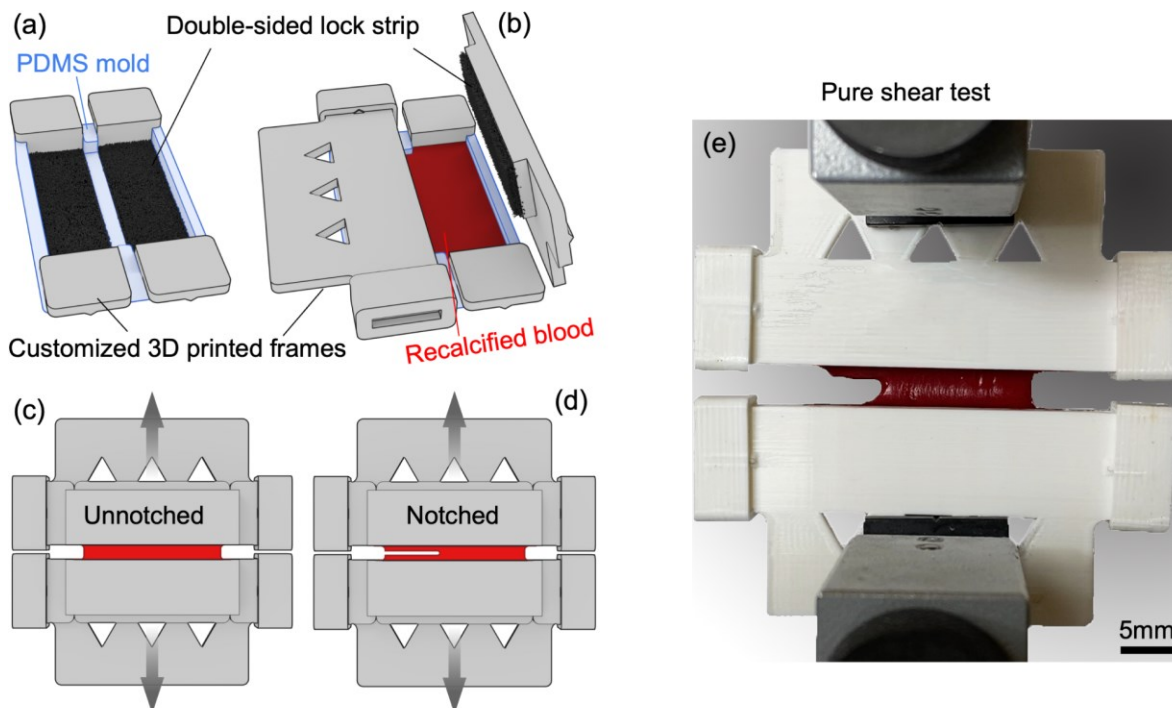


Figure 2-1 3D-printed pure-shear specimen frames. (a) Customized 3D-printed frames (components) are assembled in a PDMS mold. (b) Blood or plasma is recalcified and added into the frames and mold. (c) Unnotched specimen. (d) Notched specimen. (e) Photo of a pure-shear specimen on Instron testing machine.

To apply uniform load and secure the safe handling of the extremely fragile plasma clot, we fabricated and used a customized silicone mold to form a long and thin unnotched clot sample and placed 3D-printed components to lock on both sides of the clot specimen (40 mm × 4 mm × 3 mm for clot materials in between the 3D-printed components. See Fig. 2-1). For notched specimens, we made a 10 mm pre-notch by placing a polyester film (0.1 mm thin) into the silicone mold before clotting. The silicone mold and the attached polyester film were removed from the plasma specimens before mechanical testing. To initiate clotting, a recalcification solution was added to the plasma at a volume ratio of 1:9 (recalcification solution to plasma). Once clotting was initiated, the plasma was immediately transferred into the assembled mold using a pipette. The samples are then placed in an incubator at 37 °C for 60 minutes, while being stored within sealed moisturizing bags to prevent dehydration. These samples were stored at 4 °C overnight and tested on the second day.

2.2 Mechanical characterization

2.2.1 Rheological measurement

Rheology tests were performed to map the clotting kinetics of WB or PPP. Blood samples were recalcified as described above and deposited immediately onto the stage of a rheometer (Discovery HR-2, TA Instruments). The gap between the plate and the stage was set at 500 μm for a 160-μL blood sample. The temperature was set at 37 °C to mimic the physiological temperature. With the application of an oscillatory strain (1 %, 1 Hz) using a 20-mm parallel steel plate, the clotting kinetics was characterized by monitoring the storage (G') and loss (G'') moduli, which correspond to the elastic and viscous properties of the tested materials, respectively. The storage and loss moduli were recorded over time up to 3600 seconds. Coagulation time corresponded to the time when the storage modulus reached 90% of the value at 2000 seconds. At least 4 replicates per condition were tested.

2.2.2 Modified lap-shear tests

Modified lap shear tests were performed to measure the fracture energy of the blood clots. This method has been widely applied to characterize hydrogels and adhesives^{149,150}. Different from the conventional lap-shear tests, polyester films (100-μm thickness) were added as a rigid backing to constrain the axial tension of the specimen. The backing was glued to a collagen casing, yielding

a tissue-mimicking surface and producing appreciable adhesion with clots through the mechanisms of fibrin-collagen and platelet-collagen binding¹⁵⁰⁻¹⁵³. Such surfaces can adhere to the blood clots¹⁵⁴, transmit the loading and guarantee cohesive fracture, instead of adhesive fracture. The recalcified blood (length 35 mm, width 15 mm, and thickness 0.1 mm) was placed between two collagen-coated backings, where a polyester film of 100- μ m thickness was inserted to define the thickness of the specimen. An incision of 1-mm length was introduced as a pre-crack at the edge of the samples.

The specimens were loaded vertically at a displacement rate of 3 mm/min using the Instron machine (Instron 5966; 10-N load cell). Following an established protocol¹⁴⁹, the fracture energy, defined as the reduction of the potential energy associated with crack propagating per unit area, was calculated as the total work (*i.e.*, the area under the force-displacement curve) divided by the area of the crack surface after rupture, $\Gamma = W_t/A$. The fracture surface was the area of the debonding surface of the sample, which was the product of the sample width and the total crack length. The total crack length was the sample length subtracted by the initial crack length measured using a digital calliper with an accuracy of 0.02 mm. The shear strength was also calculated as the maximum force in the force-displacement curve divided by the initial area of the sample. The fracture surfaces were examined post-testing to confirm cohesive fracture. At least 4 replicates per condition were tested.

2.2.3 Modified double cantilever beam tests

Modified double cantilever beam tests were also performed to measure the fracture energy following a prior work¹⁵⁵. Acrylic sheets were laser-cut and glued to produce rigid cantilever beams (60 mm x 10 mm x 6 mm) and coated with collagen casing to mimic tissue surfaces. The blood sample was recalcified and immediately placed between two collagen-coated acrylic sheets; its geometry (40 mm length, 10 mm width, and 0.1 mm thickness) was defined using the polyester film. The specimens were then incubated as described above and tested with the Instron machine. The displacement-controlled loading rate was 3 mm/min. Fracture energy was calculated as the total work (area under the force-displacement curve) divided by the area of the crack surface after rupture, *i.e.*, $\Gamma = W_t/A$. At least 4 replicates per condition were tested.

2.2.4 Monotonic pure shear tests

The monotonic loading tests were performed to measure the overall fracture toughness Γ as function of the loading rate. The dimensions of the whole specimens with 3D-printed components were $80 \text{ mm} \times 80 \text{ mm} \times 13 \text{ mm}$. Both unnotched specimens and notched specimens with an edge notch of 10 mm were stretched uniformly perpendicular to the top and bottom boundaries of the specimens using an Instron machine at different displacement rates (0.04 mm/s , 0.4 mm/s , and 4 mm/s) or at single displacement rate according to the purposes of study (Fig. 2-2b). The crack propagation rates under variable loading rates were measured using the recorded high-speed videos calibrated by a ruler attached to the gripper. Since the tests were completed within 2-3 minutes, no Biobath chamber was used in these tests. For pure-shear specimens, the energy release rate takes the form $G=HW(\lambda)$, where H is the height of the undeformed specimen, and $W(\lambda)$ is the strain energy density in bulk material far ahead of the crack tip and is measured by calculating the area under the stress-strain curve up to the applied stretch $\lambda=1+S/H$, where S is the applied displacement, from pure shear tests on unnotched samples. The tests with notched specimens informed the critical stretch λ_c , when the pre-crack propagates. With the measured quantities, the overall fracture toughness Γ was calculated as $HW(\lambda_c)^{125}$.

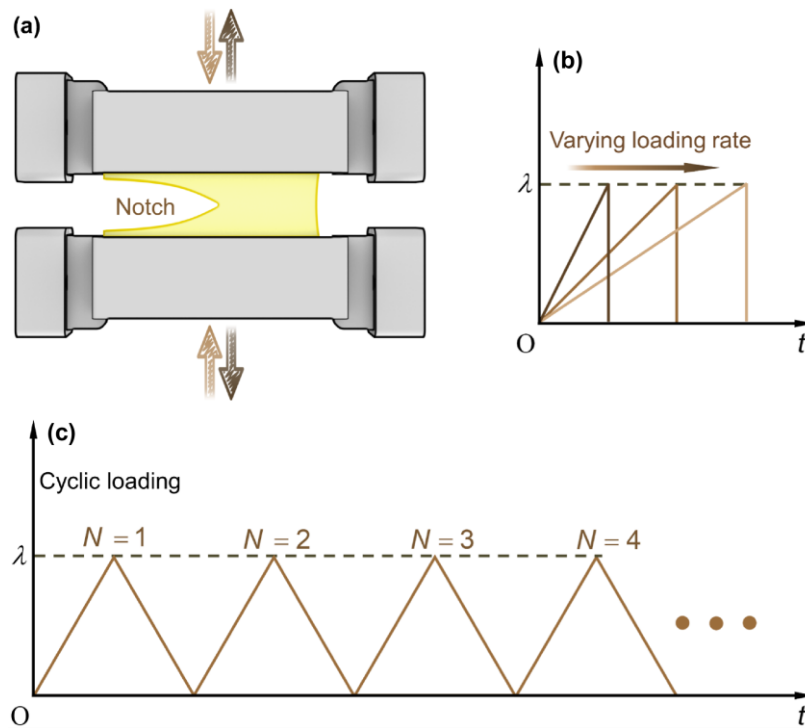


Figure 2-2 Pure shear tests. (a) Pure shear fracture test specimen used to characterize fibrin clots under cyclic and monotonic load. (b) Schematic for monotonic load profile with various loading rates. (c) Schematic for cyclic loading profile with a pre-set stretch.

2.2.5 Cyclic load tests

The fatigue cyclic uniaxial load was applied on the both unnotched and notched pure shear specimens with a pre-crack using a displacement-controlled universal testing machine (Instron Model 5965) integrated with a Biobath chamber (Fig. 2-3a). The entire test setup was immersed in a phosphate-buffered saline solution within the Biobath chamber throughout the tests to minimize dehydration (Fig. 2-3). The specimens were cyclically stretched between 0 and a prescribed stretch λ up to 10,000 cycles, while the displacement rate was fixed at 0.4 mm/s (Fig. 2-2c). The prescribed stretches correspond to the applied strain ($\varepsilon = \lambda - 1$): 0.38, 0.41, 0.44, 0.47 and 0.50. Each fatigue test conducted in this work took more than 24 hours for the loading-unloading cycles (up to 10,000 cycles) within Biobath. The range of applied strains was determined based on the critical failure strain obtained from the monotonic fracture test. The Instron machine recorded both forces and displacements throughout the test for both unnotched and notched specimens, meanwhile a digital camera recorded the crack extension (Δa) of notched specimens only, which was calibrated by a ruler attached to the gripper.

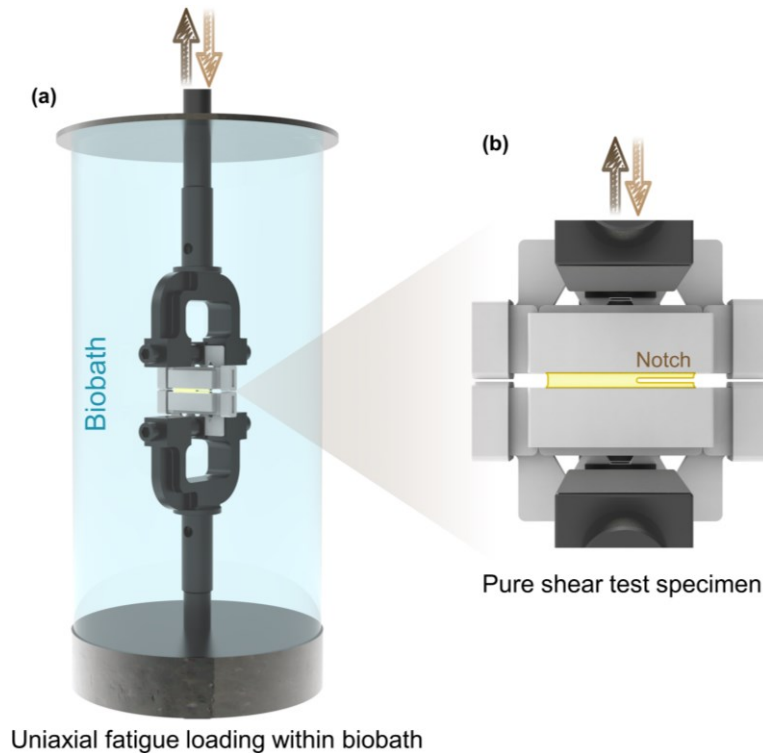


Figure 2-3 Cyclic fatigue test setup. (a) Schematic of uniaxial fatigue loading with biobath. (b) Schematic of pure shear test specimen with 3D-printed components.

2.2.6 90° peeling adhesion tests

We characterized the interfacial fracture energy of blood clots on various substrates using 90° peeling tests¹⁵⁶⁻¹⁵⁸. Rectangular substrates (30 mm x 10 mm x 2 mm) – including bovine muscle, bovine liver, porcine skin, bovine aorta, and gauze – were affixed to a rigid polyethylene terephthalate backing. A silicone mold (Ecoflex 30) with a rectangular chamber (30 mm x 10 mm x 4 mm) was positioned atop the PET plate to enclose the substrate. A 5 mm scotch tape (as a hydrophobic spacer) was applied at the initial part of the substrate to introduce an interfacial crack. Once clotting was started, the blood was pipetted into the chamber, and a flexible backing (polypropylene fabric; 100 mm x 10 mm) was laid on the liquid blood surface with sufficient blood exudation to enhance bonding between the backing and the clot. Samples were incubated at 37°C for 60 min in humidity bags. Post-incubation, samples were stored at 4°C overnight and tested the following day. We mounted samples on our Instron machine (model 5965; 10 N loading cell) with a 90° peeling setup, and applied vertical displacement on backings at 0.02 mm/s (0.01 s⁻¹), 0.2 mm/s (0.1 s⁻¹) and 2 mm/s (1 s⁻¹; the limit of the testing machine without the inertial effects) loading rates. Strain rates were calculated by dividing the loading rate by the thickness of specimens which was pre-defined by the height of the space between backing and substrate (2 mm). The interfacial fracture energy of the specimen was calculated by¹⁵⁹:

$$\Gamma_{adhesion} = P_s / b \quad (2-1)$$

where P_s is the average peeling force at the plateau where the peeling force reaches a steady state, and b is the width of peeling specimens.

2.3 Image analysis

2.3.1 Scanning electron microscopy

We employed scanning electron microscopy (SEM) to identify structural changes from variations in RBC and PLT content as well as detect interfacial fracture type. The microstructure of blood clots was captured using a field emission SEM (F450, FEI). Prior to SEM imaging, all samples underwent sequential ethanol dehydration and hexamethyldisilazane (drying to conserve their original microstructure)¹⁶⁰. The dehydrated samples were then coated with 4 nm Pt using a high-resolution sputter coater (ACE600, Leica) to enhance surface conductivity.

2.3.2 Confocal imaging

The microstructure of fibrin clots was characterized using confocal imaging and further analyzed with a semi-empirical model. A solution of fibrinogen conjugated with Alexa Fluor 488 (Thermo Fisher, Invitrogen™, Molecular Probes® F-13191) was prepared following the manufacturer's instruction and used as fluorescent probes. This solution was added to plasma samples for the final volume fraction of 2% v/v, clotted and stored using the procedure above. The samples were imaged under an LSM 800 Confocal Microscope linked with a Zeiss Axio Observer Z.1 fully motorized inverted microscopy (Pharmacology & Therapeutics, McGill University) to obtain raw confocal Z-stack images. These images were collected through 488 nm excitation at 40x 1.30 NA oil immersion plan apo-chromatic lens with 1610 x 1610 pixels. The optical resolution was 0.099 μ m in the xy plane and 0.1 μ m on the z-axis.

Additionally, we further assessed the microstructural changes of notched fibrin clot specimens before and after cyclic fatigue loading to explore the micro-mechanisms during fatigue crack growth within all over the pure-shear samples (i.e., crack tip and far from crack tip). Three unloaded notched samples and three notched samples after 10,000 cycles of fatigue cyclic loading were carefully transferred onto thin glass slides with 3D-printed components fixed to maintain the tension state of fibrin network while being imaged under the same equipment with the same setting mentioned above.

2.3.3 Data-based 3D image reconstruction and morphometric quantification

We reconstructed 3D confocal images using an open-source Python package Qiber3D to characterize the fibrin network architecture. This method can be operated without manual interactions with the software, thus compatible with large datasets. It is advantageous over other methods such as 2D maximum-intensity projections. Raw 3D confocal image stacks are loaded for resampling using the Gaussian filter. After binarization and 3D reconstruction, the fiber segments were defined by fiber between two neighboring branch points. A fibrous network from one confocal image may consist of several collections of connected fiber segments. We conducted morphometric quantification¹⁶¹ and generated a database of structural parameters, including the spatial data of all the fiber segments, and their average diameters, lengths, and fiber directions. To extract the parameters from the database, we then developed a Python-based data processing script (accessible via GitHub¹⁶²). Extensible 3D graphics were also generated based on the reconstruction

results, which were rendered using Blender to create 3D model images of fibrin networks.

In the fibrin network, several short fibers may laterally aggregate and crosslink, forming small clusters of fibers. The algorithm may identify the clusters as single fiber segments, which leads to an overestimation of average fiber segment diameters. Therefore, we adopted the interquartile range (IQR) method to identify and remove outliers statically. IQR value was calculated by subtracting the first quartile Q_1 from the third quartile Q_3 . The lower limit was defined as Q_1 minus $1.5 \cdot \text{IQR}$, while the upper limit was obtained by Q_3 plus $1.5 \cdot \text{IQR}$. Data points beyond the upper and lower limits range are considered outliers and removed from the dataset.

2.4 Finite element modeling

To model blood clot mechanical response under unconfined compression and pure shear tests, a special compressible Yeoh's strain energy function (W) along with a rate-independent Mullin's damage (η) was employed^{163,164}:

$$W = \eta W_{\text{dev}} + W_{\text{vol}} + \Phi(\eta) = \eta \sum_{i=1}^3 C_i (\bar{I}_1 - 3)^i + \frac{1}{D} (J - 1)^2 + \Phi(\eta) \quad (2-2)$$

in which \bar{I}_1 and J denote the first deviatoric strain invariant and volumetric change. C_i and D represent hyperelastic material constants^{165,166}, and η was determined from the following evolution equation¹⁶³:

$$\eta = 1 - \frac{1}{r} \operatorname{erf} \left(\frac{W_{\text{dev}}^{\max} - W_{\text{dev}}}{m + \beta W_{\text{dev}}} \right) \quad (2-3)$$

where r , β and m are material constants with erf as the error function, and W_{dev}^{\max} is the maximum deviatoric strain energy function through the loading history.

The cohesive zone model – with a bilinear triangular function – was employed to represent both the midsection of the pure shear samples along the crack plane, as well as the interfacial bonding between the blood clot and tissue^{158,167-169}. The intrinsic work of adhesion ($\Gamma_0 = \frac{1}{2} S \delta$) was defined by utilizing the interfacial strength (S) and the maximum separation distance (δ). For peeling simulations, to ensure convergence, we employed a 4-node linear plane strain quadrilateral element with hourglass control, and modeled the clot-tissue interface by a 4-node two-dimensional cohesive element. For pure shear test simulations, we used 8-node linear brick elements, and

defined cohesive elements throughout the crack plane in the bulk material.

2.5 Statistical analysis

All analyses were conducted using Originlab Pro 2018. One-way analysis of variance (ANOVA) was used to compare differences between groups of experimental data. Both F- and P-values were calculated. All data are represented as a means \pm 0.5 SD unless otherwise noted.

Chapter 3 Fracture toughness of blood clot

3.1 Preface

Blood clots are naturally derived bioadhesives that adhere to tissues, plug vascular damage and stop bleeding. Their function of hemostasis hinges on their resistance against rupture (toughness). Despite the relevance, fracture mechanics of blood clots remain largely unexplored, particularly the toughness and critical length scales governing clot fracture have not been reported. In this chapter, we study the fracture behavior of human whole blood clots and platelet-poor plasma clots. The fracture energy of whole blood clots and platelet-poor plasma clots are determined using modified lap-shear method. We find that the measured toughness is independent of the specimen geometry and loading conditions. These results reveal an important contribution of blood cells to the clot fracture, as well as the dissipative length scale and nonlinear elastic length scale governing clot fracture. This study will motivate the investigation on blood clot fracture and inspire the development of clot-mimicking bioadhesives.

3.2 Introduction

Blood clots are a class of naturally derived bioadhesives that the human body leverages to stop bleeding and heal wounds. They are essentially hydrogels composed of fibrin and other proteins, infiltrated with platelets, red blood cells (RBCs), and other cells⁶⁴. They form at wounded blood vessels to stop bleeding, a process known as *hemostasis* (Fig. 3-1a). Blood clots plug and seal the blood vessel defects, where they are exposed to shear stress, tension, and blood pressure from the local tissue environment (Fig. 3-1b)⁶⁴. Pathological blood clots can appear within intact blood vessels, causing *thrombosis*¹⁷⁰. In both circumstances, the fracture of blood clots is detrimental and even fatal. The fracture of the blood clots at wound sites results in rebleeding (Fig. 3-1d)⁶⁶. The fracture of an intravascular blood clot yields small pieces of thrombi that may disturb blood flow through the circulatory system and cause pulmonary embolism, heart attack, or stroke¹⁷¹. Thrombotic complications occur in many diseases; for instance, 31% of COVID-19 patients in intensive care units have venous and arterial thromboembolism¹⁷². Understanding the fracture mechanics of blood clots may identify new mechanisms for controlling thrombosis and hemostasis. It can also provide insights to develop new bioadhesives recapitulating blood clots for tissue repair

and regeneration.

Despite the likely importance of fracture mechanics of blood clots in human health, it is not well understood compared to the fracture of hydrogels and many other soft materials^{125,173,174}. In previous works, mechanical properties of blood clots such as stiffness, strength, and nonlinearity including viscoelasticity of blood clots^{18,64,115} are well characterized. Such properties, however, characterize blood clots that are intact and without cracks. Few works to date are reported on the toughness (*i.e.*, fracture energy required to extend a unit area of a crack) of blood clots. Recently, the toughness of fibrin clots derived from human blood plasma was determined using the single-edge notched tension method and compared with finite element simulation⁷¹. Those clots are essentially fibrin hydrogels, containing no blood cells that present at a large volume ratio in blood clots. In contrast, the blood clots formed during bleeding are composed of fibrin and blood cells such as red blood cells and platelets. The toughness of whole blood clots was not investigated. In addition to providing biological functions, the red blood cells and platelets influence the mechanical properties of blood clots such as stiffness and viscoelasticity^{18,21,27,175}. Given the difference between fibrin clots and whole blood clots and the clinical relevance of whole blood clots, it is critical to investigate the whole blood clots and the mechanisms underlying clot fracture.

As blood clots are fragile, wet, and soft, characterizing the fracture properties of blood clots is non-trivial. Because blood clots are soft and deformable, compared to engineered materials such as metals and plastics, this excludes using conventional fracture testing methods, such as three-point bending methods that are only applicable to rigid materials¹⁷⁶. Furthermore, because blood clots have low tensile strength compared to other biological materials such as blood vessels⁷¹, they are vulnerable to damage and even rupture during handling, transport, and mounting. It is problematic for many testing methods for fracture toughness, such as pure shear tests that have been extensively used to characterize the toughness of soft materials¹²⁵. Also, the wet nature of blood clots makes them difficult to grip or handle. Lastly, blood clots are delicate, dynamic biological materials. There is a limited operational time window for specimen preparation and testing, considering the biochemical components, clotting, and contraction kinetics^{5,177-180}.

In this work, we will apply fracture mechanics approaches to measure the fracture energy of human blood clots. We ask the following questions: what is the toughness of human blood clots and how does it depend on the composition and loading? To address them, we will first synthesize and

characterize human whole blood clots and platelet-poor plasma clots using rheology. We will then combine modified lap-shear and double-cantilever beam methods to measure the toughness of the blood clots. To mimic aspects of tissue surfaces, we will employ rigid substrates coated with collagen casing, which can adhere to and support the blood clots for mechanical testing. The sensitivity of the measurements to the sample size and the loading condition will be examined. We will also estimate, for the first time, the dissipative and nonlinear elastic length scales, defining the crack tip field of blood clots. These findings will advance the understanding and modeling of blood clot rupture, which is an important mechanism in thrombosis and bleeding. The gained insights could offer inspiration and strategies for the development of clot-mimicking bioadhesives.

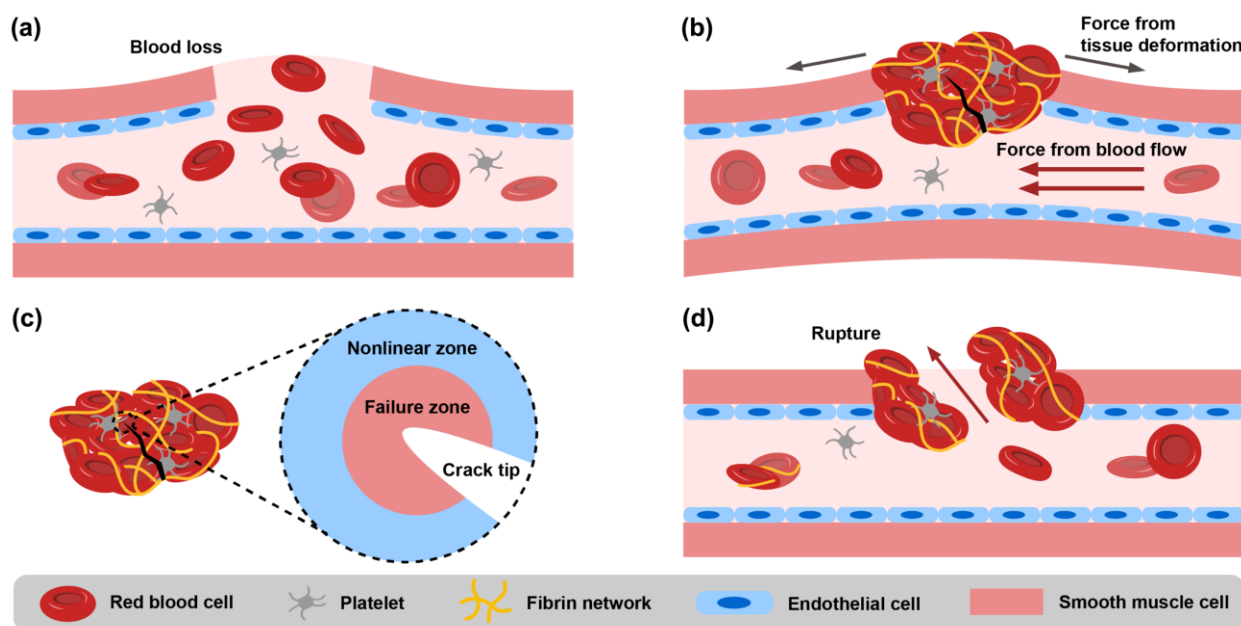


Figure 3-1 Schematics of clot formation and failure at a wound of a blood vessel. (a) Blood loss at a wound of a blood vessel. (b) A blood clot, formed to seal the defect, experiencing mechanical loading from the blood flow and the surrounding tissue, which might result in clot rupture. (c) Blood clots may rupture, causing rebleeding. (d) Schematic of the crack tip zone.

3.3 Results and discussion

3.3.1 Rheological behaviors of blood clots

We first characterized the blood clots with rheological tests to determine the shear modulus. Both WB and PPP were tested and compared for the role of blood cells in clot fracture. The blood clots were initiated with the mixture of recalcification solution and tissue factor (Fig. 3-2a). The addition

of Ca^{2+} initiated the coagulation cascade and produced thrombin, while the tissue factor further amplified the generation of thrombin by an extrinsic pathway of coagulation, converting soluble fibrinogen into an insoluble cross-linked fibrin network¹⁸¹. The kinetics of clot stiffening was mapped with rheological time-sweep tests. Fig. 3-2b shows the storage modulus surpasses the loss modulus quickly.

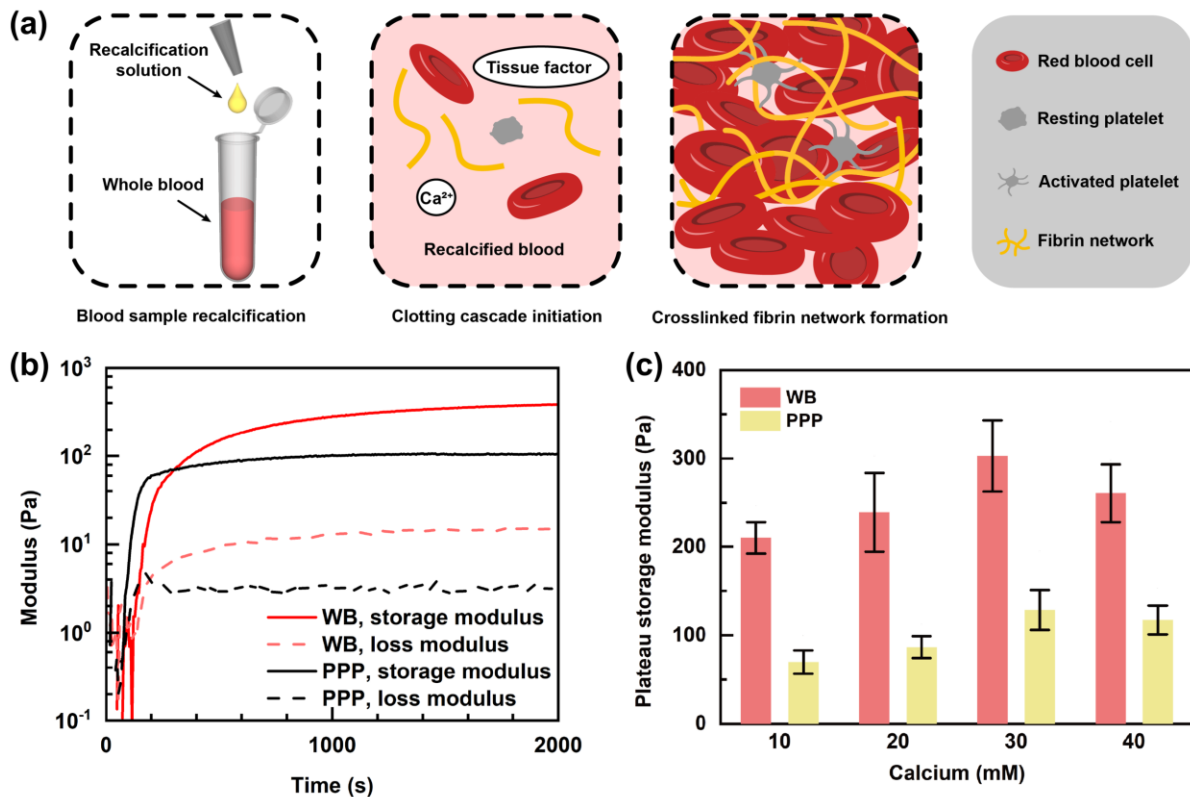


Figure 3-2 Rheological measurements of blood clots. (a) Schematics of blood clot sample preparation. (b) Gelation kinetics of clotting whole blood (WB) and platelet-poor plasma (PPP). (c) Long-term storage modulus of whole blood clots and platelet-poor plasma clots as a function of calcium concentrations, determined at 2000s. Sample size N=4; error bars, mean \pm 0.5 SD.

Blood clots stiffened with the presence of blood cells such as RBCs and platelets due to their influence on the fibrin network structure, complex elasticity of RBCs, and clot contraction due to platelets^{18,182}. To visualize the microstructure, we used SEM to image the microscopic morphology of the clots. The PPP clot is a typical cross-linked fibrin network, while the WB clot is a tight aggregation of RBCs connected by the fibrin network and platelets. As the RBCs take up to 50% of the total blood volume, they affect the structure and mechanics of fibrin fibers and the resulting

network²¹. Fiber diameter increases upon RBC incorporation and RBCs also influence the viscoelastic properties of the clot¹⁸. The incorporation of platelets leads to clot contraction and clot stiffening²⁷.

As calcium ions are reported to influence blood clot stiffness^{82,183}, we also measured the clot modulus with varying calcium concentrations. Both WB and PPP clots stiffen slightly as the calcium concentration increases from 10 mM to 30 mM (Fig. 3-2c), as calcium is responsible for the activation of coagulation factors. The effect saturates at high calcium concentrations (30 mM and 40 mM). A slight decrease is observed at 40 mM, which may be because excessive calcium could inhibit blood coagulation¹⁸⁴ and deserves further investigation. A similar trend was also observed in the change of coagulation time with increasing calcium concentration. As a result, 30 mM final calcium concentration was used in the following study on both human WB and human PPP clots. The shear modulus of human WB clots is 302.92 ± 80.42 Pa, and that of human PPP is 128.45 ± 45.18 Pa. The measurements agree well with the literature^{82,185,186}, validating the blood clot formation. They will be used later for calculating the critical length scales underlying clot fracture.

3.3.2 Lap-shear tests of blood clots

We next quantified the toughness of blood clots as fracture energy measured with modified lap shear tests. The testing method was chosen due to its applicability to soft fragile samples that might deform substantially due to gravity alone. Also, the test has been widely applied for characterizing blood clots, hydrogels, and other biomaterials^{149,150,154}. In this study, we used collagen-coated acrylic sheets, which adhere to and exert loading to blood clots. To examine the fracture behavior, we introduced a pre-crack in the middle of the sample and adjusted the alignment of the specimen and the loading direction to ensure the crack would propagate through the clot matrix (Fig. 3-3a). It was observed that the rupture started when the measured force got maximum. By examining the fracture surfaces of the specimen post-testing, we found sample residues on both sides of the backing, confirming cohesive rupture (Fig. 3-3b). From the force-displacement curves of the WB and PPP clot specimens, we determined the fracture energy of WB and PPP blood clots at 5.90 ± 1.18 J/m² and 0.96 ± 0.90 J/m², respectively (Fig. 3-3b, c). The shear strain rate was fixed at 20/min in this study. It should be noted that the loading rate is expected to play a role as the blood clots are highly viscoelastic, calling for further investigation⁹¹.

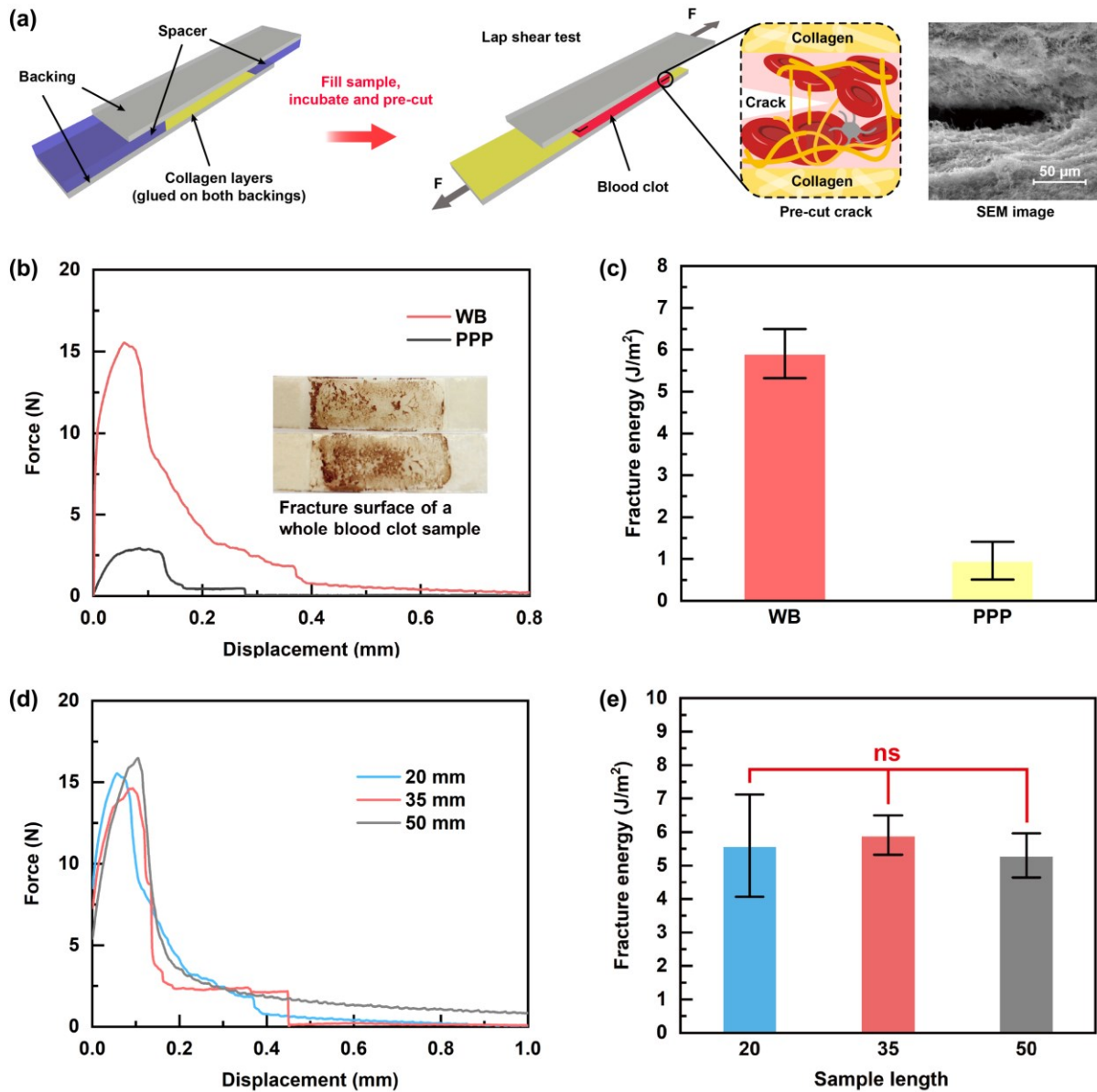


Figure 3-3 Fracture energy of blood clots measured by lap shear test were size independent. (a) Schematics of lap shear test setup. The SEM image on the right shows the crack front of human whole blood clot. (b) Force-displacement curves of lap shear tests for whole blood (WB) clots and platelet-poor plasma (PPP) clots; the inset shows the fracture surface of the WB specimen. (c) Fracture energy results of whole blood clots and platelet-poor plasma clots. Sample size N=4. (d) Representative force-displacement curves of whole blood clot lap shear tests of different sample lengths. (e) Fracture energy of whole blood clots obtained from lap shear tests of different sample lengths. Sample size N=4; error bars, mean \pm 0.5SD; ns: no significance, one-way analysis of variance (ANOVA), Tukey test.

The comparison between WB and PPP clots reveals the substantial contribution of blood cells to the fracture toughness of blood clots. RBCs and platelets influence the fibrin network, clot

formation, maturation, stability, embolization, and fibrinolysis^{18,21}. The toughening effect contributed by blood cells is intriguing and likely relates to viscoelastic and dissipative properties of blood cells¹⁸⁷, and their interactions with the fibrin network, which alter the fibrin network structure, individual fiber characteristics, and overall clot viscoelasticity¹⁸. Based on the previous study in literature and our findings, it is believed that RBCs could contribute to the energy-dissipative mechanism of deformed blood clots, supported by the increased fracture toughness and by the increased viscous contribution of complex modulus¹⁸.

3.3.3 Fracture energy measurements with varying loading

As fracture energy is expected to be invariant against the geometric factor and testing methods¹⁸⁸, we next measured toughness after varying the geometric and loading conditions. First, we performed the lap-shear tests with varying lengths of WB clot samples (20-50 mm). The force-displacement curves and the measured toughness were compared (Fig. 3-3d, e). An ANOVA was conducted and identified no significant difference with $F=0.0830$ and $P=0.9212$.

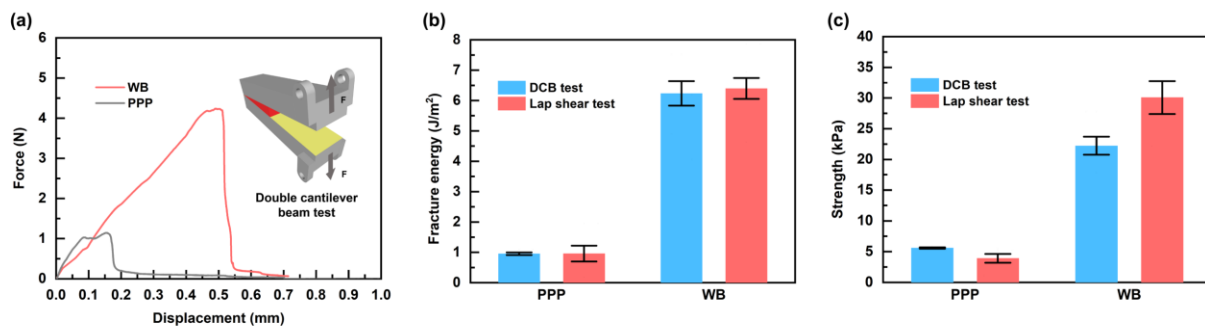


Figure 3-4 Lap shear test results were compared with double cantilever beam tests, and loading condition independence was found. (a) Schematics of double cantilever beam (DCB) testing, and representative force-displacement curves of DCB tests on WB and PPP clots. (b) Fracture energy of WB and PPP clots obtained from DCB tests and lap shear tests, respectively. (c) Strength of WB and PPP clots measured by DCB tests and lap shear tests, respectively. Strength is defined as the maximum force divided by the initial area of the sample section surface. Sample size $N=4$; error bars, mean \pm 0.5 SD.

We further changed the lap-shear method with a modified DCB method to test human PPP clots (Fig. 3-4a). In the modified DCB tests, collagen-coated acrylic sheets were used as rigid cantilever beams, which sandwiched and loaded the clot sample. For the PPP clot, the fracture energy measured by modified DCB tests and by lap shear tests was alike. A similar agreement was found between the fracture energy of the WB clot measured with the two different tests (Fig. 3-4b). In

comparison, the strength measured with DCB tests differed from that of lap-shear tests for both PPP and WB clots (Fig. 3-4c). This result demonstrated that fracture energy can be used to quantify the fracture toughness of blood clots, which was independent of sample length and loading conditions. Further tests with varying other testing conditions are needed to validate whether the measured quantity is a material property.

Chapter 4 Fatigue fracture and rate-dependent fracture of blood clot

4.1 Preface

Fibrin clot is a vital class of fibrous materials, governing the mechanical response blood clots. Fracture behavior of fibrin clots under complex physiological load is relevant for hemostasis and thrombosis. But how they fracture under cyclic and variable rate loading has not been reported. Here we conduct cyclic fatigue and monotonic variable rate loading tests on fibrin clots to characterize their fracture properties in terms of fatigue threshold and rate-dependent fracture toughness. We demonstrate that the fracture behavior of fibrin clots is sensitive to the amplitude of cyclic load and the loading rate. The cyclic fatigue tests show the fatigue threshold of fibrin clots at 1.66 J/m^2 , compared to the overall fracture toughness 15.8 J/m^2 . Furthermore, we rationalize the fatigue threshold using a semi-empirical model parameterized by 3D morphometric quantification to account for the hierarchical molecular structure of fibrin fibers. The variable loading tests reveal rate dependence of the overall fracture toughness of fibrin clots. Our analysis with a viscoelastic fracture model suggests the viscoelastic origin of the rate-dependent fracture toughness. The toughening mechanism of fibrin clots is further compared with biological tissues and hydrogels. This study advances the understanding and modeling of fatigue and fracture of blood clots and would motivate further investigation on the mechanics of fibrous materials.

4.2 Introduction

Fibrous materials are an important class of materials constituted by nature-derived and/or synthetic fibers¹⁸⁹. These materials consist of fibers with diameters typically measured in micrometers¹⁹⁰. They differ from polymer-chain based materials, where the mechanical behavior is mainly governed by entropic elasticity of the polymer chains. Fibrin clot is an exemplary fibrous material that is formed with fibrin fibers and responsible for the structural integrity and mechanical stability of blood clots (Fig. 4-1a,b,c)^{93,128,191}.

Blood clots are of clinical significance in both hemostasis (halting bleeding in injury sites) and thrombosis (clots formed in blood vessels and block the blood flow). As the main load-bearing

component of blood clot, the fibrin clot experiences complex physiological loads from the surrounding tissue environments and the blood flow (Fig. 4-1a)^{54,192,193}. For instance, there is a vast blood flow rise in humans from 2.9 L/min at rest to 7.2 L/min, during exercise through cyclic heartbeat ranging from 73 to 110 beats/min¹⁹⁴. Also, contracting muscles result in dynamic cyclic loads on the clots at the wound site. The fracture of fibrin clots could result in complications such as rebleeding, hemorrhage, ischemic stroke, arterial and venous thrombosis, and thromboembolism (an aggregate of blood clots moves in the blood flow and dams other vessels) intensified by other diseases like COVID-19^{195,196}. Clinically, understanding the underlying fracture mechanisms can inform deeper insight into blood clot failure, embolism, and integrity in both hemostasis and thrombosis^{91,197}.

To study the fracture of a material, the fracture mechanics principle is focused on the balance between the energy release rate G and the fracture toughness Γ . The former defines the driving force for extending a crack by the applied loading, and the latter characterizes the material's resistance against crack progradation and fracture¹²⁵. When G matches or exceeds Γ , the crack propagates and fracture precedes. This principle allows one to measure fracture toughness. Common fracture test specimens for hydrogel include the pure shear test¹⁴⁸, the single edge crack test¹⁴⁸, the simple extension test¹⁹⁸, and the tearing test¹⁹⁹. These configurations ease measuring the critical energy release rate G_c during crack propagation since stress and strain fields for steady crack propagation are independent of crack length¹²⁵. The fracture toughness Γ can be quantified as the critical energy release rate G_c required for crack growth ($\Gamma=G_c$). The energetic approach is more suitable for soft materials due to challenges in determining the state of stress and deformation fields near the crack tip, particularly for the large-deformation fracture. For fibrin clots and other hydrogels exhibiting nonlinear mechanical response, the measured fracture toughness is often the sum of the intrinsic fracture toughness and the contribution from dissipative processes such as viscoelasticity and poroelasticity. Deciphering each contribution to the overall fracture toughness is important for understanding and predicting the fracture behavior. Achieving this decoupling necessitates a combination of mechanical testing methods such as cyclic fatigue tests and variable rate tests. The cyclic loading could deplete dissipative processes and eventually reveal the minimum energy required to break a layer of polymer chains at the crack tip²⁰⁰. By varying loading rate, one could examine the rate dependency of the overall fracture toughness in order to probe the contribution from rate-dependent processes such as viscoelasticity²⁰⁰. Fatigue threshold models

for soft fibrous materials meanwhile need to yet be established so that the viscoelastic fracture toughness of these material systems can theoretically be assessed. The Lake-Thomas model is one of the few available models that can be extended for fibrous materials²⁰¹.

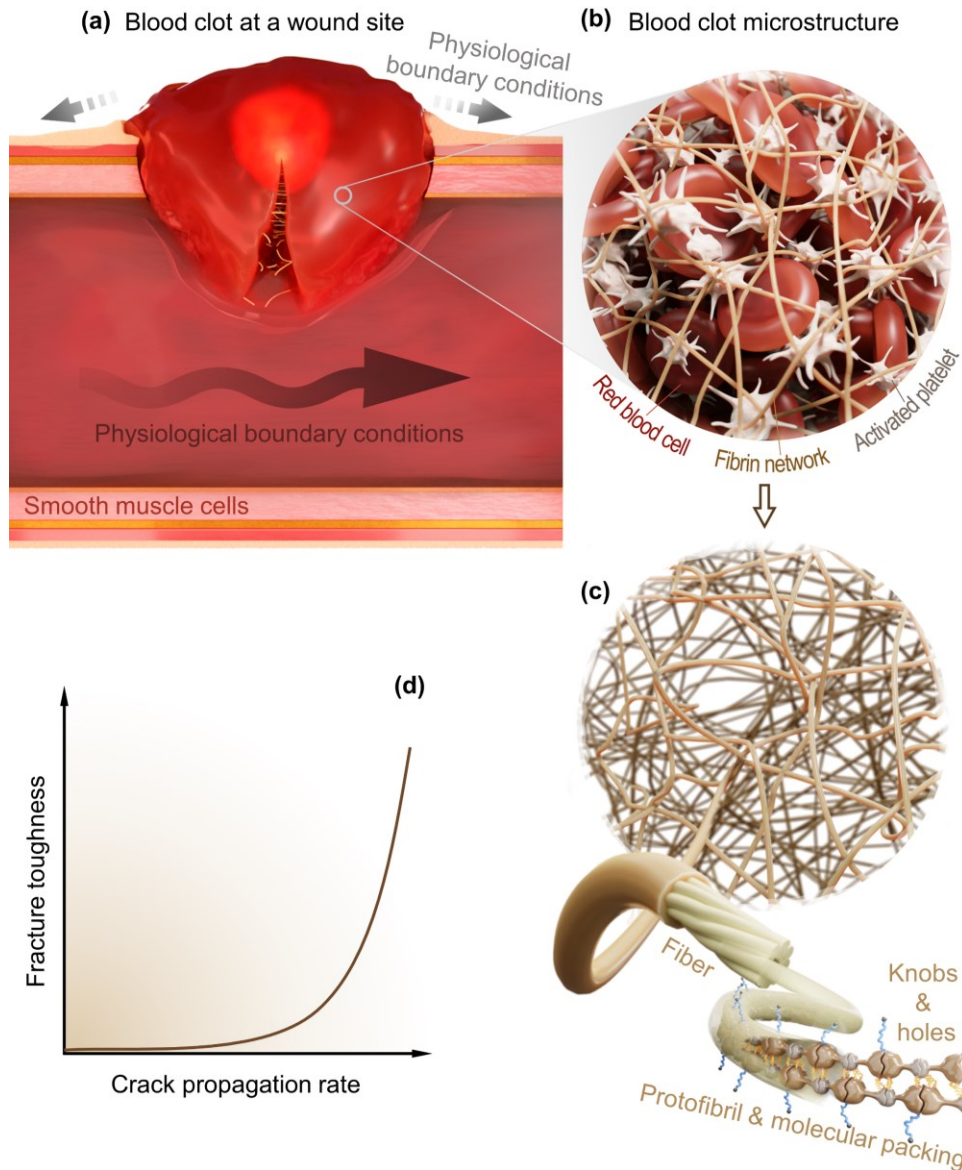


Figure 4-1 Structure and mechanical responses of blood clots under complex loading. (a) Blood clot ruptures under physiological environments and its fracture mechanisms due to its hierarchical microstructure. (b) Blood clot mainly comprises red blood cells, fibrin network, platelets and other substances. (c) Hierarchical molecular structures of fibrin network, fiber, protofibril and molecular packing with knobs and holes interactions. (d) Schematic for the rate-dependent fracture behavior of viscoelastic fibrin clots.

While the physiological load exposed to fibrin clots is difficult to replicate and complex for analysis, it can be characterized by monotonic and cyclic loads^{91,202,203}. Although the fracture

behavior of blood and fibrin clots has been studied recently^{71,91,128,156}, the reported tests primarily center on fixed-rate monotonic loading. The fracture behavior of fibrin clots under varying-rate monotonic and cyclic loading has yet been reported. In addition, the existence and magnitude of fatigue threshold and toughening mechanisms of fibrin clots remain largely unexplored. In a broader context, research on fatigue crack growth and fracture of natural fibrous materials remains much less explored compared to other polymer-chain based materials such as hydrogels²⁰⁴. Given the significant structural and mechanical differences between natural fibrous and other polymer-chain based materials, it is imperative to investigate the fatigue and fracture of fibrin clots under complex load conditions and understand the toughening mechanisms of fibrin clots, featuring other fibrous materials which are known for their highly nonlinear mechanical properties (visco- and poro-elasticity) (Fig. 4-1a,b,c)^{48,111}. Similar mechanisms have been reported for skin²⁰⁵, aorta²⁰⁶, muscle²⁰⁷, single- and double-network hydrogels^{205,206,208}, among others²⁰⁹. Understanding and learning the toughness enhancement of soft biological materials can be a key point for biomimetic and bio-inspired fibrous materials; for example, various hydrogels integrated with different dissipation mechanisms still are fatigue intolerant while they benefit from high monotonic fracture toughness²¹⁰.

In this work, we adopt the fracture mechanics approach to study the fracture of fibrin clots under complex loading. Specifically, we will perform two representative loadings under pure shear configuration: fatigue cyclic loading and monotonic variable rate loading. In the cyclic tests, we examine the energy release rate and the crack growth versus the number of applied cycles. The results further inform the fatigue threshold below which a crack does not extend. In the monotonic tests, we measure the overall fracture toughness as function of loading and crack rate. By doing so, we can decouple the overall fracture toughness into two contributors: intrinsic fracture toughness and viscoelastic dissipation. To rationalize these results, we further characterize the microstructure of fibrin clots, develop and validate semi-empirical models by taking the hierarchical molecular structure of fibrin fibers into account. The estimated fatigue threshold agrees very well with the experimentally measured value and that fitted from the data of monotonic loading tests. Finally, we comparatively highlight the toughening mechanism of fibrin clots compared to other biological materials and hydrogels. This study provides insights into the blood clot behavior in hemostasis and thrombosis and will motivate further investigation of clot fracture under physiological conditions.

4.3 Results and discussion

4.3.1 Confocal image 3D reconstruction and data-based image analysis

We obtained confocal images of the fibrin network in undeformed fibrin clot samples and performed 3D reconstruction and image analysis using a Python script based method modified by myself. A representative confocal image is shown in Figure 4-2a., the corresponding 3D reconstructed fibrin network is shown in Figure 4-2b. All fiber segment diameter and fiber segment length results are extracted and stored as a dataset, and the kernel density estimations of histograms for the average diameter and length of fiber segments of three confocal replicated unloaded samples were plotted in Figure 4-2c, d.

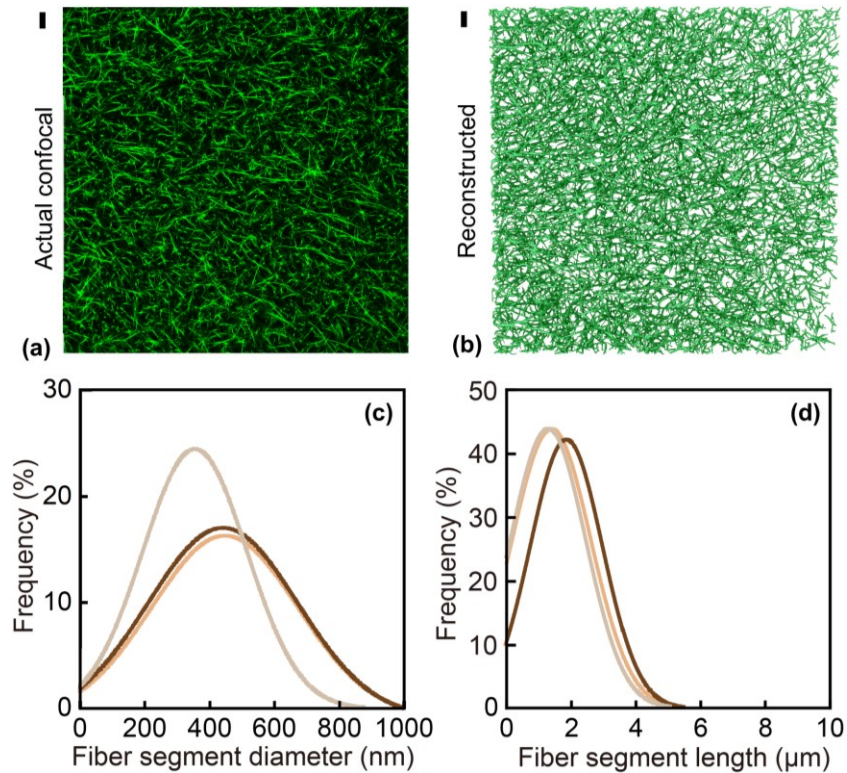


Figure 4-2 Microstructure of fibrin clots. (a) Top view of a typical 3D confocal image of a fibrin clot. (b) Top view of 3D reconstructed the same fibrin network using Qiber3D. Kernel density estimation of fiber segment diameter (c) and fiber segment length (d) of fibrin fibers from morphologic measurements of three replicates.

In the fibrin network, several short fibers may laterally aggregate and crosslink, forming small clusters of fibers. The algorithm may identify the clusters as single fiber segments, which leads to an overestimation of average fiber segment diameters. Therefore, we adopted the interquartile range (IQR) method to identify and remove outliers statically. Data points beyond the upper and

lower limits range are considered outliers and removed from the dataset. All histograms are shown in Figure 4-3.

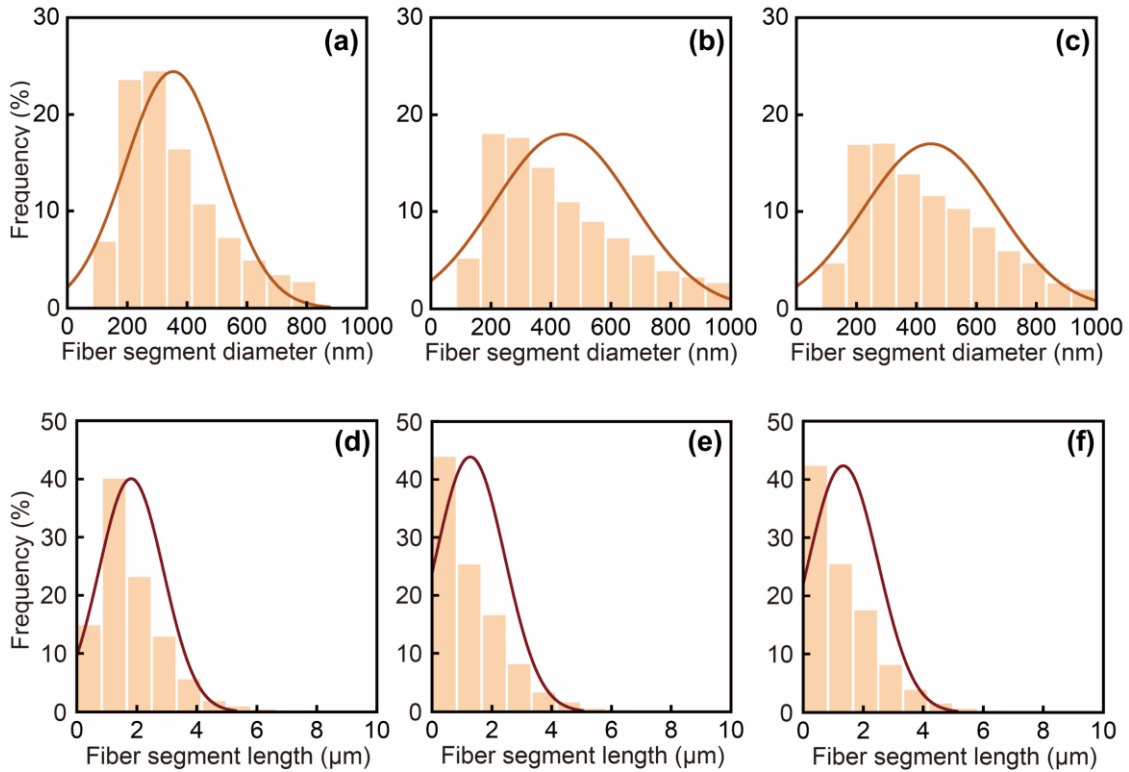


Figure 4-3 Histograms of fiber segment diameter and length. (a, b and c) Histograms of fiber segment diameter of three fibrin clot samples. (d, e and f) Histograms of fiber segment diameter of three fibrin clot samples.

4.3.2 Shakedown under cyclic load

We recorded the force-displacement curve of each pure-shear specimen over cycles and monitored the crack length throughout the test. We calculated the nominal stress (i.e., the applied force divided by the cross-sectional area in the undeformed state) and the stretch $\lambda=1+ S/H$, where S represents the displacement and H represents the initial height of the specimen. Figure 4-4a plots the nominal stress as function of the stretch, showing that the specimen softens and accumulates plastic strains over cycles. The areas of hysteresis loops between the loading and unloading curves are large in the first few cycles, and gradually shrunken as the number of cycles increases. Under the same maximum stretch, the maximum load becomes smaller over cycles. This phenomenon is known as shakedown, reflecting the accumulative damage within the fibrin network. It can be attributed to the breaking of cross-links²¹¹, the irreversible protein unfolding⁵⁴ and the loss of dissipative mechanisms under prolonged cyclic load due to the poro-visco-elastic behaviors of

clots¹¹¹. Another reason is the crack extension under cyclic load, which is characterized and discussed in the next section. Eventually, after thousands of cycles, the stress-stretch curve reaches a steady state (Fig. 4-4a). During the 5,000th to 10,000th cycles, the hysteresis becomes negligible, suggesting that the material behaves nearly elastically. Accordingly, we observed that both the maximum stress and energy release rate in each cycle drop through increasing cycles and reach a plateau (steady state) (Fig. 4-4b, c). In this state, the load is mainly carried by the elastic fibrous network, where the energy dissipative processes that could occur under that maximum stretch have been depleted. It is noted that the corresponding strain rate is 0.1 s^{-1} in fatigue testing which in general is physiologically relevant to the shear rate in blood vessels²¹², and it allows an accurate fatigue testing on the universal testing machine without unnecessary experimental challenges.

The shakedown behavior depends on the applied loading. To alter the applied load, we varied the maximum stretch, or the applied strain ($\varepsilon=\lambda-1$), while fixing the displacement rate (0.4 mm/s). Following the fracture mechanics approach, we quantified the applied load with energy release rate G , which was calculated as $G=HW(\lambda)$, where H is the height of the undeformed specimen, and the strain energy density $W(\lambda)$ is the area under the stress-stretch curve of a specific cycle (Fig. 4-4a). This method has been extensively utilized for hydrogels and elastomers^{67,208,209,213}. Figure 4-4c shows that the energy release rate G varies with the cycle number. Specifically, G first drops sharply in the first few cycles, and then plateaus beyond 2,000 cycles. The results are reminiscent of the cyclic fatigue responses of tough hydrogels and other hydrogels that exhibit energy dissipation^{149,209}.

4.3.3 Crack growth during cyclic load and fatigue threshold calculation

We next examine the crack growth over cycles as function of applied strain. Figure 4d shows the crack grows gradually under relatively large strains, and that the growth rate increases with the applied strains. Under small strains ($\varepsilon = 0.38, 0.41$), we observed no crack extension throughout the test up to 10,000 cycles, indicating fibrin clots are immune against fatigue fracture under that small load. The energy release rate of unnotched samples under fatigue cyclic loading is calculated as $G=HW_f(\lambda)$ ²¹³, where H is the initial height of clot sample, and the strain energy density $W_f(\lambda)$ is the area under the 10,000th cycle curve in which the fibrin clot samples reach a steady state with negligible hysteresis (Fig. 4-4a).

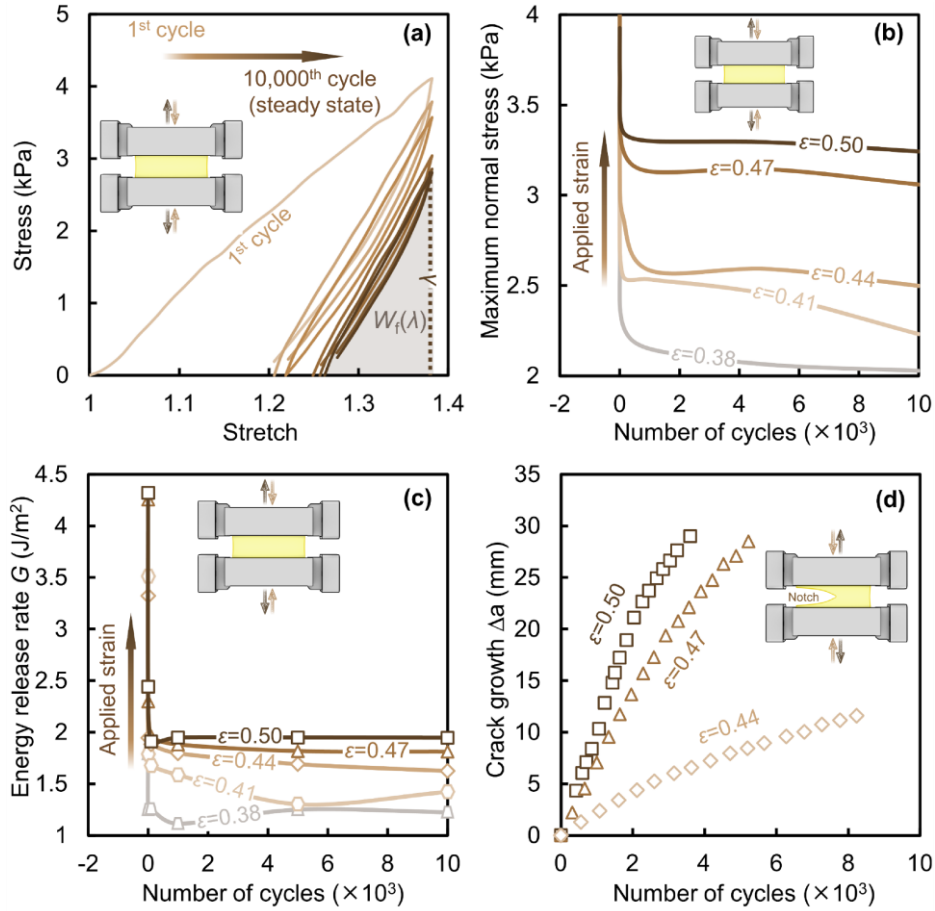


Figure 4-4 Mechanical responses of fibrin clots under cyclic load. (a) Typical stress-stretch curves of unnotched samples under cyclic load; 1st, 10th, 100th, 1000th, and 10000th cycles are shown, where the strain energy density $W_f(\lambda)$ is the area under the 10000th cycle curve in which the fibrin clot samples reach a steady state with negligible hysteresis. (b) Maximum stress of unnotched samples decreases with cycles and approaches a steady state for different applied strains. (c) Energy release rate of unnotched samples as function of the number of cycles for various applied strains. (d) Crack growth of notched samples as function of the number of cycles for various applied strains (for $\epsilon = 0.38$ and 0.41, no crack growth is observed throughout the test).

The fatigue threshold I_0 of the clot is defined as the critical energy release rate, below which the pre-cut crack of the notched specimens under same applied strains remains stationary. We then calculated the crack growth per cycle (da/dN) of notched samples in the steady state for each applied strain. By pairing the crack growth rate of notched samples and the corresponding energy release rate of unnotched samples under the same applied strains in the fatigue cyclic loading, we plot da/dN as function of G (Fig. 4-5a). Linear fitting of this relation gives an intersection at G axis, around 1.66 J/m^2 . This parameter is known as fatigue threshold, below which the cyclic loading cannot extend the crack. The fatigue threshold has been reported for various soft materials,

including hydrogels and elastomers^{204,213,214}. Our results prove the existence of fatigue threshold for fibrin clots, and its value is comparable to those measured with hydrogels⁶⁷. Fig. 4-4d shows the crack extension per cycle da/dN in the steady state. The crack does not propagate under small strain ($\epsilon = 0.38, 0.41$) cycles, but gradually propagates by increasing the strain.

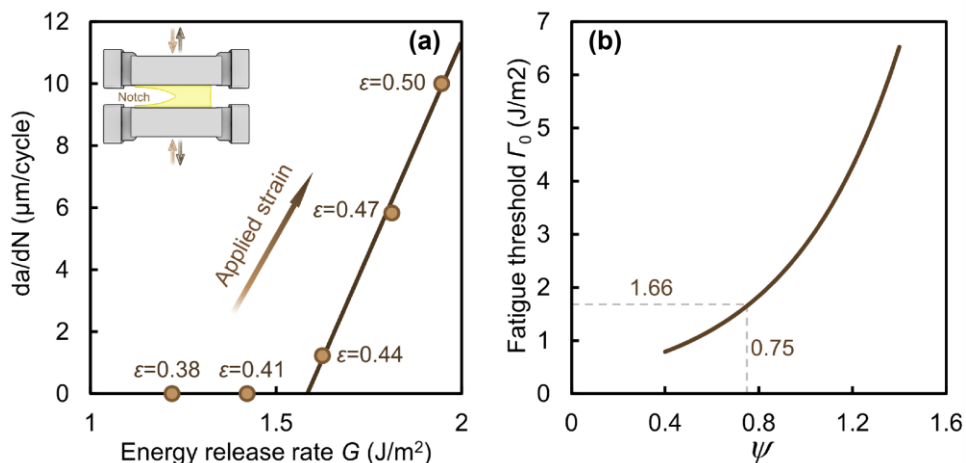


Figure 4-5 Fatigue threshold experimental and theoretical estimation. (a) Crack growth rate per cycle (da/dN) of notched samples in the steady state as function of energy release rate G of paired unnotched samples with same applied strains as marked. (b) Fatigue threshold estimation value as function of the exponent ψ related to the activation- and diffusion-limited aggregation effect.

To reveal how the cyclic loading affects the microstructure of fibrin clots, we further conducted confocal imaging on the unloaded and cyclic-loaded notched samples with focus on two regions: (i) far from crack tip and (ii) the vicinity of crack (Fig. 4-6). In the unloaded notched reference samples, images showed that the fibrin fibers were in a untensed state in far from the crack tip and at the vicinity of crack tip. The fiber configurations were altered by the cyclic loading. In the cyclic-loaded notched samples, the fibers far from the crack tip were tensed and slightly straightened, and those at the vicinity of crack tip appear much denser likely due to the local stress field and the fibrin matrix contraction²¹⁵. These characteristic microscopic structural changes align with those reported with single edge notched tension specimens⁷¹. Interestingly, we also found that the fatigue crack path deviated from the trajectory of the pre-notch. This crack micro-deflection could be attributed to the fiber alignment along the loading direction at the crack tip. The resulting anisotropy would drive the crack toward the softer region for growth. This mechanism can be considered as a toughening mechanism in fibrin clots during cyclic fatigue crack growth. This observation echoes with previous studies on the fatigue resistance of hydrogels^{201,216,217} or tear resistance of soft fibrous tissue²¹⁸.

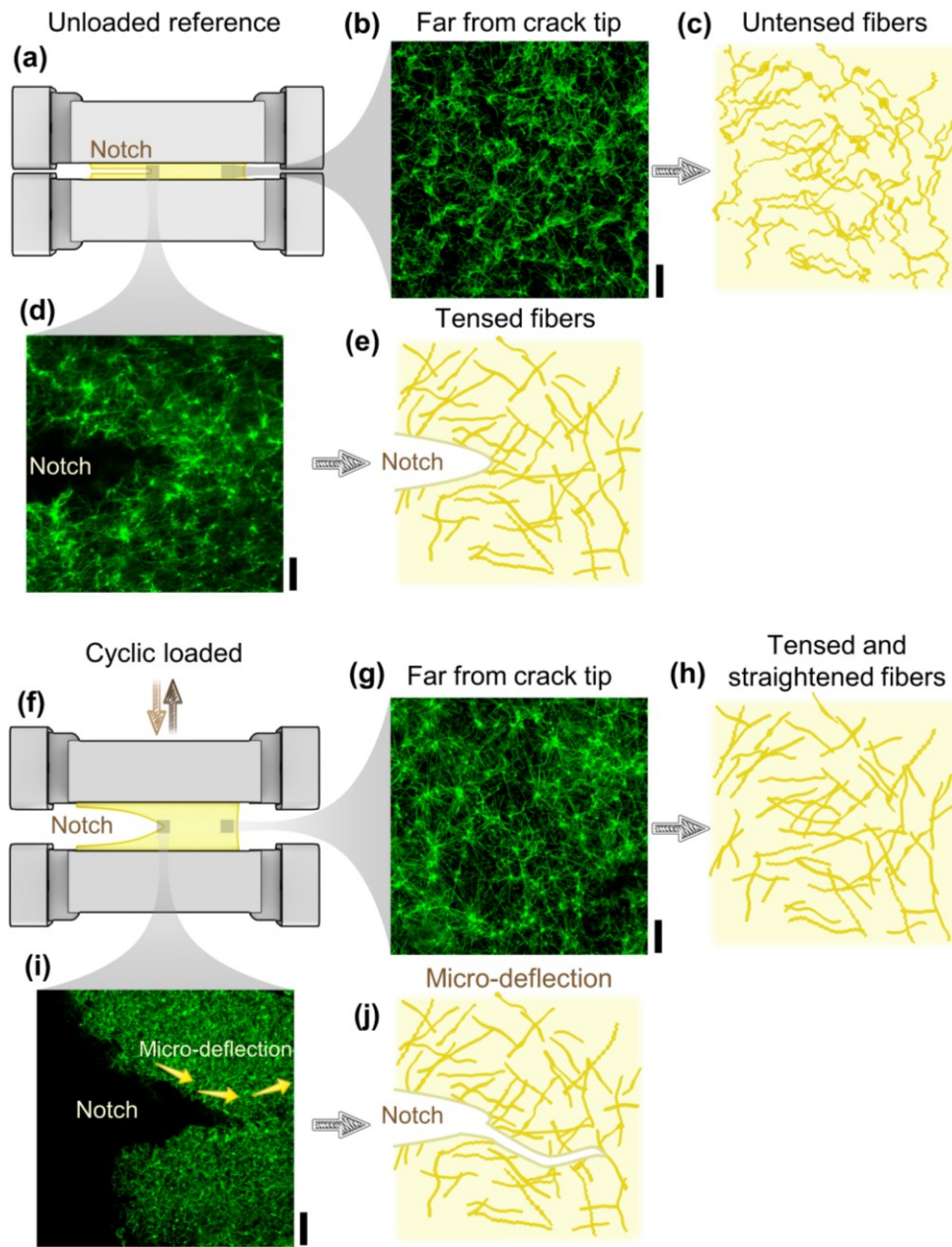


Figure 4-6 Micro-deflection mechanisms of fatigue crack growth. (a) Schematic of unloaded reference of notched samples. (b) Confocal image of unloaded reference of notched samples showing fibrin network in the region far from crack tip and (c) illustration of untensed fibers in confocal images. (d) Confocal image of unloaded reference of notched samples showing fibrin network in the region at crack tip of the pre-cut notch and (e) illustration of tensed fibers in confocal images. (f) Schematic of cyclically loaded notched samples. (g) Confocal image of cyclically loaded notched samples showing fibrin network in the region far from crack tip and (h) illustration of tensed and straightened fibers in confocal images. (i) Confocal images and (j) illustration of cyclically loaded notched samples showing micro-deflection mechanism of crack growth in the fibrin network surrounding crack tip. Note that all the scale bars represent 20 μm .

4.3.4 Theory for fibrin clot fatigue threshold

To interpret the fatigue threshold, we next extend the Lake-Thomas model for the fibrin clot, taking into account the microstructure of fibrin fibers. The Lake-Thomas model predicts very well the fatigue threshold of polymer chain networks, including polyacrylamide hydrogels²¹³. In analogy to the fatigue crack growth in polymer chain networks, the fatigue threshold, referred to as Γ_0 , is mainly attributed to the energy needed to break a single layer of fibers at the crack path. Note that other energy dissipation processes have been depleted after prolonged cyclic load.

Fibrin fibers are hierarchical proteins composed of double-stranded oligomers known as protofibrils^{93,219}, which are assembled by fibrinogen monomers (Fig. 4-1d). By considering the hierarchy nature of fibrin fibers, we adopt the following model for the fatigue threshold of fibrin clots, which is the sum of the fracture energy of a single layer of fibrin fibers at the crack growth path²⁰¹:

$$\Gamma_0 = \alpha n_{\text{fiber}} U_{\text{fiber}} L_{\text{fiber}} \quad (4-1)$$

where α is a non-dimensional enhance factor, and its value is around 3 for fibrous polymer networks²²⁰, n_{fiber} is the number of fibers per unit volume of the fibrous network in the swollen state, L_{fiber} is the average length of the fiber segments between adjacent branching points of the fibrous network in the undeformed state, and U_{fiber} is the energy required to fracture a single fiber which can be defined as follows:

$$U_{\text{fiber}} = \frac{L_{\text{fiber}}}{r_0} N_p U_{\text{monomer}} \quad (4-2)$$

where $r_0 = 22.5$ nm is the length of the regularly repeating unit of protofibril, which approximates one-half the length of the fibrinogen protein due to its half-staggered molecular structure and regular para-crystalline arrangement of packing into a fiber¹⁶ (Fig. 4-1d). U_{monomer} is the energy required to rupture a fiber per monomer which is $2400 \text{ kJ} \times \text{mol}^{-1}/N_A$ ⁹². This value was determined by rupturing single fibrin fibers, and the measured rupture force per monomer was similar to the force required to rupture the knob-hole interactions between monomers. N_p is the number of protofibrils per fiber, which is estimated as follows. An investigation into the mechanical characteristics of individual fibrin fibers, using atomic force microscopy and fluorescence microscopy, revealed that clot formation might occur through activation-limited aggregation

involving clusters of rod-like particles¹⁸³. When applied to the assembly of individual fibers, these activation- or diffusion-limited aggregation mechanisms would lead to a fractal fiber cross-section, where the protofibril density decreases as the diameter increases, and as a result, the number of protofibrils per fiber has a power law relationship with the diameter of fiber d which can be expressed as $N_p \propto d^\Psi$ ¹⁸³. Here the value of N_p for our samples can be estimated as:

$$N_p = N_{p0} \left(\frac{d}{d_0} \right)^\Psi \quad (4-3)$$

where $N_{p0}=400$ and $d_0=50\text{nm}$ are the numbers of protofibrils per fiber and fiber diameter, respectively. They are derived from a previous study, characterizing the molecular packing structure of fibrin fiber using X-ray scattering and molecular modelling²²¹. The exponent Ψ is related to the activation- and diffusion-limited aggregation effect, ranging from 0.4 to 2 which depends on the protofibril aggregation patterns. The previous work reported a small exponent $\Psi=0.4$, suggesting that fibrin fibers initiate with a well-connected semicrystalline core of protofibrils, but as more protofibrils aggregate, the fiber undergoes a transition to a more porous and disorganized state¹⁸³. In our work, we took Ψ ranging from 0.4 to 1.4 for further discussion.

The required morphometric parameters of fibers (L_{fiber} , d , and n_{fiber}) were measured by reconstructing 3D confocal images as shown in Fig 4-2. The values used in this fatigue threshold estimation model include $L_{\text{fiber}}=1.47\pm 0.29 \mu\text{m}$, $d=0.41\pm 0.05 \mu\text{m}$ and $n_{\text{fiber}}=0.21\pm 0.07 \mu\text{m}^{-3}$. Altogether using Eq. 1-3, we estimated the theoretical fatigue threshold Γ_0 of fibrin clots as function of the exponent Ψ (Fig. 4-5b), while the obtained Γ_0 in the experiments was 1.66 J/m^2 . The estimated fatigue threshold starts at 0.79 J/m^2 when $\Psi=0.4$, and increases to 6.53 J/m^2 if the exponent Ψ scale up to 1.4. When the estimated fatigue threshold agrees with the experimental measure value $\Gamma_0=1.66 \text{ J/m}^2$, the corresponding exponent $\Psi=0.75$ which falls in the suggested range, indicating that the density of connected protofibrils decreases with increasing fiber segment diameter. The agreement demonstrates that the intrinsic fracture toughness mechanism of fibrin clots is mainly attributed to the energy required to fracture a layer of fibrin fiber on the crack growth path. The difference of exponent Ψ in this work with the abovementioned literature could be attributed to other processes likely occurring at the crack tip.

4.3.5 Rate-dependence overall fracture toughness

We here assess the rate-dependence of the fracture toughness by varying the loading rate over two orders of magnitudes (strain rates include 0.01 s^{-1} , 0.1 s^{-1} , and 1 s^{-1} , respectively) using monotonic pure shear tests (Fig. 4-8a). The resulting crack propagation rate is correlated with load speeds (Fig. 4-7). Fracture toughness is determined by the critical energy release rate G_c given the fracture criterion $\Gamma=G_c$. In the pure shear specimen and the steady-state condition of crack propagation, the critical energy release rate can be calculated by measuring the applied stretch at the onset of crack growth as $G=HW(\lambda_c)^{125}$, where H is the initial height of clot sample, $W(\lambda_c)$ is the strain energy density function which is the area under the stress-stretch curve of an unnotched sample up to the critical stretch λ_c and λ_c is the critical stretch at the onset of crack growth measured from the stress-stretch curves of notched samples (Fig. 4-8b). Interestingly, the critical stretches of notched specimens show a limited rate dependence (Fig. 4-8c), and in conjugation with the rate-dependent stress-stretch curves of unnotched samples, they lead to a positive correlation between the overall fracture toughness and the crack propagation rate (Fig. 4-8d). The results suggest an important role of rate-dependent dissipation processes for the clot fracture. Previous studies on fibrin fracture reported a range of fracture toughness of fibrin gels from 1 to 15 J/m^2 ^{71,128,156}. The variances could be attributed to the difference in testing methods, and synthesis conditions including fibrin concentration and clotting agents. The detailed testing conditions such as loading rate might play a role as well, which is the focus of the current work. The known difference between fibrin clots and whole clots necessitates further investigation on the rate dependence and fatigue fracture of whole clots.

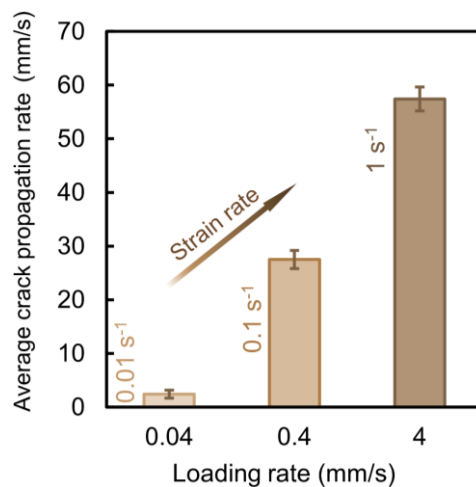


Figure 4-7 Crack propagation rates of fibrin clot pure shear specimens increase with loading rates or strain rates in the monotonic variable rate loading tests.

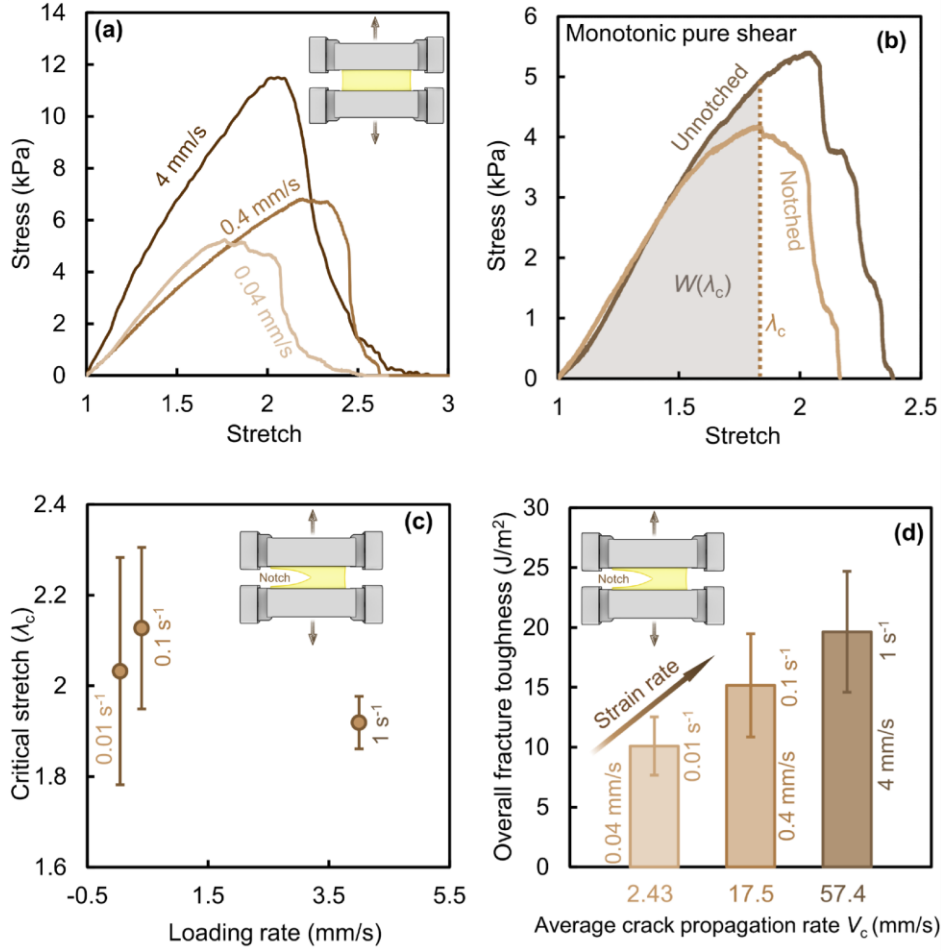


Figure 4-8 Mechanical responses of fibrin clots under variable rate loading. (a) Typical stress-stretch curves of unnotched samples under different monotonic variable rate loads. (b) Typical stress-stretch curves of unnotched and notched samples under monotonic pure shear load, where the critical stretch λ_c is the applied stretch at the onset of crack growth in the notched sample by which the strain energy density $W(\lambda_c)$ is defined as the area under the unnotched sample curve. (c) Critical stretch of notched samples under different monotonic pure shear variable rate loads. (d) Overall fracture toughness of fibrin clots with different crack propagation rates due to strain rate changes.

4.3.6 Theory for the overall fracture toughness of fibrin clots

To better understand the overall fracture toughness of fibrin clots and its rate dependence, we decouple the overall fracture toughness into two contributors as follows²²²:

$$\Gamma(V_c) = \Gamma_{in} + \Gamma_V(V_c) \quad (4-4)$$

where Γ_{in} is intrinsic fracture toughness and Γ_V is the rate-dependent fracture toughness, which can be further expressed as a function of crack propagation velocity V_c . The intrinsic fracture toughness Γ_{in} is considered rate-independent since it is attributed to the scission of a layer of fibrin

fibers at the crack tip. As such, we can approximate it with the fatigue threshold measured from the cyclic fatigue tests ($\Gamma_{in} = \Gamma_0$). The rate-dependent fracture toughness Γ_v is attributed to the bulk energy dissipation mechanisms such as viscoelasticity, water migration (or poroelasticity), and other dissipative processes¹¹².

As fibrin clots exhibit both viscoelastic and poroelastic behavior under deformation, Γ_v could be attributed to viscoelasticity and poroelasticity. Measuring the exact contribution from each mechanism is challenging, so we start by examining the critical length scales underpinning water migration and fracture. On one hand, the water transport is confined in a zone surrounding the crack tip with a length scale of D/V_c ²²³, where D is the effective diffusivity of water in the gel. Based on the reported diffusion coefficient of blood clots $D \approx 2 \times 10^{-7} \text{ m}^2/\text{s}$ ¹¹¹ and our measured V_c from our experiments, we calculated $D/V_c \approx 0.1 \text{ mm}$ and 0.004 mm for the fast- and slow-loading conditions. On the other hand, the size of the process zone at the crack tip during fracture is characterized by another length scale ζ , calculated as Γ_{in}/W^* , where Γ_{in} is the intrinsic fracture toughness and W^* is the work of rupture. Our measurements give ζ on the order of 0.1 mm . Comparing the two length scales, we find that the poroelastic process is confined within the process zone at the crack tip so that its effect is absorbed in Γ_{in} and contributes less to Γ_v . Additionally, we measured the volume of fluid that came out from these specimens using tissue paper, which was placed on the surfaces of the crack front and fracture surface. The volume ratio of mitigated fluid to the sample volume was less than 5%.

The contribution of water migration to fracture deserves additional discussion. Tutwiler and coworkers found the dependence of fibrin gel fracture toughness on dissipation arising from fluid motion ranged from 2-16% for fibrin concentration of 1-10 mg/mL, indicating a relatively small impact¹²⁸. This dependence heightened with increasing fibrin concentration, as reduced porosity led to more energy dissipation through fluid motion. Considering the comparatively low fibrin content in our samples, we anticipate a high level of porosity, a notion supported by our observation of immediate shrinkage in fibrin clots when manually cut and released from the gripper (refer to Video 4S in Supplementary Information). These observations may suggest a limited contribution of fluid migration to the overall fracture toughness.

Based on these considerations, we hypothesize that the viscoelasticity plays a predominant role in contributing to Γ_v . As such, at a given constant temperature T (room temperature), the rate-

dependent fracture toughness would follow a power-law relationship, $\Gamma_V \sim V_c^\eta$, and the overall fracture toughness can be expressed as²²⁴:

$$\Gamma(V_c) = \Gamma_{in} (1 + kV_c^\eta) \quad (4-5)$$

where k and η are constants. To validate our hypothesis, we performed a power-law curve fitting using Matlab, while setting Γ_{in} as 1.66 J/m² from our measured fatigue threshold. Figure 4-8 shows the overall fracture toughness as function of crack propagation rate, following $\Gamma(V_c) = 1.66(1 + 4.61V_c^{0.246})$ with $R^2 = 0.86$. We also make a linear extrapolation, as a linear relation was previously reported for gelatin hydrogels and associated with the viscous pullout of polymer chains⁶⁷. A discrepancy is found between the linear extrapolation and our fitted viscoelastic model (Fig. 4-9). For further validation, we related the rate-dependent fracture toughness to the time-dependent relaxation modulus, which scales with $G(t) \sim t^{-p}$. Based on the rheological measurements of fibrin clots¹¹⁷, we obtain $p=0.318$ by linear regression analysis and, following^{224,225}, find the corresponding $\eta = \frac{p}{1+p}$. Interestingly, the estimation based on the relaxation modulus matches with the value 0.246 fitted from our viscoelastic fracture toughness model. The agreement supports the viscoelastic origin of the rate-dependent fracture toughness of fibrin clots.

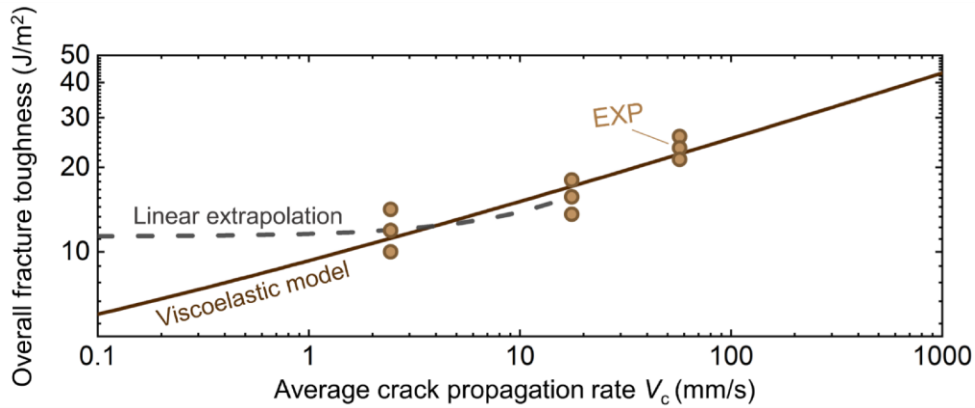


Figure 4-9 Semi-empirical prediction of overall fracture toughness of fibrin clots as function of their crack propagation rate. A linear extrapolation of relatively low crack propagation rate results ($V_c=2.43$ and 17.5 mm/s) gives an intersect which indicates the value of zero-rate fracture toughness.

Chapter 5 Adhesive and cohesive fracture modalities

5.1 Preface

Fracture of blood clots within vascular systems and at injury sites could cause life-threatening conditions. The fracture modalities include fracture within the clot's bulk material (cohesive fracture) or at the clot-tissue interface (adhesive fracture) or the mixed of the two mechanisms (mixed mode fracture). While the cohesive fracture within the bulk material has already been characterized, the adhesive fracture – as an independent and sophisticated mode of failure – is still unexplored. In this chapter, we employ an integrated experimental-computational approach to evaluate the adhesive and cohesive fracture behavior of bovine blood clots by incorporating mechanical factors (e.g., loading rate, failure modes) as well as cellular components, such as red blood cells (RBCs) and platelets. Among biological substrates, the blood clot showed the largest interfacial fracture energy to the muscle and the least adhesion to the inner arterial lining, consistent with its biological role. Both interfacial and bulk fracture energy exhibited notable rate dependency, suggesting the role of dissipation as a toughening mechanism. An elevation in RBC content increased interfacial/bulk fracture energy, without influencing the clot's hysteresis, and this phenomenon – as substantiated by our finite element model – was due to an increase in intrinsic toughness. Increasing the platelet content enhances interfacial fracture energy to a level where the failure mode in the peeling tests shifted from adhesive to mixed-mode fracture, underscoring the crucial role platelets of in adhesion. These findings significantly expand our understanding of clot mechanics, bearing important clinical implications that may optimize the management of clot-related disorders, and pave the way for developing innovative therapies.

5.2 Introduction

Blood clot formation is a complicated and dynamic process, involving a number of biochemical and cellular activities that may be split into several discrete stages important for their future usage as a biomaterial. Fibrin, a major component of whole blood, has been studied and used as surgical glues since the 1940s for its unique mechanical and biological properties²²⁶. The formation and structure of the clot's fibrin matrix, as well as the participation of various proteins in the clotting process, are critical features of blood clot structure. While significant research has been conducted

on the biochemistry of clot formation, the mechanical properties of clots as a whole have received little attention, despite their potential importance in therapeutic applications and tissue regeneration.

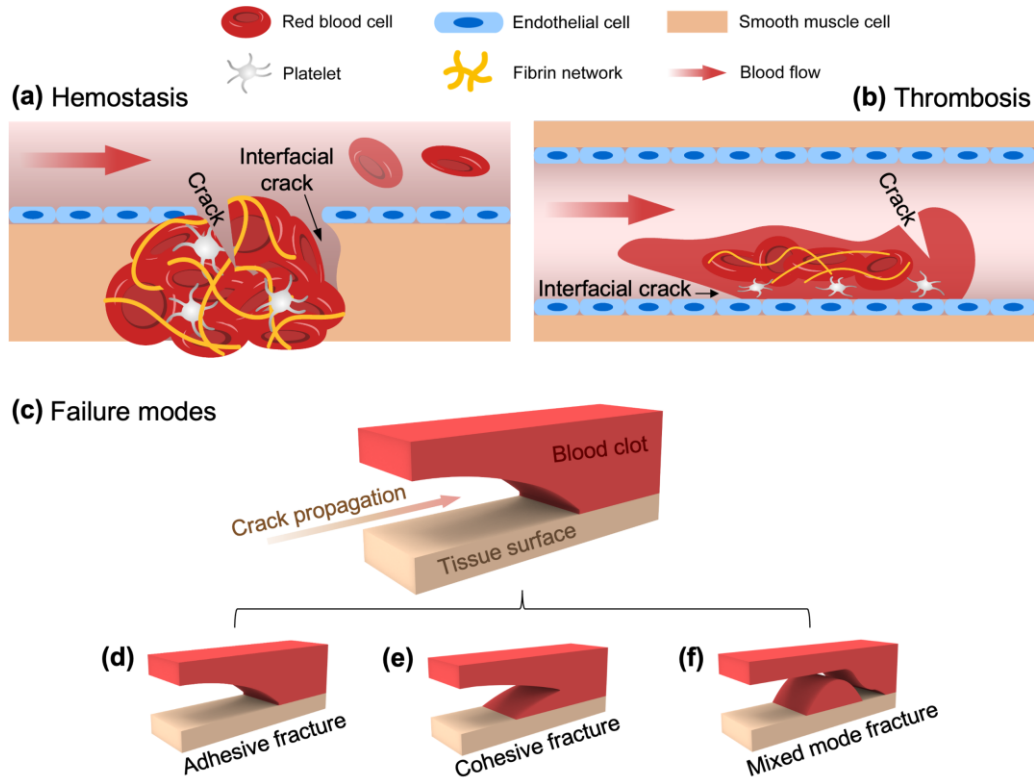


Figure 5-1 Schematic of adhesive and cohesive fracture of blood clot in homeostasis and thrombosis conditions. (a) Adhesive and cohesive fracture of blood clot in hemostasis, led by the propagation of interfacial crack and crack within clots, respectively. (b) Adhesive and cohesive fracture of blood clot in thrombosis, led by the propagation of interfacial crack and crack within clots, respectively. (c, d, e and f) Different failure modes in blood clot on tissue surface, including adhesive, cohesive and mixed mode fracture.

Mechanical failure and fracture of blood clots, at injury sites or within the vascular system, may result in severe and potentially fatal complications such as excessive bleeding, embolism, and thrombosis – which can be exacerbated by conditions such as COVID-19²²⁷. Current understandings around clot failure have been centered around the cohesive fracture arising from cracks within the clot's bulk material^{71,156,193}. Yet, an independent and sophisticated failure mode resulting from the progression of an interfacial crack between the clot and a substrate tissue is often overlooked (Fig. 5-1)⁶⁶. Central to the latter mechanism is the interplay between the clot's bulk and adhesion properties to the substrate tissue. When the interfacial crack extends solely along the clot-tissue boundary, the phenomenon is called an adhesive fracture; however, when the crack

(near the interface) propagates within one material, without crossing the boundary, cohesive fracture occurs (Fig. 5-1). In a mixed-mode fracture case, the fracture takes place partly along the interface (adhesive) and partly within one of the materials (cohesive). Hence, interfacial fracture energy is the term for describing the energy required to create a unit area of an interfacial crack which can involve a mixed-mode fracture^{228,229}. Correspondingly, bulk fracture energy, also known as fracture toughness, is used for describing the energy required for a unit area of crack growth solely within one material (cohesive fracture)²³⁰. The complexities of interfacial crack propagation demand a deep understanding of both the adhesive and cohesive properties of blood clots.

Incorporating adhesive and cohesive fracture in clot failure mechanisms presents a holistic framework to understand the fracture mechanics of the clot, and accurate characterization of these mechanisms needs distinct methodologies in physiologically relevant conditions. Recent studies have measured the bulk fracture energy of the clot using modified lap shear and edge-notched samples^{71,156,193}; nevertheless, exploring alternative methodologies could provide additional insights into the cohesive fracture behavior of blood clots under different loading conditions. In addition, the interfacial fracture energy of a material fundamentally derives from both intrinsic adhesion to a substrate as well as the energy dissipation within the bulk material¹⁹⁹. Characterizing the coupling between bulk properties and apparent adhesion is critical to the comprehensive understanding and modeling of blood clot fracture.

A blood clot – as a bio-composite material with multiple constituents such as red blood cells (RBCs), platelets and fibrin – has a complex mechanical response^{27,64,91}, and exploring the role of these components in different fracture modalities is crucial for uncovering the underlying causes of failure with direct clinical implications. Various disorders or conditions can alter these constituents, such as polycythemia leading to high RBC count, and thrombocytopenia causing low platelet count. While the influence of fibrin content on cohesive fracture has been evaluated¹⁹³, the effects of cellular constituents (specifically RBCs and platelets) on clot fracture have not been assessed, and exploring these factors remains critical to expanding our knowledge and developing targeted treatments for clot-related complications.

Therefore, this study employs an integrated experimental-computational approach to evaluate the fracture behavior of bovine blood clots by incorporating mechanical factors (e.g., loading rate,

failure modes) as well as cellular components, such as RBCs and platelets. We performed peeling tests on various substrates (such as muscle, skin and artery) along with pure shear tests to characterize interfacial and bulk fracture energy, respectively. Additionally, we evaluate the effects of the loading rate, as well as platelets and RBCs contents on adhesion and cohesive fracture of blood clots. Furthermore, a constitutive model is calibrated to predict the mechanical behavior of blood clots and their fracture responses. This comprehensive framework lays the groundwork for the assessment and prediction of adhesive and cohesive fracture behavior and sets a benchmark for measuring the fracture performance of innovative therapeutic strategies.

5.3 Results and discussion

5.3.1 Interfacial fracture energy

We used peeling tests to characterize the energy per unit area needed to detach blood clots from various substrates (e.g., skin and liver; Fig. 5-2d) and found that blood clots exhibited the strongest adhesion with gauze, reaching an interfacial fracture energy of $8.22 \pm 0.88 \text{ J/m}^2$, followed by the muscle ($5.63 \pm 2.01 \text{ J/m}^2$) while the weakest adhesion was with the inner aorta ($1.35 \pm 0.39 \text{ J/m}^2$), and the liver ($2.59 \pm 0.89 \text{ J/m}^2$); Figure 5-2c. As the loading rate increased from 0.01 s^{-1} to 0.1 s^{-1} or 1 s^{-1} , the interfacial fracture energy nearly doubled; however, this rate dependency was non-uniform, and the effects diminished at larger rates, which highlights the complex relationship between blood clot adhesion and various substrates.

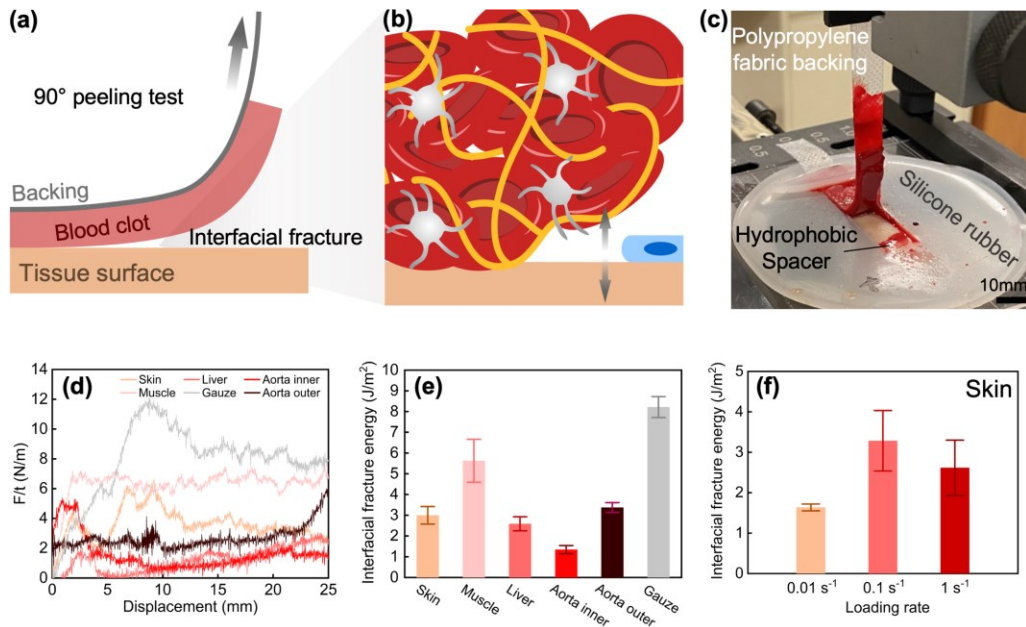


Figure 5-2 Characterization of interfacial fracture energy. (a and b) 90° peeling test experimental setup schematic and (c) photo. (d) Selected force-displacement responses of blood clot on different substrates under 90° peeling test. (e) Measured interfacial fracture energy of blood clots on different substrates (n=4). (f) The effect of loading rate on interfacial fracture energy of blood clot (n=4).

5.3.2 Bulk fracture energy

We measured the bulk fracture energy of the bovine blood clots using pure shear tests at $18.27 \pm 1.45 \text{ J/m}^2$ (rate = 0.01 s^{-1}), Figure 5-3, and the measured fracture toughness remained insensitive to variations in crack length (Fig. 5-3d) partly because the initial crack length was much larger than the estimated dissipative length – i.e., the length of the stress concentration zone; $5.3 \text{ mm} \pm 0.5 \text{ mm}$. In addition, a strong rate dependency was noted in the mechanical stress-strain responses (Fig. 5-3e), which led to a marked increase in the fracture toughness (Fig. 5-3f). Specifically, the fracture toughness at a loading rate of 0.01 s^{-1} was found to be 18.27 J/m^2 , whereas at a higher rate of 1 s^{-1} , the fracture toughness was increased by 70% (38.12 J/m^2).

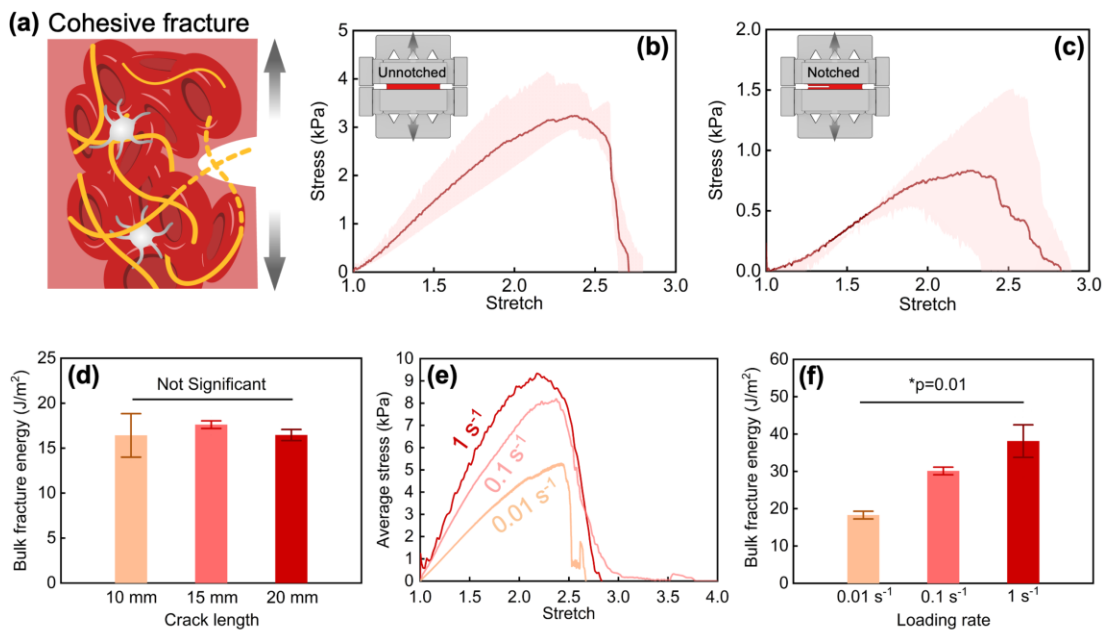


Figure 5-3 Characterization of bulk fracture energy: (a) Schematic illustration of crack growth in the blood clot. Average stress-stretch curves of (b) intact and (c) notched samples in pure shear tests (shaded area represents the experimental range; n=4). (d) Fracture toughness of blood clot is insensitive to crack length (n=4). (e) Average stress-stretch curves of unnotched samples in pure shear tests under different loading rates (0.01, 0.1 and 1 s^{-1} ; n=4). (f) Fracture toughness of blood clot under different loading rates (at each group n=4). For statistical analyses, one-way ANOVA was carried out.

5.3.3 Effects of RBC and platelet

We assessed the impact of modulating RBC and platelet contents on the mechanical properties of clots. When the RBC content was increased to 70%, the interfacial fracture energy of the clot increased by 80% (Fig. 5-4); and elevating the platelet content from 1x to 3x nearly doubled the interfacial fracture energy (Fig. 5-6). SEM images and visual observations corroborated that samples with increased platelet count (3x) displayed a mixed mode fracture (i.e., combined adhesive and cohesive fracture) at the interface under the peeling test, with residual clots serving as evidence of cohesive fracture (Fig. 5-7). Contrarily, the control group with a standard platelet content (1x) showed negligible traces of clot residue on the muscle substrate, indicative of an adhesive fracture (Fig. 5-7).

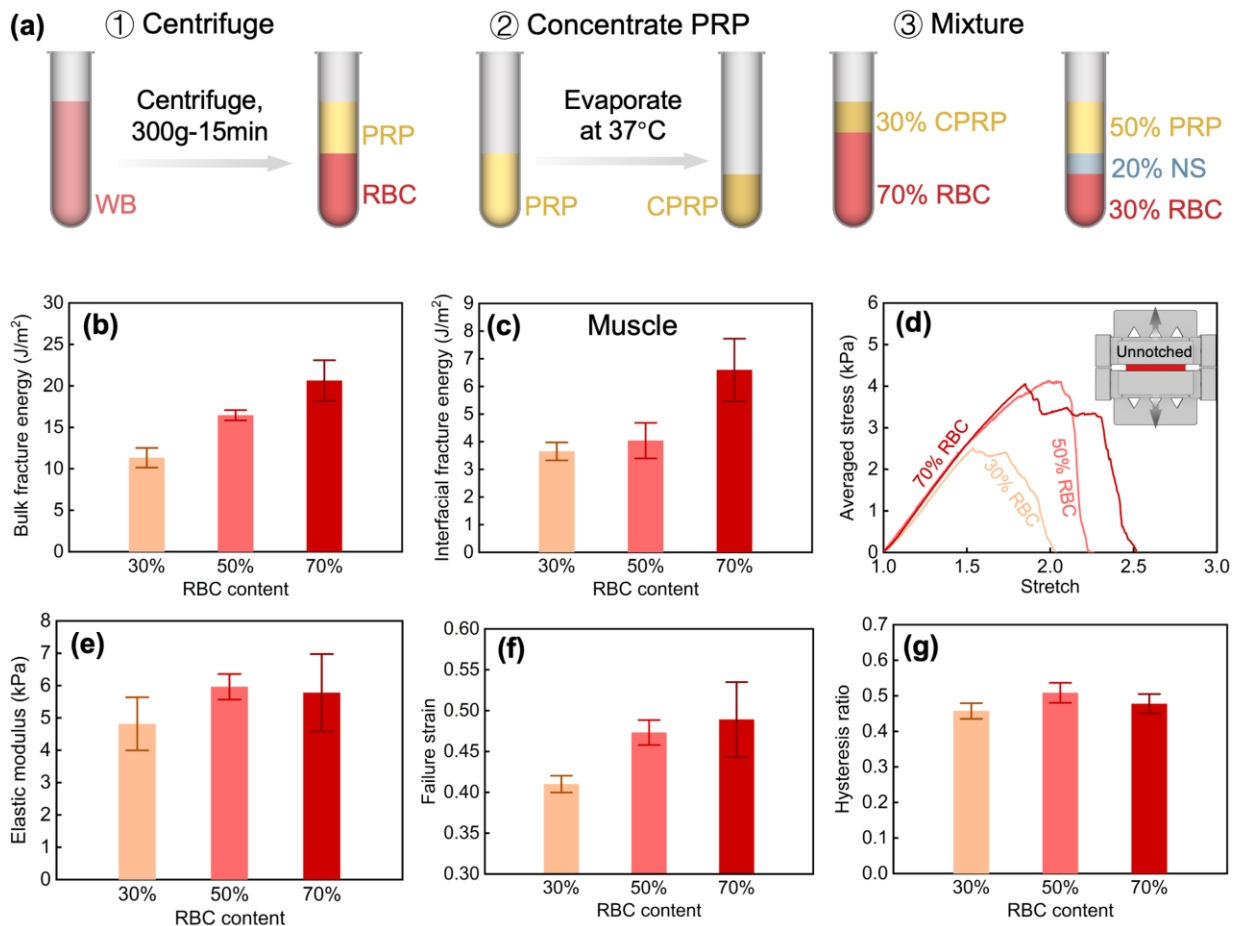


Figure 5-4 The effects of RBC on mechanical properties of the blood clot. (a) Preparation process of blood with different RBC content (WB: whole blood; PRP: platelet rich plasma; RBC: red blood cell; CPRP: concentrated platelet rich plasma; NS: normal saline). (b) Fracture toughness of blood clot for different RBC content measured from pure shear test (n=4). (c) Interfacial fracture energy of blood clot on muscle for different RBC content estimated from 90°

peeling test (n=4). Average elastic modulus (d) and average stress-stretch response (e) of the blood clot under pure shear test (intact sample) for different RBC content (n=4). The effect of RBC content on (f) failure strain and (g) hysteresis ratio of the blood clot under pure shear test.

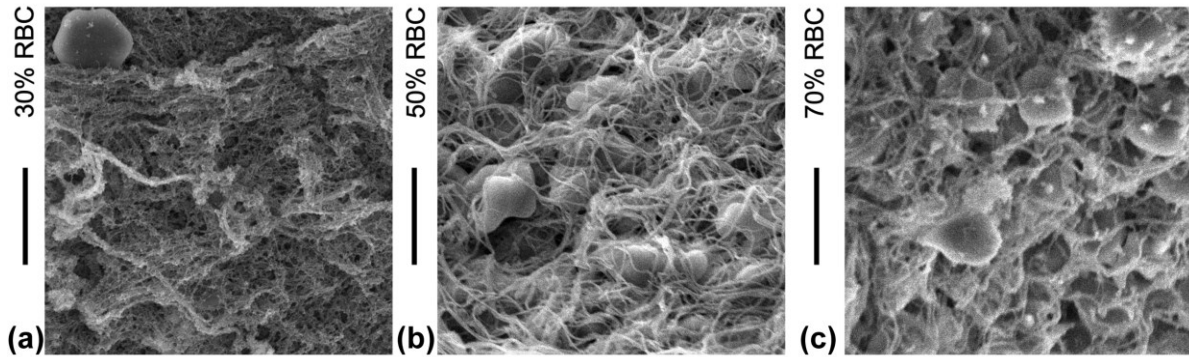


Figure 5-5 SEM images of blood clots for different RBC content. (a) 30%, (b) 50% or control group, and (c) 70%.

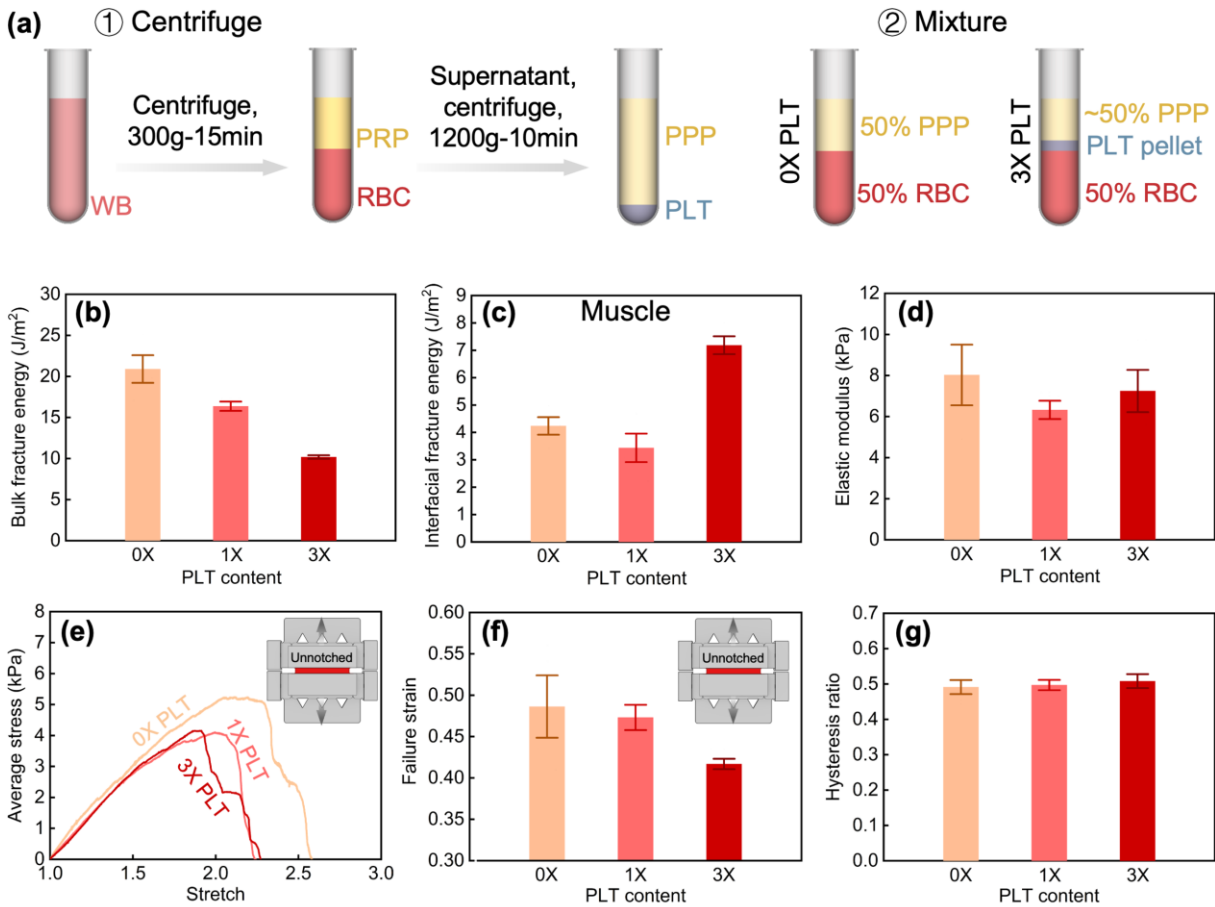


Figure 5-6 The effects of PLT content on mechanical properties of the blood clot. (a) Preparation process of blood with different PLT content (WB: whole blood; PRP: platelet rich plasma; PPP: platelet poor plasma; RBC: red blood cell; PLT: platelet). (b) Fracture toughness of blood clot for different PLT content measured from pure shear test (n=4).

(c) Interfacial fracture energy of blood clot on muscle for different PLT content estimated from 90° peeling test (n=4). Average elastic modulus (d) and average stress-stretch responses (e) of the blood clot under pure shear test (intact sample) for different PLT content (n=4). The effect of PLT content on (f) failure strain and (g) hysteresis ratio of the blood clot under pure shear test.

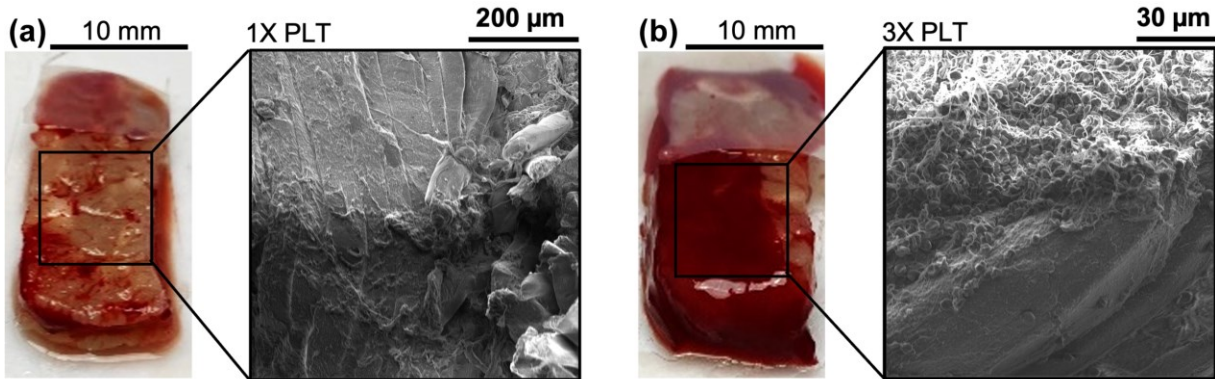


Figure 5-7 SEM images of (a) control and (b) 3x PLT blood clot samples after peeling tests showing residues on bovine muscle substrates after peeling test.

Changing the RBC and platelet contents substantially influenced the failure strain (or stress) of the blood clot (Fig. 5-4 and 5-6). An increase in RBC content led to higher failure strain, and therefore higher bulk fracture energy (Fig. 5-4), yet larger platelet contents decreased the bulk fracture energy (Fig. 5-7). Altering clot constituents did not significantly affect the stiffness or hysteresis (energy dissipation under cyclic loading) of the blood clot (Fig. 5-4 and 5-7). SEM imaging confirmed the differences in the content of RBC and platelets within the blood clot, yet no noticeable changes in the fibrin network structure were observed due to variations in RBC and platelet contents (Fig. 5-5). These findings underscore the critical role of RBC and platelets in determining the mechanical properties and adhesion behavior of blood clots.

5.3.4 Finite element model

We built two finite element models to simulate cohesive and adhesive fracture of blood clots, respectively, using a coupled cohesive-zone and Mullins-effect model validated by our experiments. The fracture model simulates the clot fracture under pure shear configuration. We calibrated a rate-independent constitutive model that combined the Yeoh hyperelastic model ($C_1 = 0.47 \text{ kPa}$; $C_2 = 0.17 \text{ kPa}$; $C_3 = -0.01 \text{ kPa}$; $D = 0.06 \text{ kPa}^{-1}$) with Mullin's effect ($r = 1.00$; $\beta = 0.26$; $m = 0.87 \text{ J}$). Our model could well capture the stress-stretch responses of the blood clot under both tension and compression loads (Fig. 5-8). We employed cohesive zone models to

simulate the crack propagation phenomenon. The cohesive zone model defines a traction-separation law, which relates the tractions (or stresses) across the crack surfaces to the relative displacement between them. This traction-separation law is characterized by parameters such as the intrinsic fracture energy (Γ_0) and the maximum normal stress (S). While these two parameters are unknown, we performed a series of simulations using various combinations of Γ_0 and S , yielding the corresponding predictions of bulk and interfacial fracture energy (Fig. 5-8). From these results, we could identify the range of Γ_0 and S that match the experimental and computational results. The presented model successfully captured the rate-independent multi-modal behavior of the blood clot, as well as the interfacial/bulk crack propagation (Fig. 5-9).

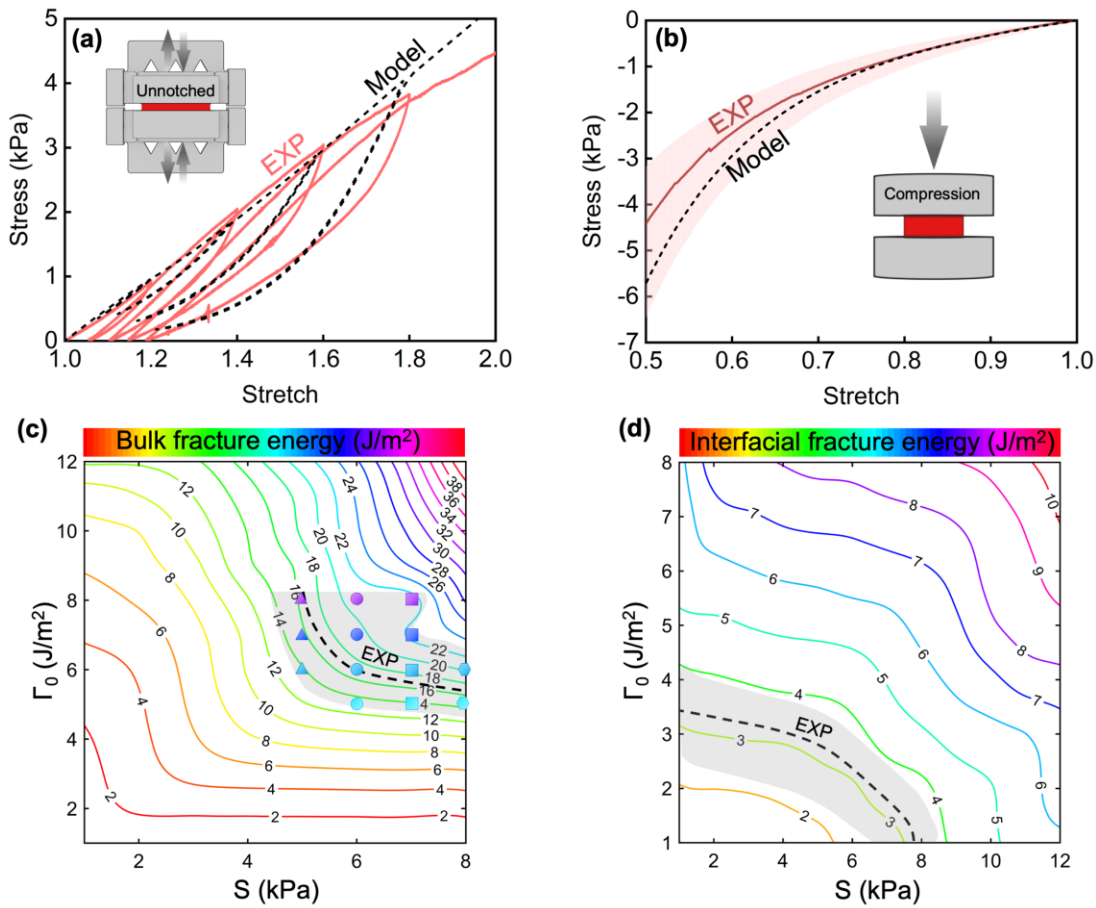


Figure 5-8 Rate independent model of the blood clot. Measured and estimated responses of the blood clot under (a) measured (red) and estimated (black) cyclic pure shear and (b) measured (red) and estimated (black) unconfined compression loadings. (c) Estimated bulk fracture energy of the blood clot for various cohesive zone model parameters (intrinsic toughness: Γ_0 ; maximum stress: S). (d) Estimated interfacial fracture energy of the blood clot for various cohesive zone model parameters (intrinsic toughness: Γ_0 ; maximum stress: S).

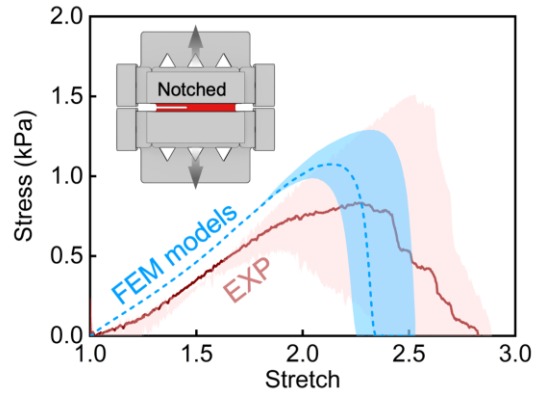


Figure 5-9 Comparison between measured (red) and rate-independent model estimated (blue) force-displacement responses of the notched sample under pure shear loading.

In our study, we observed that the fracture mode of blood clots, whether cohesive or adhesive fracture, can be influenced by various factors. The interplay between cohesive and adhesive fracture modes is crucial in understanding the mechanical behavior of blood clots in hemostasis and thrombosis, particularly in scenarios involving complex loading conditions and interfaces. Cohesive failure occurs within the material itself, while adhesive failure occurs at interfaces between different materials. By comparing cohesive and adhesive fracture toughness, we can gain insights into how the clot may behave under different loading conditions and environments. According to our experimental results and FEM results, it is found that the cohesive fracture toughness of whole blood clot is generally higher than its adhesive fracture toughness on various substrates. It suggests a greater tendency for the crack to propagate at the interface, resulting in an adhesive fracture mode. On some surfaces where the clot adhesive fracture toughness approaches clot cohesive fracture toughness, the fracture mode may transform into a combined-mode fracture or cohesive fracture, leading to a clot rupture or a formation of clot fragments. Our finite element modeling results provide a means to predict and understand these fracture modes by simulating the crack propagation phenomenon and assessing the stress distribution within the clot. Clinically, this information is crucial for predicting the efficacy of therapeutic strategies aimed at preventing or treating blood clot-related disorders.

Chapter 6 Discussion and future work

6.1 Discussion

6.1.1 Pure shear configuration

The pure shear test was first proposed by Rivlin and Thomas¹⁴⁸ to test fracture of rubber samples and has been broadly adopted to characterize gel fracture¹²⁵. This measurement involves two kinds of samples with identical geometry: unnotched and notched samples. Our specimens were a long thin strip with a width ($L=40$ mm) significantly greater than its height ($H=4$ mm) and thickness ($b=3$ mm). For notched samples, a long crack of length $c=10$ mm ($c \gg H$) was introduced in the middle of the strip. All samples were securely affixed at the upper and lower boundaries by gluing with rigid grippers and subjected to a uniform vertical displacement imposed by the Instron machine.

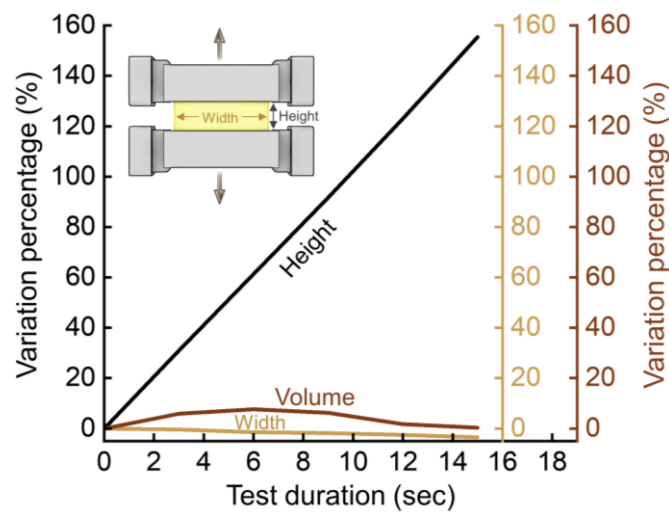


Figure 6-1 Variation percentage of height, width and volume change of unnotched pure shear specimen of fibrin clot versus the test duration during monotonic uniaxial loading.

To examine the dimensional change during testing, we captured the front and side views of the unnotched specimen under monotonic load, and measured specimen height, width and volume until rupture occurred. The variation percentages of these geometrical factors were calculated and plotted in Fig. 6-1. We confirmed that the width showed minimal alteration, while the height uniformly increased with the applied displacement. The total volume showed slight changes before rupture, and no significant water expulsion was observed throughout the test. These results affirm

that our specimens generally satisfy the pure shear conditions mentioned above. To examine the contraction of our specimen, we manually cut the undeformed specimen in the middle, and observed immediate shrinkage of the released fibrin clots. This observation suggests that the presence of pre-strain developed in the contracting clots, as well as the significant boundary constraints at the upper and lower grippers. Given that all clots were prepared using platelet-poor plasma, the contraction is presumed to result from intrinsic fibrin matrix contraction²¹⁵. Further investigation is warranted to explore how fibrin clot contraction influences fracture behavior.

6.1.2 Fracture toughness of blood clots

We demonstrated that fracture toughness is a well-defined material property of clots through experiments and simulations. The measured quantity was found to be crack length invariant and specimen geometries invariant, consistent with prior reports in literature. Therefore, the failure of clots is governed by crack propagation. Fibrin clots and whole blood clots exhibit a low toughness compared to biological materials such as collagen and cartilage²³¹, and synthetic hydrogels²⁰⁴. The uniqueness of clot fracture lies in their multiscale processes, such as fibrous network geometry (Chapter 4), cellular components effect (Chapter 5), molecular unfolding and fiber bundling⁷¹, which are usually out of scope in studies on elastomers or synthetic hydrogels.

The specimens were prepared in pure-shear configuration. We fabricated and used a customized silicone mold to form a long and thin unnotched clot sample ($40 \times 4 \times 3$ mm), and placed 3D-printed components to lock on both sides of the clot specimen. For notched specimens, we made a 10-mm pre-notch by placing a polyester film (0.1 mm thin) into the silicone mold before clotting. The silicone mold and the attached polyester film were removed from the plasma specimens before mechanical testing. The materials for the fabrication of the silicone mold and 3D printed part were carefully chosen based on experimental trials to allow uniform load and secure the safe handling of the extremely fragile plasma clot throughout the entire process of clot preparation, assembling, transferring, storing, grip clamping, and loading.

6.1.3 Critical length scales during clot fracture

The fracture of blood clots involves mechanical, physical, and biochemical processes, given the structural and compositional complexity of blood clots⁶⁴. A running crack in a blood clot is expected to encounter complex stress/strain fields at the crack tip. Characterizing these complex

fields is technically challenging so that we intended to estimate the critical length scales governing the physical processes around the crack tip area, which are key to understand and model the fracture. They are manifested with a failure zone where dissipation occurs and a nonlinear elastic zone where the material elements are deformed nonlinearly. The critical length scales to define the failure zone and nonlinear zone are known as the dissipative length scale and the nonlinear length scale, respectively²³². Specifically, the dissipative length reflects the critical flaw size, above which the clots sensitize to the crack²³³.

The critical length scales underlying the clot fracture remain elusive. Therefore we estimated the critical length scales governing the fracture of blood clots: the dissipative length scale ξ and the nonlinear elastic length scale²³³ based on the experimental results in Chapter 3. The former describes the size of the process zone near the crack tip during fracture and reflects the flaw sensitivity of a material, while the latter depicts the size of materials undergoing nonlinear deformation at the crack tip (as illustrated in Figure 3-1c)²³². The dissipative length scale was estimated by the ratio of the fracture energy to the work to rupture, $\xi = \Gamma/W$. The fracture energy G was measured with lap-shear tests as shown in Figure 3-3. The work to rupture W was characterized by loading specimens without a cut to rupture using the same setup (lap shear test in this study) and defined by the area under the stress-strain curve. The nonlinear elastic length scale, also known as the elasto-adhesive length, can be represented by the ratio of the fracture energy to the Young's modulus, $l = \Gamma/E$. The Young's modulus was estimated by $E = G \cdot 2(1+\nu)$, where G was the shear modulus measured from rheologic measurements and the Poisson's ratio ν was 0.5, since blood clots can be considered incompressible as hydrogels²³⁴. As can be seen, the length scales were on the order of 0.1-1 mm, reflective of large deformability and dissipative capacity of blood clots (Table 6-1).

Our estimations are supported by confocal imaging and finite element (FE) modeling. In a recent study on human blood plasma-derived fibrin clots⁷¹, the unfolding of fibrin fibers occurred at a characteristic length scale of 0.1 mm at the crack tip, while the alignment of fibrin fibers and large deformation appeared across the whole specimen. The fiber unfolding and alignment are associated with the dissipative and deformation behavior of blood clots⁹³. Similar results were obtained by us in a separate study of finite element modelling, where we mapped the large deformation and dissipation of whole blood clots under simple shear in lap-shear tests. Further

research is needed to map the strain field within blood clots using some techniques like force traction microscope or digital image correlation (DIC).

The two length scales benchmark the crack tip field. These critical length scales have been extensively investigated for soft materials such as hydrogels and elastomers^{232,233}. In addition to this study, further investigation is needed to establish the two length scales for blood clot fracture. For example, when the crack size exceeds the dissipative length scale, the failure is governed by crack growth (fracture mechanics). Given a crack smaller than the dissipative length scale, the material is insensitive to cracking (flaw-insensitive) and thus follows the strength criteria instead²³². For highly deformable viscoelastic materials, the nonlinear length scale represents the area where the deformation is appreciably nonlinear and considerable energy dissipation occurs²³³.

Table 6-1: Critical length scales.

Length scales	Whole blood	Platelet-poor plasma
Dissipative length scale (mm)	0.17	0.15
Nonlinear elastic length scale (mm)	6.50	3.00

To further compare the blood clots with other materials, we collected the dissipative and nonlinear elastic length scales for various materials. Figure 6-2 illustrates the values for human WB and PPP clots from this work, and those reported in literature for fibrin gel⁷¹, blood vessel^{235,236}, skin²⁰⁵, natural rubber¹⁴⁸, alginate gels²⁰⁵, double-network (DN) gels^{233,237}, polyacrylamide (PAAm) gels²⁰⁵, PAAm-alginate gels²⁰⁵, agar gels²³⁸, and tetra-arm polyethylene glycol (Tetra-PEG) gels²²⁰. Compared with the fibrin clot⁷¹, the WB clots have a smaller flaw sensitivity length scale (~0.2 mm) and larger nonlinear length scale (~7 mm), which could be attributed to a large fraction of blood cells in WB. Interestingly, the two length scales of human blood clots are comparable with that of double-network hydrogel and natural rubber. This finding implies that blood clots are relatively flaw insensitive and highly deformable, therefore have a great potential for fracture resistance.

The impressive length scales are associated with the unique structure and composition of blood clots. The porous fibrin network, as the main structural protein, endows high deformation and

softness, while maintaining a sufficient permeability to allow effective enzymatic decomposition. Platelets attach to the fibrin fibers to stiffen and densify the clot, thereby providing a mechanically stable seal. The incorporation of soft and viscoelastic filler, RBCs, can deconcentrate stress and dissipate energy under strain. They are manifested as the hysteresis, Mullins effect, and rate-dependent effect (viscoelasticity) of blood clots under cyclic loadings⁹¹. The detailed toughening mechanisms should be further investigated.

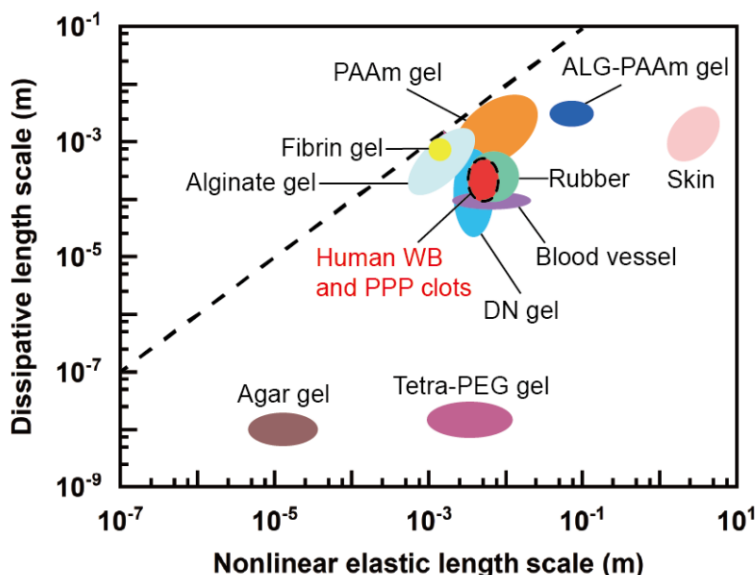


Figure 6-2 Dissipative and nonlinear elastic length scales for soft and biological materials. Data of human whole blood and platelet-poor plasma clots is from my work presented in this thesis, others are from previous studies^{71,148,205,220,233,235-238}. Dash line represents that the material’s dissipative length scale and nonlinear length scale are equal.

6.1.4 Toughening mechanism of fibrin clots

The ratio of fracture toughness to fatigue threshold (termed as toughening ratio) reflects the bulk dissipation ability and toughening mechanism of soft materials²³⁹. At the load speed of 0.4 mm/s, the overall fracture toughness of fibrin clot was measured at 15.8 J/m², in contrast to the measured fatigue threshold at the same rate 1.66 J/m². Our study attributes the large toughening ratio 9.13 to the viscoelastic dissipation mechanism within fibrin clots. Since fibrin serves as the key structural component of whole blood clots, we expect the same mechanism to be the main contributor of the fracture toughness of whole blood clots. This conjecture requires further investigation to confirm. Given the key role of fibrin network, further improving the toughening

ratio could be realized by increasing the volume fraction of fibrinogen¹²⁸. While we used the plasma containing relatively low physiological fibrinogen level in this study, there is potential room for further toughness improvement.

The fracture of fibrin clots could involve various mechanical responses of individual fibers and their network. Previous studies collectively offer insights into a range of processes spanning length- and time-scales, including fiber deformation, alignment, recoiling, and protein unfolding as strains increase^{54,240}. These processes represent potential toughening mechanisms during fibrin clot fracture. Notably, fibrin fibers exhibit rapid recoil from strains under 100% on submillisecond timescales, a phenomenon occurring thousands of times faster than protein refolding²⁴¹. Admittedly the detailed molecular processes remain to explore, we consider the breakage of knobs-hole interactions (or amine-carboxylate bonds)^{192,211} as a key mechanism, which is rate-dependent. This is likely to be accompanied by the breakage of certain covalent bonds, such as γ - γ -crosslinking and α - γ -crosslinking bonds) formed between monomers and oligomers¹⁶. Another possible toughening mechanism is the bonding and interactions between fibers under deformation⁶¹. They could influence the stiffness, dimension, and alignment of fibers, as well as the connectivity and density of the network, ultimately affecting the stress field and fracture toughness. The detailed contributions of these physical processes are important for future investigation.

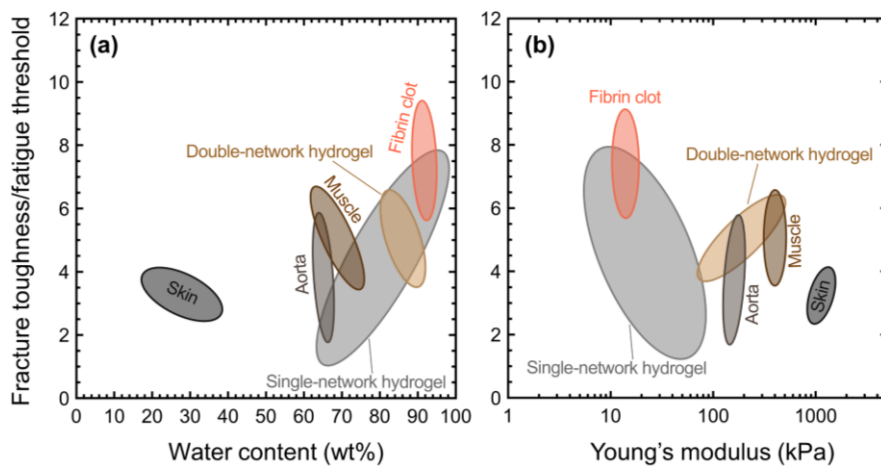


Figure 6-3 Comparative toughness enhancement ratio (fracture toughness over fatigue threshold) versus (a) water content and (b) Young's modulus for fibrin clots in this work, single- and double-network hydrogels^{205,206,208}, and other biological materials, including skin²⁰⁵, aorta²⁰⁶ and muscle²⁰⁷.

To put the toughening of fibrin clots under the context of soft materials, we compared the toughness ratio of fibrin clot with hydrogels and biological tissues, including skin, aorta and

muscle, as function of water content (Fig. 6-4a) and elastic modulus (Fig. 6-4b)^{205-208,242}. Although viscoelasticity is commonly seen among biological materials^{125,239,243-245}, fibrin clots stand out with a high toughening ratio, despite high water content (low solid content given fibrinogen level in bovine plasma is approximately w:v=0.5%²⁴⁶) and low Young's modulus. As a single-network fibrous hydrogel, fibrin clots outperform other single-network hydrogels and double-network hydrogels. This unique fracture property of fibrin clots deserves further investigation. This comparison can shed light on the energy dissipation potential of fibrin clots and offer a route enabling mimicking this material system for possible biomedical applications.

6.1.5 Adhesive fracture and cohesive fracture

Mechanical failure of blood clots could result in serious health issues such as excessive blood loss and thrombosis. Our study further investigates cohesive fracture as one of the failure modes. For bovine blood, the measured bulk fracture energy ($18.3 \pm 1.5 \text{ J/m}^2$) in pure shear tests was larger than the earlier measured values from lap shear (6.5 J/m^2) and edge notch (8 J/m^2 ; ovine blood) tests¹⁹³. Such differences could be in part due to the difference of testing mode and setup. As blood clot is extremely delicate, we designed a customized jig to test the blood clot with minimum handling, manipulation, and processing to maintain clot's structural integrity. Furthermore, we found that a crack length greater than 10 mm does not affect the fracture toughness since this was much larger than the fracto-sensitive length of the clot (estimated at $5.3 \text{ mm} \pm 0.5 \text{ mm}$).

In earlier studies, the focus has been predominantly on cohesive fracture within the bulk material, yet interfacial crack propagation, as an independent mode of failure, has been often overlooked. In this failure mechanism, the blood clot detaches from substrate tissues (such as skin or arteries), and through this process adhesive, cohesive and mixed-mode fracture can take place (Fig. 5-1). In comparison to fracture toughness within the bulk material (Fig. 5-3), we measured much lower interfacial fracture energy across all tested biological tissues (Fig. 5-2), suggesting a higher likelihood for interfacial fracture. This observation underscores the importance of adhesion in the blood clot failure. Our peeling tests further confirmed the predominance of adhesive fracture, with SEM imaging revealing only small residuals of the blood clot left on the substrate tissue (Fig. 5-7a). It is worth noting that mixed mode fracture when the platelet content was increased 3x from the normal concentration (Fig. 5-7b). We characterized interfacial and bulk fracture energies using different tests (peeling and pure shear), and a direct comparison of these values should be

approached with caution.

Interfacial fracture energy arises from both the surface-to-surface bonds between adjacent materials (i.e., intrinsic adhesion) as well as energy dissipation within the bulk material. Blood clots exhibit a rate-dependent mechanical response with a hysteresis of 46% (Fig. 5-4g), indicating a strong potential for internal energy dissipation, which in turn augments adhesion. Our finite element model for peeling tests reveals that eliminating bulk material dissipation (i.e., simulating an elastic response devoid of the Mullin effect) reduces the interfacial fracture energy by 31%, underscoring the coupling between surface interactions and internal material characteristics. This indicates that studying adhesion should not only include interfacial properties but also bulk material properties.

Our measurements indicate that among biological substrates, the blood clot had the largest adhesion to the muscle tissue and the least adhesion to the inner arterial lining (Fig. 5-2), a phenomenon that harmonizes with the clot's biological role. The natural design necessitates that blood exhibits minimal adhesion with the interior of blood vessels, facilitating smooth flow and mitigating clot formation. This is achieved through the production of anti-adhesive molecules such as heparan sulfate, prostacyclin, and nitric oxide by the endothelial cells within blood vessels, thereby inhibiting blood cells from adhering to the vessel walls²⁴⁷. Conversely, in muscle injury, the exposed collagen fibers in the vessel wall attract platelets to stop bleeding. This attraction is mediated by the von Willebrand factor acting as a bridge, while platelets can also bind directly to collagen via integrin $\alpha2\beta1$ and GPVI receptors²⁴⁷.

6.1.6 Rate dependency of clot fracture

Understanding the mechanical responses and fracture mechanics of blood clots under continuous dynamic loads, similar to the conditions posed by blood flow, is crucial. Our results demonstrated that the clot has a strong rate-dependent response (Fig. 5-2 and 5-3). Bulk fracture energy within the bulk material exhibited a consistent increase with an increasing loading rate (0.01 s⁻¹ and 1 s⁻¹ loading rate); Figure 5-2. On the other hand, interfacial fracture energy showed a rather different trend; while an increase in interfacial fracture energy was observed at smaller loading rates (from 0.01 s⁻¹ to 0.1 s⁻¹), the effect appeared to be small at larger rates (>0.1 s⁻¹); Figure 5-3. These time-dependent responses can be partly attributed to the poro-visco-elastic nature of the clot. In our mechanical tests, the poro-elastic time constant ($\tau = D^2/4Ek$, where τ is the time constant, D is

the characteristic length, and E and τ represent the elastic modulus and permeability) was estimated at 1 to 3 s, and given the applied loading rates, fluid had sufficient time to exit the tissue. The effect of poro-elasticity on fibrin clot fracture¹²⁸ was estimated at a maximum of 15%; therefore, the observed rate effects on bulk fracture energy are primarily due to the viscoelasticity of the fibrin network. As the rate increases, the fibrin network's viscoelastic response becomes more dominant, resulting in a more resilient clot structure due to increased inter-fibrin interactions, and strain-hardening.

6.1.7 Cell inclusions

Both RBC and platelets markedly influenced the fracture mechanics and mechanical properties of blood clots. Increasing the RBC content led to an elevation in the failure strain as well as its bulk/interfacial fracture energies without inducing additional hysteresis (Fig. 5-4). According to the general fracture mechanics theory, fracture toughness ($\Gamma = \Gamma_0 + \Gamma_D$) could be decoupled into two contributions: the breaking of interfacial bonds (intrinsic toughness; Γ_0) and the bulk material's ability to dissipate energy (Γ_D). Interestingly, our results show a weak dependence of the hysteresis (or energy dissipation) on the tested range of RBC content (Fig. 5-4g), indicating that RBCs directly impact Γ_0 . This is in alignment with finite element simulations, which demonstrated that an increase in Γ_0 augments the overall bulk/interfacial fracture energy of the material (Fig. 5-8). This rise in Γ_0 due to RBC might be attributed to the fact that the inclusion of RBCs results in a more organized fibrin network¹⁸. Our findings highlight the need for future studies to uncover the underlying mechanisms through which RBC enhances the intrinsic cohesive/adhesive fracture toughness.

The influence of platelets on the mechanical properties of blood clots^{27,108,124,175}, particularly on adhesion^{33,66,248}, provides key insights into clot behavior. The contractile elements within platelets, such as actin and myosin, allow them to induce contraction in the clot, generating a pre-stress/strain state²⁴⁹. In our pure shear tests, clots were constrained, resulting in pre-strain levels of 11%-15%. With an increase in platelet content, this pre-strain is amplified. Although one might expect that additional platelets could improve the structural integrity²⁵⁰, such potential improvement appears to be counterbalanced by the effects of platelet-induced contraction, resulting in a net reduction in the clot's bulk fracture energy (Fig. 5-6). Nonetheless, a higher platelet count significantly enhanced interfacial fracture energy by a factor of two (Fig. 5-6c). This also shifted failure mode

in peeling tests; while control samples (with normal platelet content) predominantly underwent adhesive fracture – as confirmed visually and via SEM imaging – an increased platelet content transitioned this behavior towards mixed-mode fracture within the bulk material (Fig. 5-6). These observations underline the critical role platelets play in modulating the mechanical behavior of clots, particularly adhesion property, as well as the complex interplay between platelet-induced pre-strain and the resulting impacts on clot strength and adhesion, thus providing valuable insights into clot formation, stability, and potential failure mechanisms.

6.1.8 Clinical relevance

Understanding the mechanics of blood clots, including the distinct roles of adhesive and cohesive fracture in clot failure and the impact of RBC and platelet counts, has important clinical implications. By providing insights into the complex mechanical responses of blood clots, the study could contribute to improving therapeutic strategies for clot-related diseases. Pathological conditions such as polycythemia and thrombocytopenia, characterized by abnormal RBC and platelet counts^{251,252}, respectively, are likely to alter the mechanical properties of clots, thereby influencing clot failure. Furthermore, the findings regarding the role of platelets and RBCs in clot adhesion and fracture toughness offer potential avenues for tailoring therapies based on individual patient's blood composition. The finite element model that accurately captures the mechanical behavior of blood clots under different conditions can be a valuable tool for predicting clot behavior and assessing the effectiveness of therapeutic strategies.

Consider the application of wound management. An ideal wound dressing should balance its adhesion to the tissue and clot; it should attach firmly to the surrounding tissue to efficiently stop bleeding, yet maintain minimal adhesion to the clot itself to avoid disruption and potential re-bleeding upon removal. However, gauze – the most common wound dressing material – seems to contradict this notion. In a skin injury, the gauze has almost zero adhesion to the skin, rendering it unable to adequately seal the wound site. Meanwhile, our peeling tests have shown that gauze exhibits the highest adhesion to the clot (Fig. 5-3). This elevated clot adherence can lead to cohesive breakage within the clot during dressing removal, triggering a re-bleeding event, a situation familiar to many healthcare practitioners and patients. These insights underscore the need for the development of novel wound dressing materials that better align with these ideal properties.

6.1.9 Limitations

The blood clot under study was formed under static conditions, whereas the clot formation under physiological conditions is a dynamic process. Influences such as thrombin flux and flow shear rate can impact fibrin network formation²⁵³, and consequently alter structural features of the blood clot, such as fibrin network isotropy/anisotropy. These factors could also potentially modify the mechanical properties of the clot^{87,254}. Despite these differences, thrombin-induced clots from bovine blood have demonstrated mechanical properties similar to those of human blood clots formed in arteries⁸⁷. However, it is worth noting that using *in vivo* formed clots for this study was not feasible due to restrictions related to sample size and technical considerations. The role of platelets in affecting the mechanical properties of the blood clot is also significant⁶⁸. However, the delay associated with shipping time, typically around 24 hours, is expected to render most platelets in the blood source inactive, which could influence the results^{255,256}. Our finite element modeling was rate-independent and also did not account for the effect of permanent deformation or plasticity^{102,257}, but given that we were examining a single rate, this assumption remained adequate for our study's purposes.

There has been extensive investigation into coagulation factors involved in clot formation, yet the roles and mechanisms of coagulation factors have not been touched in this thesis. Remarkably, blood clots possess the ability to self-assemble and organize into diverse architectures. *In vivo*, a natural blood clot is produced from a two-stage hemostasis process, known as primary and secondary hemostasis. Primary hemostasis is triggered by vessel injury, inducing endothelial activation, denudation, secretion, and deposition of von Willebrand factor (vWF). Additionally, collagen and tissue factor-bearing cells are exposed at the injury site, initiating platelet adhesion and activation¹⁸¹. Simultaneously, tissue factor exposure facilitates the propagation of the extrinsic pathway of coagulation, generating thrombin that activates various coagulation factors in the intrinsic pathway²⁵⁸. Activated platelets accumulate through fibrinogen-mediated interplay with platelet surface integrin, forming a platelet plug that arrests hemorrhage, marking the completion of primary hemostasis²⁵⁹. The surface of aggregated active platelets brings negatively charged phospholipids that enable colocalization and additional activation of clotting factors to create the prothrombinase complex in presence of calcium chloride, resulting in an amplified generation of thrombin that breaks down fibrinogen into fibrin; fibrin self-assembles and undergoes further

crosslinking by the activity of Factor XIIIa to form a packed biopolymeric mesh that creates the hemostatic clot and halts loss of blood components, marking the completion of secondary hemostasis⁶⁵. It could offer valuable insights to propel further investigations into the impact of hemostasis mechanisms on the fracture behavior of blood clots.

The pure shear test method adopted in this work relies on an approximate loading condition assumption. The pure shear test was first proposed by Rivlin and Thomas¹⁴⁸ to test fracture of rubber samples and has been broadly adopted to characterize gel fracture¹²⁵. The undeformed sample in our work is a long thin strip of width $L=40$ mm, height $H=4$ mm and thickness $b=3$ mm with $L \gg H$ and b . A long crack of length $c=10$ mm ($c \gg H$) lies in the middle between the top and bottom boundaries of the strip which are clamped to the loading device. Typically, a uniform vertical displacement is imposed on the top and bottom of the strip. The condition that L and $c \gg H$ enables the translational invariance of the stress and strain fields, i.e. they remain unchanged in a moving coordinate system centered at the crack tip as the crack propagates. In addition, if $L \gg c$, the material far ahead of the crack tip is under spatially uniform deformation with principle stretches $\lambda_1 = 1$, $\lambda_2 = \lambda_s$, $\lambda_3 = 1/\lambda_s$, where the subscripts 1, 2, and 3 denote the direction parallel to the undeformed crack, perpendicular to the undeformed crack and along the thickness, respectively. According to observations during experiments, a sign of clot contraction and pre-strain occurred in the clot samples. While the fracture toughness calculation in this thesis under a pure shear configuration does not involve constitutive equations, additional clarification is needed on how clot contraction and pre-strain influence the stress-strain field during fracture tests.

6.2 Future work

Combining knowledge of fracture mechanics and biomaterial engineering could help develop advanced hemostasis strategies to effectively stem bleeding in various severe hemorrhage conditions. Although mechanical properties of blood components have been studied extensively, the fracture properties of blood clots remain largely unexplored, which are mission-critical to hemostasis as well as developing approaches for diagnosis, therapy, and treatment. Therefore, the aim of this work is to establish the foundational knowledge of the mechanics of blood clot fracture, yet questions remain within the scope of this field and urge for deeper studies.

The biomechanics of blood clots is intricated by the multiple blood cells and coagulation factors involved in coagulation that may determine the multiscale structural features, mechanical

properties, and biological functions. Future work is needed to test whole blood clots, where blood cells such as red blood cells and platelets might affect the fracture and fatigue behavior. Notably, von Willebrand factor (VWF) is an adhesive protein that contributes to platelet function by mediating the initiation and progression of thrombus formation at sites of vascular injury²⁶⁰. Due to its biochemical functions, vWF is believed to play a vital role in the adhesion of blood clots. Hence, future research should investigate the influence of vWF on the adhesion of blood clots.

Furthermore, advancements in constitutive and computational modeling methods would have a significant impact on understanding and predicting the mechanical behavior of blood clots particularly the fracture properties. Most of the constitutive models described above are built upon an assumption that the material is incompressible, isotropic, and homogeneous. Results from the experiments, however, showed that this assumption is questionable under the context of blood clots^{54,98}. Moreover, the constitutive model could capture the mechanics of cells and the effects of active cell components, such as platelets, which play vital roles in the cohesive and adhesive fracture of blood clots. Therefore, despite the advance, there is still much room for improvement in the development of constitutive models for clots. Besides, existing approaches to modeling macroscopic blood clots often overlook the mechanics of individual fibers, which determine the structure of the clot. Multiscale models combine material behavior at the macro and micro scales, giving a more detailed representation of the material behavior. Through coupling the fracture and biochemistry of blood clots, the developed knowledge could inform the development of advanced hemostatic technology of diagnosis, therapy, and treatment.

Chapter 7 Concluding remarks

In this thesis, we first extensively reviewed the challenges and background of coagulation and blood clot composition, summarizing existing studies and proposing future directions for advancing biomechanical understanding. We highlighted the rationale, objectives, and hypotheses. The experimental methods covered blood clot initiation, sample preparation, mechanical characterization, image analysis, and finite element modeling, along with ethical considerations and statistical analysis.

We investigated the fracture mechanics of human blood clots in Chapter 3. We measured the fracture energy of human WB clots and PPP clots, as well as the critical length scales of blood clots near the crack tip. We characterized the fracture energy with modified lap-shear tests and found that it was insensitive to the sample size. The fracture energy measured with the lap-shear and DCB tests was in good agreement. We further calculated the dissipative length scale and the nonlinear elastic length scale of the blood clots. They provide valuable insights into the stress-strain field in the crack tip during blood clot rupture. Our study concludes that blood clots are highly deformable, dissipative, and relatively flaw-insensitive. The underlying mechanisms are expected to link with the elastic nonlinearity and dissipation of the fibrin network and the blood cells, which calls for future investigations. This work will motivate further investigation of the fracture mechanics and properties of blood clots, and may propel the development of improved bioadhesive and hemostatic materials.

Fibrin clot is a soft fibrous gel, exhibiting nonlinear mechanical responses under complex physiological loads. It is the main load-bearing constituent of blood clots where red blood cells, platelets and other cells are trapped. How the fibrin clot fractures under complex mechanical loads is critical for hemostasis and thrombosis. Therefore, we first characterized the fatigue threshold and rate-dependent fracture toughness of fibrin clots by conducting cyclic fatigue and monotonic variable rate loading tests. To rationalize our results, we reconstructed the 3D geometry of the fibrin network and implemented the morphometric quantification, and fed the measured values into a semi-empirical model to estimate the fatigue threshold of fibrin clots. Further, we interpreted the rate-dependent fracture toughness by adopting the viscoelastic fracture toughness model. The theoretical predictions agreed well with the experimental data. We compared and highlighted the

toughness enhancement ratio of fibrin clots measured in this work with other similar biomaterial systems. Our main conclusions are as follows: (1) Fatigue crack growth in fibrin clots occurs when the applied loading exceeds the fatigue threshold 1.66 J/m^2 or the applied strain is larger than 65%. (2) The semi-empirical model extended from the Lake-Thomas model, parameterized with our structural characterization, could output the fatigue threshold matching that obtained in cyclic fatigue tests. (3) The hierarchical microstructure of fibrin fibers plays an important role in the fatigue and rupture resistance of fibrin clots. (4) The overall fracture toughness of fibrin clots substantially increased with the loading rate and the crack growth rate. (5) The scission of fibers at the vicinity of the crack tip involved in fatigue resistance (threshold) as well as the viscoelastic bulk energy dissipation were two main toughening mechanisms determining the overall fracture toughness and rupture resistance of fibrin clots. These outcomes advance the understanding of fibrin clot fracture under complex loading and offer valuable insights into the fracture of fibrous materials and blood clots, which could facilitate material development and modeling for wound healing, hemostasis, and tissue regeneration applications.

Fracture of blood clots within vascular systems and at injury sites could cause life-threatening conditions. The fracture modalities include fracture within the clot's bulk material or at the clot-tissue interface. While the cohesive fracture within the bulk material has already been characterized, the adhesive fracture – as an independent and sophisticated mode of failure – is still unexplored. To further explore the pivotal role of rate-dependent response, RBCs, and platelets in clot fracture modalities, we investigated the cohesive and adhesive fracture mechanics of bovine blood clots in Chapter 5. The bulk fracture energy exhibited significant rate-dependency while remaining minimally impacted by variations in crack length. Interfacial fracture energy also increased with the loading rate although this influence tapered off at higher rates. In addition, we found that gauze exhibited the highest adhesion to the clot (larger than other biological substrates) and paradoxically failed to adhere to the skin to efficiently seal the wound, risking disruption and potential re-bleeding upon removal. An elevation in RBC content amplified both interfacial and bulk fracture energy, without influencing the clot's hysteresis, and this phenomenon – as substantiated by our finite element model – could be attributed to an increase in intrinsic toughness. Moreover, elevating the platelet content enhances interfacial fracture energy to a level where the failure mode in the peeling tests shifted from adhesive to mixed-mode fracture, underscoring the crucial role platelets of in adhesion. We also developed a finite element model which captured the

complex loading-unloading blood clots behavior in different loading conditions as well as crack propagation within the bulk material and interface. These findings significantly expand our understanding of clot mechanics, bearing important clinical implications that may optimize the management of clot-related disorders, and pave the way for developing innovative, more efficient wound dressings.

Overall, this thesis represents a comprehensive investigation into the fracture mechanics of blood clots, shedding light on the intricate behavior of these naturally derived bioadhesives. The studies conducted by the author have uncovered the dissipative nature of blood clots, their fatigue threshold, and rate-dependent fracture toughness, as well as the crucial roles played by major blood constituents of fibrin, RBCs and platelets. In addition to the scientific contribution to biomechanics, these findings lay the groundwork for the development of improved bioadhesives and hemostatic materials, with potential applications in wound healing, hemostasis, and tissue regeneration.

Bibliography

1. Hickman, D. A., Pawlowski, C. L., Sekhon, U. D. S., Marks, J. & Gupta, A. S. Biomaterials and Advanced Technologies for Hemostatic Management of Bleeding. *Adv. Mater.* **30** (2018).
2. Spahn, D. R. *et al.* Management of bleeding and coagulopathy following major trauma: an updated European guideline. *Crit. Care* **17**, R76 (2013).
3. Kauvar, D. S., Lefering, R. & Wade, C. E. Impact of hemorrhage on trauma outcome: an overview of epidemiology, clinical presentations, and therapeutic considerations. *J. Trauma Acute Care Surg.* **60**, S3-S11 (2006).
4. Park, J. & Koh, J.-w. Era of Bloodless Surgery: Spotlights on Hemostatic Materials and Techniques. *Hanyang Med. Rev.* **38**, 3-15 (2018).
5. Tran, R. *et al.* Biomechanics of haemostasis and thrombosis in health and disease: from the macro- to molecular scale. *J. Cell. Mol. Med.* **17**, 579-596 (2013).
6. Weisel, J. W. Biomechanics in hemostasis and thrombosis. *J. Thromb. Haemost.* **8**, 1027-1029 (2010).
7. Weisel, J. W. Structure of fibrin: impact on clot stability. *J. Thromb. Haemost.* **5**, 116-124 (2007).
8. Evans, P. *et al.* Rheometry and associated techniques for blood coagulation studies. *Med. Eng. Phys.* **30**, 671-679 (2008).
9. Janmey, P. A., Winer, J. P. & Weisel, J. W. Fibrin gels and their clinical and bioengineering applications. *J. R. Soc. Interface* **6**, 1-10 (2009).
10. Mosesson, M. W. Fibrinogen and fibrin structure and functions. *J. Thromb. Haemost.* **3**, 1894-1904 (2005).
11. Welsch, N., Brown, A. C., Barker, T. H. & Lyon, L. A. Enhancing clot properties through fibrin-specific self-cross-linked PEG side-chain microgels. *Colloids Surf. B* **166**, 89-97 (2018).
12. Kattula, S., Byrnes, J. R. & Wolberg, A. S. Fibrinogen and fibrin in hemostasis and thrombosis. *Arterioscler. Thromb. Vasc. Biol.* **37**, e13-e21 (2017).
13. Weisel, J. W. Fibrin assembly. Lateral aggregation and the role of the two pairs of fibrinopeptides. *Biophys. J.* **50**, 1079-1093 (1986).

14. Weisel, J. W. Fibrinogen and fibrin. *Adv. Protein Chem.* **70**, 247-299 (2005).
15. Undas, A. & Ariëns, R. A. Fibrin clot structure and function: a role in the pathophysiology of arterial and venous thromboembolic diseases. *Arterioscler. Thromb. Vasc. Biol.* **31**, e88-e99 (2011).
16. Weisel, J. W. & Litvinov, R. I. Fibrin Formation, Structure and Properties. *Subcell. Biochem.* **82**, 405-456 (2017).
17. Weisel, J. W. & Nagaswami, C. Computer modeling of fibrin polymerization kinetics correlated with electron microscope and turbidity observations: clot structure and assembly are kinetically controlled. *Biophys. J.* **63**, 111-128 (1992).
18. Gersh, K. C., Nagaswami, C. & Weisel, J. W. Fibrin network structure and clot mechanical properties are altered by incorporation of erythrocytes. *Thromb. Haemost.* **102**, 1169-1175 (2009).
19. Cines, D. B. *et al.* Clot contraction: compression of erythrocytes into tightly packed polyhedra and redistribution of platelets and fibrin. *Blood* **123**, 1596-1603 (2014).
20. Varin, R. *et al.* Whole blood clots are more resistant to lysis than plasma clots-greater efficacy of rivaroxaban. *Thromb. Res.* **131**, 100-109 (2013).
21. Litvinov, R. I. & Weisel, J. W. Role of red blood cells in haemostasis and thrombosis. *ISBT Sci. Ser.* **12**, 176-183 (2017).
22. Rother, R. P., Bell, L., Hillmen, P. & Gladwin, M. T. The clinical sequelae of intravascular hemolysis and extracellular plasma hemoglobin: a novel mechanism of human disease. *Jama* **293**, 1653-1662 (2005).
23. Camus, S. M. *et al.* Circulating cell membrane microparticles transfer heme to endothelial cells and trigger vasoocclusions in sickle cell disease. *Blood* **125**, 3805-3814 (2015).
24. van Beers, E. J. *et al.* Circulating erythrocyte-derived microparticles are associated with coagulation activation in sickle cell disease. *Haematologica* **94**, 1513-1519 (2009).
25. Gao, Y., Lv, L., Liu, S., Ma, G. & Su, Y. Elevated levels of thrombin-generating microparticles in stored red blood cells. *Vox Sang.* **105**, 11-17 (2013).
26. Wohner, N. *et al.* Lytic resistance of fibrin containing red blood cells. *Arterioscler. Thromb. Vasc. Biol.* **31**, 2306-2313 (2011).
27. Lam, W. A. *et al.* Mechanics and contraction dynamics of single platelets and implications for clot stiffening. *Nat. Mater.* **10**, 61-66 (2011).

28. Jiroušková, M., Jaiswal, J. K. & Collier, B. S. Ligand density dramatically affects integrin α IIb β 3-mediated platelet signaling and spreading. *Blood* **109**, 5260-5269 (2007).
29. Jen, C. J. & McIntire, L. V. The structural properties and contractile force of a clot. *Cell Motil.* **2**, 445-455 (1982).
30. Greulich, P. E., Carr, M. E., Zekert, S. L. & Dent, R. M. Quantitative assessment of platelet function and clot structure in patients with severe coronary artery disease. *Am. J. Med. Sci.* **307**, 15-20 (1994).
31. Tutwiler, V. *et al.* Kinetics and mechanics of clot contraction are governed by the molecular and cellular composition of the blood. *Blood* **127**, 149-159 (2016).
32. Le Minh, G. *et al.* Impaired contraction of blood clots as a novel prothrombotic mechanism in systemic lupus erythematosus. *Clin. Sci.* **132**, 243-254 (2018).
33. Qiu, Y. *et al.* Platelet mechanosensing of substrate stiffness during clot formation mediates adhesion, spreading, and activation. *PNAS* **111**, 14430-14435 (2014).
34. Myers, D. R. *et al.* Single-platelet nanomechanics measured by high-throughput cytometry. *Nat. Mater.* **16**, 230-235 (2017).
35. Kita, A. *et al.* Microenvironmental geometry guides platelet adhesion and spreading: a quantitative analysis at the single cell level. *PloS one* **6**, e26437 (2011).
36. Stalker, T. J. *et al.* Hierarchical organization in the hemostatic response and its relationship to the platelet-signaling network. *Blood* **121**, 1875-1885 (2013).
37. Jiang, S., Liu, S., Lau, S. & Li, J. Hemostatic biomaterials to halt non-compressible hemorrhage. *J. Mater. Chem. B* **10**, 7239-7259 (2022).
38. Kriz, N., Rinder, C. S. & Rinder, H. M. Physiology of hemostasis: with relevance to current and future laboratory testing. *Clin. Lab. Med.* **29**, 159-174, v (2009).
39. Ruggeri, Z. M. & Mendolicchio, G. L. Adhesion Mechanisms in Platelet Function. *Circ. Res.* **100**, 1673-1685 (2007).
40. Tomokiyo, K. *et al.* Von Willebrand factor accelerates platelet adhesion and thrombus formation on a collagen surface in platelet-reduced blood under flow conditions. *Blood* **105**, 1078-1084 (2005).
41. Hoffman, M. Remodeling the blood coagulation cascade. *J. Thromb. Thrombolysis* **16**, 17-20 (2003).
42. Versteeg, H. H., Heemskerk, J. W., Levi, M. & Reitsma, P. H. New fundamentals in

- hemostasis. *Physiol Rev.* **93**, 327-358 (2013).
43. Periyah, M. H., Halim, A. S. & Mat Saad, A. Z. Mechanism Action of Platelets and Crucial Blood Coagulation Pathways in Hemostasis. *Int. J. Hematol. Oncol. Stem Cell Res.* **11**, 319-327 (2017).
 44. Weisel, J. W. & Litvinov, R. I. The biochemical and physical process of fibrinolysis and effects of clot structure and stability on the lysis rate. *Cardiovasc. Hematol. Agents Med. Chem.* **6**, 161-180 (2008).
 45. van Herrewegen, F., Meijers, J. C., Peters, M. & van Ommen, C. H. Clinical practice: the bleeding child. Part II: disorders of secondary hemostasis and fibrinolysis. *Eur. J. Pediatr.* **171**, 207-214 (2012).
 46. Evans, P. A., Hawkins, K., Williams, P. R. & Williams, R. L. Rheometrical detection of incipient blood clot formation by Fourier transform mechanical spectroscopy. *J. Nonnewton Fluid Mech.* **148**, 122-126 (2008).
 47. Kumar, V. & Chapman, J. R. Whole blood thrombin: development of a process for intra-operative production of human thrombin. *J. Extra Corpor. Technol.* **39**, 18-23 (2007).
 48. Weisel, J. W. The mechanical properties of fibrin for basic scientists and clinicians. *Biophys. Chem.* **112**, 267-276 (2004).
 49. Liu, W. *et al.* Fibrin fibers have extraordinary extensibility and elasticity. *Science* **313**, 634-634 (2006).
 50. Weisel, J. W. Enigmas of blood clot elasticity. *Science* **320**, 456-457 (2008).
 51. Pratt, K. P., Côté, H. C. F., Chung, D. W., Stenkamp, R. E. & Davie, E. W. The primary fibrin polymerization pocket: Three-dimensional structure of a 30-kDa C-terminal γ chain fragment complexed with the peptide Gly-Pro-Arg-Pro. *PNAS* **94**, 7176-7181 (1997).
 52. Litvinov, R. I., Gorkun, O. V., Owen, S. F., Shuman, H. & Weisel, J. W. Polymerization of fibrin: specificity, strength, and stability of knob-hole interactions studied at the single-molecule level. *Blood* **106**, 2944-2951 (2005).
 53. Kononova, O. *et al.* Molecular mechanisms, thermodynamics, and dissociation kinetics of knob-hole interactions in fibrin. *J. Biol. Chem.* **288**, 22681-22692 (2013).
 54. Brown, A. E. X., Litvinov, R. I., Discher, D. E., Purohit, P. K. & Weisel, J. W. Multiscale mechanics of fibrin polymer: gel stretching with protein unfolding and loss of water. *Science* **325**, 741-744 (2009).

55. Weisel, J. W. Cross-linked gamma-chains in a fibrin fibril are situated transversely between its strands. *J. Thromb. Haemost.* **2**, 1467-1469; discussion 1469-1473 (2004).
56. Rosenfeld, M. A. *et al.* Covalent structure of single-stranded fibrin oligomers cross-linked by FXIIIa. *Biochem. Biophys. Res. Commun.* **461**, 408-412 (2015).
57. Matsuka, Y. V., Medved, L. V., Migliorini, M. M. & Ingham, K. C. Factor XIIIa-catalyzed cross-linking of recombinant α C fragments of human fibrinogen. *Biochemistry* **35**, 5810-5816 (1996).
58. Standeven, K. F. *et al.* Functional analysis of fibrin γ -chain cross-linking by activated factor XIII: determination of a cross-linking pattern that maximizes clot stiffness. *Blood* **110**, 902-907 (2007).
59. Chernysh, I. N., Nagaswami, C., Purohit, P. K. & Weisel, J. W. Fibrin clots are equilibrium polymers that can be remodeled without proteolytic digestion. *Sci. Rep.* **2**, 1-6 (2012).
60. Lim, B. C., Ariëns, R. A., Carter, A. M., Weisel, J. W. & Grant, P. J. Genetic regulation of fibrin structure and function: complex gene-environment interactions may modulate vascular risk. *The Lancet* **361**, 1424-1431 (2003).
61. Britton, S. *et al.* Contribution of nascent cohesive fiber-fiber interactions to the non-linear elasticity of fibrin networks under tensile load. *Acta Biomater.* **94**, 514-523 (2019).
62. Kurniawan, N. A. *et al.* Fibrin networks support recurring mechanical loads by adapting their structure across multiple scales. *Biophys. J.* **111**, 1026-1034 (2016).
63. Vos, B. E. *et al.* Programming the mechanics of cohesive fiber networks by compression. *Soft matter* **13**, 8886-8893 (2017).
64. Qiu, Y., Myers, D. R. & Lam, W. A. The biophysics and mechanics of blood from a materials perspective. *Nat. Rev. Mater.* **4**, 294-311 (2019).
65. Marcus E. Carr, J. Development of Platelet Contractile Force as a Research and Clinical Measure of Platelet Function. *Cell Biochem. Biophys.* **38**, 55-78 (2003).
66. Chan, K. Y. T. *et al.* The adhesion of clots in wounds contributes to hemostasis and can be enhanced by coagulation factor XIII. *Sci. Rep.* **10**, 20116 (2020).
67. Bai, R., Yang, J. & Suo, Z. Fatigue of hydrogels. *Eur. J. Mech. A/Solids* **74**, 337-370 (2019).
68. Pathare, S. J., Eng, W., Lee, S.-J. J. & Ramasubramanian, A. K. Fibrin prestress due to platelet aggregation and contraction increases clot stiffness. *Biophys. Rep.* **1**, 100022

- (2021).
69. Sugerman, G. P. *et al.* A whole blood thrombus mimic: Constitutive behavior under simple shear. *J. Mech. Behav. Biomed. Mater.* **115**, 104216 (2021).
 70. He, D., Kim, D. A., Ku, D. N. & Hu, Y. Viscoporoelasticity of coagulation blood clots. *Extreme Mech. Lett.* **56**, 101859 (2022).
 71. Tutwiler, V. *et al.* Rupture of blood clots: Mechanics and pathophysiology. *Sci. Adv.* **6**, eabc0496 (2020).
 72. Di Martino, E. *et al.* Biomechanics of abdominal aortic aneurysm in the presence of endoluminal thrombus: experimental characterisation and structural static computational analysis. *Eur. J. Vasc. Endovasc. Surg.* **15**, 290-299 (1998).
 73. Gasser, T. C., Görgülü, G., Folkesson, M. & Swedenborg, J. Failure properties of intraluminal thrombus in abdominal aortic aneurysm under static and pulsating mechanical loads. *J. Vasc. Surg.* **48**, 179-188 (2008).
 74. Geest, J. P. V., Sacks, M. S. & Vorp, D. A. A planar biaxial constitutive relation for the luminal layer of intra-luminal thrombus in abdominal aortic aneurysms. *J. Biomech.* **39**, 2347-2354 (2006).
 75. Kavanagh, E. G., Grace, P. A., McGloughlin, T. M. & Doyle, B. J. The biaxial mechanical behaviour of abdominal aortic aneurysm intraluminal thrombus: classification of morphology and the determination of layer and region specific properties. *J. Biomech.* **47**, 1430-1437 (2014).
 76. Teng, Z. *et al.* Layer-and direction-specific material properties, extreme extensibility and ultimate material strength of human abdominal aorta and aneurysm: a uniaxial extension study. *Ann. Biomed. Eng.* **43**, 2745-2759 (2015).
 77. Wang, D. H., Makaroun, M., Webster, M. W. & Vorp, D. A. Mechanical properties and microstructure of intraluminal thrombus from abdominal aortic aneurysm. *J. Biomech. Eng.* **123**, 536-539 (2001).
 78. Robinson, R. A. *et al.* Limitations of using synthetic blood clots for measuring in vitro clot capture efficiency of inferior vena cava filters. *Med. devices (Auckl.)* **6**, 49 (2013).
 79. Duffy, S. *et al.* Novel methodology to replicate clot analogs with diverse composition in acute ischemic stroke. *J. Neurointerv. Surg.* **9**, 486-491 (2017).
 80. Gralla, J. *et al.* Mechanical Thrombectomy for Acute Ischemic Stroke: Thrombus–Device

- Interaction, Efficiency, and Complications In Vivo. *Stroke* **37**, 3019-3024 (2006).
81. Karšaj, I. & Humphrey, J. D. A mathematical model of evolving mechanical properties of intraluminal thrombus. *Biorheology* **46**, 509-527 (2009).
 82. Ryan, E. A., Mockros, L. F., Weisel, J. W. & Lorand, L. Structural origins of fibrin clot rheology. *Biophys. J.* **77**, 2813-2826 (1999).
 83. Ashton, J. H., Geest, J. P. V., Simon, B. R. & Haskett, D. G. Compressive mechanical properties of the intraluminal thrombus in abdominal aortic aneurysms and fibrin-based thrombus mimics. *J. Biomech.* **42**, 197-201 (2009).
 84. Krasokha, N. *et al.* Mechanical properties of blood clots—a new test method. *Materialwiss. Werkstofftech.* **41**, 1019-1024 (2010).
 85. Lai, V. K., Lake, S. P., Frey, C. R., Tranquillo, R. T. & Barocas, V. H. Mechanical behavior of collagen-fibrin co-gels reflects transition from series to parallel interactions with increasing collagen content. *J. Biomech. Eng.* **134**, 011004 (2012).
 86. Xie, H. *et al.* Correspondence of ultrasound elasticity imaging to direct mechanical measurement in aging DVT in rats. *Ultrasound Med. Biol.* **31**, 1351-1359 (2005).
 87. Chueh, J. Y. *et al.* Mechanical characterization of thromboemboli in acute ischemic stroke and laboratory embolus analogs. *Am. J. Neuroradiol.* **32**, 1237-1244 (2011).
 88. Kim, O. V., Litvinov, R. I., Weisel, J. W. & Alber, M. S. Structural basis for the nonlinear mechanics of fibrin networks under compression. *Biomaterials* **35**, 6739-6749 (2014).
 89. Saldívar, E., Orje, J. N. & Ruggeri, Z. M. Tensile destruction test as an estimation of partial proteolysis in fibrin clots. *Am. J. Hematol.* **71**, 119-127 (2002).
 90. van Dam, E. A. *et al.* Non-linear viscoelastic behavior of abdominal aortic aneurysm thrombus. *Biomech. Model. Mechanobiol.* **7**, 127-137 (2008).
 91. Sugerman, G. P., Parekh, S. H. & Rausch, M. K. Nonlinear, dissipative phenomena in whole blood clot mechanics. *Soft Matter* **16**, 9908-9916 (2020).
 92. Liu, W., Carlisle, C. R., Sparks, E. A. & Guthold, M. The mechanical properties of single fibrin fibers. *J. Thromb. Haemost.* **8**, 1030-1036 (2010).
 93. Litvinov, R. I. & Weisel, J. W. Fibrin mechanical properties and their structural origins. *Matrix Biol.* **60-61**, 110-123 (2017).
 94. Johnson, S., McCarthy, R., Gilvarry, M., McHugh, P. E. & McGarry, J. P. Investigating the Mechanical Behavior of Clot Analogues Through Experimental and Computational

- Analysis. *Ann. Biomed. Eng.* **49**, 420-431 (2021).
95. Lakshmanan, R. S., Efremov, V., O'Donnell, J. S. & Killard, A. J. Measurement of the viscoelastic properties of blood plasma clot formation in response to tissue factor concentration-dependent activation. *Anal. Bioanal. Chem.* **408**, 6581-6588 (2016).
 96. Johnson, S. *et al.* Review of Mechanical Testing and Modelling of Thrombus Material for Vascular Implant and Device Design. *Ann. Biomed. Eng.* **45**, 2494-2508 (2017).
 97. van Dam, E. A. *et al.* Determination of linear viscoelastic behavior of abdominal aortic aneurysm thrombus. *Biorheology* **43**, 695-707 (2006).
 98. van Kempen, T. H., Peters, G. W. & van de Vosse, F. N. A constitutive model for the time-dependent, nonlinear stress response of fibrin networks. *Biomech. Model. Mechanobiol.* **14**, 995-1006 (2015).
 99. Schmitt, C., Henni, A. H. & Cloutier, G. Characterization of blood clot viscoelasticity by dynamic ultrasound elastography and modeling of the rheological behavior. *J. Biomech.* **44**, 622-629 (2011).
 100. Slaboch, C. L., Alber, M. S., Rosen, E. D. & Ovaert, T. C. Mechano-rheological properties of the murine thrombus determined via nanoindentation and finite element modeling. *J. Mech. Behav. Biomed. Mater.* **10**, 75-86 (2012).
 101. Rausch, M. K., Sugerman, G. P., Kakaletsis, S. & Dortdivanlioglu, B. Hyper-viscoelastic damage modeling of whole blood clot under large deformation. *Biomech. Model. Mechanobiol.*, 1-13 (2021).
 102. van Kempen, T. H., Donders, W. P., van de Vosse, F. N. & Peters, G. W. A constitutive model for developing blood clots with various compositions and their nonlinear viscoelastic behavior. *Biomech. Model. Mechanobiol.* **15**, 279-291 (2016).
 103. Kaibara, M. & Fukada, E. Dynamic viscoelastic study for the structure of fibrin networks in the clots of blood and plasma. *Biorheology* **6**, 329-339 (1970).
 104. Gerth, C., Roberts, W. W. & Ferry, J. D. Rheology of fibrin clots II: Linear viscoelastic behavior in shear creep. *Biophys. Chem.* **2**, 208-217 (1974).
 105. Kim, O. V. *et al.* Foam-like compression behavior of fibrin networks. *Biomech. Model. Mechanobiol.* **15**, 213-228 (2016).
 106. Chaudhuri, O., Cooper-White, J., Janmey, P. A., Mooney, D. J. & Shenoy, V. B. Effects of extracellular matrix viscoelasticity on cellular behaviour. *Nature* **584**, 535-546 (2020).

107. Blombäck, B. & Okada, M. Fibrin gel structure and clotting time. *Thromb. Res.* **25**, 51-70 (1982).
108. Tutwiler, V., Wang, H., Litvinov, R. I., Weisel, J. W. & Shenoy, V. B. Interplay of Platelet Contractility and Elasticity of Fibrin/Erythrocytes in Blood Clot Retraction. *Biophys. J.* **112**, 714-723 (2017).
109. Zheng, X., Yazdani, A., Li, H., Humphrey, J. D. & Karniadakis, G. E. A three-dimensional phase-field model for multiscale modeling of thrombus biomechanics in blood vessels. *PLoS Comput. Biol.* **16**, e1007709 (2020).
110. Xu, S. *et al.* Model predictions of deformation, embolization and permeability of partially obstructive blood clots under variable shear flow. *J. R. Soc. Interface* **14** (2017).
111. Ghezelbash, F., Liu, S., Shirazi-Adl, A. & Li, J. Blood clot behaves as a poro-visco-elastic material. *J. Mech. Behav. Biomed. Mater.*, 105101 (2022).
112. Hu, Y. & Suo, Z. Viscoelasticity and poroelasticity in elastomeric gels. *Acta Mech. Solida Sin.* **25**, 441-458 (2012).
113. Hu, Y., Zhao, X., Vlassak, J. J. & Suo, Z. Using indentation to characterize the poroelasticity of gels. *Appl. Phys. Lett.* **96**, 121904 (2010).
114. Zhao, X., Huebsch, N., Mooney, D. J. & Suo, Z. Stress-relaxation behavior in gels with ionic and covalent crosslinks. *J. Appl. Phys.* **107**, 063509 (2010).
115. Puig-De-Morales-Marinkovic, M., Turner, K. T., Butler, J. P., Fredberg, J. J. & Suresh, S. Viscoelasticity of the human red blood cell. *Am. J. Physiol. Cell Physiol.* **293**, C597-C605 (2007).
116. Moeendarbary, E. *et al.* The cytoplasm of living cells behaves as a poroelastic material. *Nat. Mater.* **12**, 253-261 (2013).
117. Janmey, P. A., Amis, E. J. & Ferry, J. D. Rheology of fibrin clots. VI. Stress relaxation, creep, and differential dynamic modulus of fine clots in large shearing deformations. *J. Rheol.* **27**, 135-153 (1983).
118. Undas, A. *et al.* Fibrin clot properties are altered in patients with chronic obstructive pulmonary disease. *Thromb. Haemost.* **102**, 1176-1182 (2009).
119. Undas, A. *et al.* Reduced clot permeability and susceptibility to lysis in patients with acute coronary syndrome: effects of inflammation and oxidative stress. *Atherosclerosis* **196**, 551-557 (2008).

120. Undas, A. *et al.* Altered fibrin clot structure/function in patients with idiopathic venous thromboembolism and in their relatives. *Blood* **114**, 4272-4278 (2009).
121. Pieters, M. *et al.* An international study on the standardization of fibrin clot permeability measurement: methodological considerations and implications for healthy control values. *J. Thromb. Haemost.* **10**, 2179-2181 (2012).
122. Drabik, L., Wołkow, P. & Undas, A. Fibrin Clot Permeability as a Predictor of Stroke and Bleeding in Anticoagulated Patients With Atrial Fibrillation. *Stroke* **48**, 2716-2722 (2017).
123. Frączek, P., Krzysztofik, M., Stanisiz, A. & Undas, A. Clinical outcomes and plasma clot permeability and lysability in patients with venous thromboembolism on rivaroxaban: a cohort study. *Pol. Arch. Intern. Med.* **129** (2019).
124. Wufsus, A. R., Macera, N. E. & Neeves, K. B. The Hydraulic Permeability of Blood Clots as a Function of Fibrin and Platelet Density. *Biophys. J.* **104**, 1812-1823 (2013).
125. Long, R. & Hui, C.-Y. Fracture toughness of hydrogels: measurement and interpretation. *Soft Matter* **12**, 8069-8086 (2016).
126. Savushkin, A. Clots of blood plasma. *J. Eng. Phys. Thermophys.* **76**, 645-647 (2003).
127. Riha, P., Wang, X., Liao, R. & Stoltz, J. Elasticity and fracture strain of whole blood clots. *Clin. Hemorheol. Microcirc.* **21**, 45-49 (1999).
128. Garyfallogiannis, K. *et al.* Fracture toughness of fibrin gels as a function of protein volume fraction: Mechanical origins. *Acta Biomater.* **159**, 49-62 (2023).
129. Sierra, D. H., Eberhardt, A. W. & Lemons, J. E. Failure characteristics of multiple-component fibrin-based adhesives. *J. Biomed. Mater. Res.* **59**, 1-11 (2002).
130. Hart, R. G. *et al.* Embolic strokes of undetermined source: the case for a new clinical construct. *Lancet Neurol.* **13**, 429-438 (2014).
131. Xu, Z., Kamocka, M., Alber, M. & Rosen, E. D. Computational approaches to studying thrombus development. *Arterioscler. Thromb. Vasc. Biol.* **31**, 500-505 (2011).
132. Bodnar, T. & Sequeira, A. Numerical simulation of the coagulation dynamics of blood. *Comput. Math. Methods Med.* **9**, 83-104 (2008).
133. Kim, E. *et al.* Correlation between fibrin network structure and mechanical properties: an experimental and computational analysis. *Soft Matter* **7** (2011).
134. Hrapko, M., Van Dommelen, J., Peters, G. & Wismans, J. The mechanical behaviour of brain tissue: large strain response and constitutive modelling. *Biorheology* **43**, 623-636

- (2006).
135. Weisel, J. W., Rixen, D., Koning, O., van Bockel, J. & Hamming, J. Development of fibrinous thrombus analogue for in-vitro abdominal aortic aneurysm studies. *J. Biomech.* **40**, 289-295 (2007).
 136. van Kempen, T. H. S., Bogaerds, A. C. B., Peters, G. W. M. & van de Vosse, F. N. A constitutive model for a maturing fibrin network. *Biophys. J.* **107**, 504-513 (2014).
 137. Babushkina, E. S., Bessonov, N. M., Ataulkhanov, F. I. & Panteleev, M. A. Continuous modeling of arterial platelet thrombus formation using a spatial adsorption equation. *PLoS One* **10** (2015).
 138. Liu, K., VanLandingham, M. R. & Ovaert, T. C. Mechanical characterization of soft viscoelastic gels via indentation and optimization-based inverse finite element analysis. *J. Mech. Behav. Biomed. Mater.* **2**, 355-363 (2009).
 139. Noailly, J., Van Oosterwyck, H., Wilson, W., Quinn, T. M. & Ito, K. A poroviscoelastic description of fibrin gels. *J. Biomech.* **41**, 3265-3269 (2008).
 140. Fogelson, A. L. & Guy, R. D. Immersed-boundary-type models of intravascular platelet aggregation. *Comput. Methods Appl. Mech. Eng.* **197**, 2087-2104 (2008).
 141. Pivkin, I. V., Richardson, P. D. & Karniadakis, G. Blood flow velocity effects and role of activation delay time on growth and form of platelet thrombi. *PNAS* **103**, 17164-17169 (2006).
 142. Xu, Z., Kim, O., Kamocka, M., Rosen, E. D. & Alber, M. Multiscale models of thrombogenesis. *Wiley Interdiscip. Rev. Syst. Biol. Med.* **4**, 237-246 (2012).
 143. Hun Yeon, J. *et al.* A biochemical network can control formation of a synthetic material by sensing numerous specific stimuli. *Sci. Rep.* **5**, 10274 (2015).
 144. Raditya, P. P. R. & Hernaningsih, Y. Platelet Counts Analysis of Platelet-Poor Plasma (PPP) Produced by Several Centrifugation Techniques. *Indian J. Med. Forensic Med. Toxicol.* **14** (2020).
 145. Sugerman, G. P., Chokshi, A. & Rausch, M. K. Preparation and Mounting of Whole Blood Clot Samples for Mechanical Testing. *Curr. Protoc.* **1** (2021).
 146. Zohdi, T. I., Kuypers, F. A. & Lee, W. C. Estimation of red blood cell volume fraction from overall permittivity measurements. *Int. J. Eng. Sci.* **48**, 1681-1691 (2010).
 147. Dhurat, R. & Sukesh, M. Principles and Methods of Preparation of Platelet-Rich Plasma: A

- Review and Author's Perspective. *J. Cutan. Aesthet. Surg.* **7**, 189-197 (2014).
148. Rivlin, R. S. & Thomas, A. G. Rupture of rubber. I. Characteristic energy for tearing. *J. Polym. Sci.* **10**, 291-318 (1953).
149. Ni, X., Chen, C. & Li, J. Interfacial fatigue fracture of tissue adhesive hydrogels. *Extreme Mech. Lett.* **34**, 100601 (2020).
150. Wang, Y., Yang, X., Nian, G. & Suo, Z. Strength and toughness of adhesion of soft materials measured in lap shear. *J. Mech. Phys. Solids* **143**, 103988 (2020).
151. Reyhani, V. *et al.* Fibrin binds to collagen and provides a bridge for $\alpha V\beta 3$ integrin-dependent contraction of collagen gels. *Biochem. J.* **462**, 113-123 (2014).
152. Fu, H. *et al.* Flow-induced elongation of von Willebrand factor precedes tension-dependent activation. *Nat. Commun.* **8** (2017).
153. Rana, A., Westein, E., Niego, B. E. & Hagemeyer, C. E. Shear-dependent platelet aggregation: Mechanisms and therapeutic opportunities. *Front. Cardiovasc. Med.* **6** (2019).
154. Chan, K. Y. T. *et al.* Adhesion of blood clots can be enhanced when copolymerized with a macromer that is crosslinked by coagulation Factor XIIIa. *Biomacromolecules* **17**, 2248-2252 (2016).
155. Dastjerdi, A. K., Pagano, M., Kaartinen, M. T., McKee, M. D. & Barthelat, F. Cohesive behavior of soft biological adhesives: experiments and modeling. *Acta Biomater.* **8**, 3349-3359 (2012).
156. Liu, S., Bao, G., Ma, Z., Kastrup, C. J. & Li, J. Fracture mechanics of blood clots: Measurements of toughness and critical length scales. *Extreme Mech. Lett.* **48**, 101444 (2021).
157. Yuk, H., Zhang, T., Lin, S., Parada, G. A. & Zhao, X. Tough bonding of hydrogels to diverse non-porous surfaces. *Nat. Mater.* **15**, 190-196 (2016).
158. Yang, Z., Ma, Z., Liu, S. & Li, J. Tissue adhesion with tough hydrogels: Experiments and modeling. *Mech. Mater.* **157**, 103800 (2021).
159. Bao, G. *et al.* Liquid-infused microstructured bioadhesives halt non-compressible hemorrhage. *Nat. Commun.* **13** (2022).
160. Hazrin-Chong, N. H. & Manfield, M. An alternative SEM drying method using hexamethyldisilazane (HMDS) for microbial cell attachment studies on sub-bituminous coal. *J. Microbiol. Methods* **90**, 96-99 (2012).

161. Jaeschke, A., Eckert, H. & Bray, L. J. Qiber3D—an open-source software package for the quantitative analysis of networks from 3D image stacks. *GigaScience* **11** (2022).
162. Liu, S. *FibNetQuantifyTool*,
<<https://github.com/XAVI4U/PyClotFracture/releases/tag/v1.0.1>> (2023).
163. Ogden, R. W. & Roxburgh, D. G. A pseudo-elastic model for the Mullins effect in filled rubber. *Proc. R. Soc. A: Math. Phys. Eng. Sci.* **455**, 2861-2877 (1999).
164. Yeoh, O. H. Some Forms of the Strain Energy Function for Rubber. *Rubber Chem. Technol.* **66**, 754-771 (1993).
165. Ghezelbash, F. *et al.* Modeling of human intervertebral disc annulus fibrosus with complex multi-fiber networks. *Acta Biomater.* **123**, 208-221 (2021).
166. Holzapfel, A. G. *Nonlinear solid mechanics II.* (2000).
167. Wei, Y. & Hutchinson, J. W. Interface strength, work of adhesion and plasticity in the peel test. *Int. J. Fract.* **93**, 315–333 (1998).
168. Tvergaard, V. & Hutchinson, J. W. The influence of plasticity on mixed mode interface toughness. *J. Mech. Phys. Solids* **41**, 1119-1135 (1993).
169. Hui, C. Y., Ruina, A., Long, R. & Jagota, A. Cohesive Zone Models and Fracture. *J. Adhes.* **87**, 1-52 (2011).
170. Furie, B. & Furie, B. C. Mechanisms of thrombus formation. *N. Engl. J. Med.* **359**, 938-949 (2008).
171. Søgaard, K. K., Schmidt, M., Pedersen, L., Horváth–Puhó, E. & Sørensen, H. T. 30-year mortality after venous thromboembolism. *Circulation* **130**, 829-836 (2014).
172. Malas, M. B. *et al.* Thromboembolism risk of COVID-19 is high and associated with a higher risk of mortality: A systematic review and meta-analysis. *EClinicalMedicine* **29-30**, 100639 (2020).
173. Kang, J., Wang, C. & Cai, S. Cavitation to fracture transition in a soft solid. *Soft Matter* **13**, 6372-6376 (2017).
174. Ni, X., Yang, Z. & Li, J. Scaling behavior of fracture properties of tough adhesive hydrogels. *ACS Macro Lett.* **10**, 180-185 (2021).
175. Wufsus, A. R. *et al.* Elastic behavior and platelet retraction in low- and high-density fibrin gels. *Biophys. J.* **108**, 173-183 (2015).
176. Bower, A. F. *Applied mechanics of solids.* (CRC press, 2009).

177. Wu, D.-W., Li, Y.-M. & Wang, F. How long can we store blood samples: A systematic review and meta-analysis. *EBioMedicine* **24**, 277-285 (2017).
178. Kim, O. V., Litvinov, R. I., Alber, M. S. & Weisel, J. W. Quantitative structural mechanobiology of platelet-driven blood clot contraction. *Nat. Commun.* **8** (2017).
179. Sun, Y. *et al.* Platelet heterogeneity enhances blood clot volumetric contraction: An example of asynchrono-mechanical amplification. *Biomaterials* **274**, 120828 (2021).
180. Kunnakattu, S.-J. *et al.* Dynamic and quantitative assessment of blood coagulation status with an oscillatory rheometer. *Appl. Sci.* **8**, 84 (2018).
181. Davie, E. W., Fujikawa, K. & Kisiel, W. The coagulation cascade: initiation, maintenance, and regulation. *Biochemistry* **30**, 10363-10370 (1991).
182. Windberger, U. & Lauger, J. Blood clot phenotyping by rheometry: Platelets and fibrinogen chemistry affect stress-softening and -stiffening at large oscillation amplitude. *Molecules* **25** (2020).
183. Li, W. *et al.* Fibrin fiber stiffness is strongly affected by fiber diameter, but not by fibrinogen glycation. *Biophys. J.* **110**, 1400-1410 (2016).
184. Hilgard, P. Experimental hypercalcaemia and whole blood clotting. *J. Clin. Pathol.* **26**, 616-619 (1973).
185. Evans, P. *et al.* Studies of whole blood coagulation by oscillatory shear, thromboelastography and free oscillation rheometry. *Clin. Hemorheol. Microcirc.* **38**, 267-277 (2008).
186. McIntire, L. V. Rheology and blood coagulation. *Br. J. Haematol.* **36**, 299-304 (1977).
187. Yoon, Y. Z., Kotar, J., Yoon, G. & Cicuti, P. The nonlinear mechanical response of the red blood cell. *Phys. Biol.* **5**, 036007 (2008).
188. Zhao, X. Multi-scale multi-mechanism design of tough hydrogels: building dissipation into stretchy networks. *Soft Matter* **10**, 672-687 (2014).
189. Hu, J., Jahid, M. A., Harish Kumar, N. & Harun, V. in *Handbook of Fibrous Materials* 1-36 (2020).
190. Chen, W., Kumari, J., Yuan, H., Yang, F. & Kouwer, P. H. J. Toward Tissue-Like Material Properties: Inducing In Situ Adaptive Behavior in Fibrous Hydrogels. *Adv. Mater.* **34**, 2202057 (2022).
191. Kurniawan, N. A. *et al.* Buffers Strongly Modulate Fibrin Self-Assembly into Fibrous

- Networks. *Langmuir* **33**, 6342-6352 (2017).
192. Beudert, M., Gutmann, M., Lühmann, T. & Meinel, L. Fibrin Sealants: Challenges and Solutions. *ACS Biomater. Sci. Eng.* **8**, 2220-2231 (2022).
 193. Fereidoonzehad, B., Dwivedi, A., Johnson, S., McCarthy, R. & McGarry, P. Blood clot fracture properties are dependent on red blood cell and fibrin content. *Acta Biomater.* **127**, 213-228 (2021).
 194. Taylor, C. A. *et al.* In Vivo Quantification of Blood Flow and Wall Shear Stress in the Human Abdominal Aorta During Lower Limb Exercise. *Ann. Biomed. Eng.* **30**, 402-408 (2002).
 195. Bonaventura, A. *et al.* Endothelial dysfunction and immunothrombosis as key pathogenic mechanisms in COVID-19. *Nat. Rev. Immunol.* **21**, 319-329 (2021).
 196. Levi, M., Thachil, J., Iba, T. & Levy, J. H. Coagulation abnormalities and thrombosis in patients with COVID-19. *Lancet Haematol.* **7**, e438-e440 (2020).
 197. Wakefield, T. W., Myers, D. D. & Henke, P. K. Mechanisms of venous thrombosis and resolution. *Arterioscler. Thromb. Vasc. Biol.* **28**, 387-391 (2008).
 198. Greensmith, H. W. Rupture of rubber. X. The change in stored energy on making a small cut in a test piece held in simple extension. *J. Appl. Polym. Sci.* **7**, 993-1002 (1963).
 199. Gent, A. N. Adhesion and Strength of Viscoelastic Solids. Is There a Relationship between Adhesion and Bulk Properties? *Langmuir* **12**, 4492-4496 (1996).
 200. Lake, G. J. & Thomas, A. G. The strength of highly elastic materials. *Proc. R. Soc. A: Math. Phys. Eng. Sci.* **300**, 108-119 (1967).
 201. Ni, J. *et al.* Strong fatigue-resistant nanofibrous hydrogels inspired by lobster underbelly. *Matter* **4**, 1919-1934 (2021).
 202. Good, B. C. The influence of blood composition and loading frequency on the behavior of embolus analogs. *J. Mech. Behav. Biomed. Mater.* **140**, 105738 (2023).
 203. Patki, P., Simon, S., Manning, K. B. & Costanzo, F. Computational analysis of effects of clot length on Acute ischemic stroke recanalization under different cyclic aspiration loading conditions. *Int. J. Numer. Methods Biomed. Eng.* **39** (2023).
 204. Kim, J., Zhang, G., Shi, M. & Suo, Z. Fracture, fatigue, and friction of polymers in which entanglements greatly outnumber cross-links. *Science* **374**, 212-216 (2021).
 205. Li, J., Illeperuma, W. R. K., Suo, Z. & Vlassak, J. J. Hybrid hydrogels with extremely high

- stiffness and toughness. *ACS Macro Lett.* **3**, 520-523 (2014).
206. Tonsomboon, K., Butcher, A. L. & Oyen, M. L. Strong and tough nanofibrous hydrogel composites based on biomimetic principles. *Mater. Sci. Eng. C Mater. Biol. Appl.* **72**, 220-227 (2017).
 207. Ashby, M. F. *The CES EduPack database of natural and man-made materials*. (Cambridge University and Granta Design, 2008).
 208. Lin, S. *et al.* Anti-fatigue-fracture hydrogels. *Sci. Adv.* **5**, eaau8528 (2019).
 209. Bai, R. *et al.* Fatigue fracture of tough hydrogels. *Extreme Mech. Lett.* **15**, 91-96 (2017).
 210. Sun, J. Y. *et al.* Highly stretchable and tough hydrogels. *Nature* **489**, 133-136 (2012).
 211. Brown, A. C. & Barker, T. H. Fibrin-based biomaterials: Modulation of macroscopic properties through rational design at the molecular level. *Acta Biomater.* **10**, 1502-1514 (2014).
 212. Sakariassen, K. S., Orning, L. & Turitto, V. T. The impact of blood shear rate on arterial thrombus formation. *Future Sci. OA* **1** (2015).
 213. Tang, J., Li, J., Vlassak, J. J. & Suo, Z. Fatigue fracture of hydrogels. *Extreme Mech. Lett.* **10**, 24-31 (2017).
 214. Hua, M. *et al.* Strong tough hydrogels via the synergy of freeze-casting and salting out. *Nature* **590**, 594-599 (2021).
 215. Montero, A. *et al.* Contraction of fibrin-derived matrices and its implications for in vitro human skin bioengineering. *J. Biomed. Mater. Res. A* **109**, 500-514 (2021).
 216. Sun, D. *et al.* Enhance Fracture Toughness and Fatigue Resistance of Hydrogels by Reversible Alignment of Nanofibers. *ACS Appl. Mater. Interfaces* **14**, 49389-49397 (2022).
 217. Lin, S., Liu, J., Liu, X. & Zhao, X. Muscle-like fatigue-resistant hydrogels by mechanical training. *PNAS* **116**, 10244-10249 (2019).
 218. Bircher, K., Zündel, M., Pensalfini, M., Ehret, A. E. & Mazza, E. Tear resistance of soft collagenous tissues. *Nat. Commun.* **10** (2019).
 219. Piechocka, I. K., Bacabac, R. G., Potters, M., Mackintosh, F. C. & Koenderink, G. H. Structural hierarchy governs fibrin gel mechanics. *Biophys. J.* **98**, 2281-2289 (2010).
 220. Akagi, Y., Sakurai, H., Gong, J. P., Chung, U.-I. & Sakai, T. Fracture energy of polymer gels with controlled network structures. *J. Chem. Phys.* **139**, 144905 (2013).

221. Jansen, K. A. *et al.* Molecular packing structure of fibrin fibers resolved by X-ray scattering and molecular modeling. *Soft Matter* **16**, 8272-8283 (2020).
222. Xiao, Z. *et al.* Rate-dependent fracture behavior of tough polyelectrolyte complex hydrogels from biopolymers. *Mech. Mater.* **156**, 103785 (2021).
223. Long, R., Lefranc, M., Bouchaud, E. & Hui, C.-Y. Large deformation effect in Mode I crack opening displacement of an Agar gel: A comparison of experiment and theory. *Extreme Mech. Lett.* **9**, 66-73 (2016).
224. Persson, B. N. J. & Brener, E. A. Crack propagation in viscoelastic solids. *Phys. Rev. E* **71** (2005).
225. Sun, T. L. *et al.* Bulk Energy Dissipation Mechanism for the Fracture of Tough and Self-Healing Hydrogels. *Macromolecules* **50**, 2923-2931 (2017).
226. Park, C. H. & Woo, K. M. Fibrin-Based Biomaterial Applications in Tissue Engineering and Regenerative Medicine. *Adv. Exp. Med. Biol.* **1064**, 253-261 (2018).
227. Ackermann, M. *et al.* Pulmonary Vascular Endothelialitis, Thrombosis, and Angiogenesis in Covid-19. *N. Engl. J. Med.* **383**, 120-128 (2020).
228. Lau, D., Broderick, K., Buehler, M. J. & Büyüköztürk, O. A robust nanoscale experimental quantification of fracture energy in a bilayer material system. *PNAS* **111**, 11990-11995 (2014).
229. He, M. Y., Turner, M. R. & Evans, A. G. Analysis of the double cleavage drilled compression specimen for interface fracture energy measurements over a range of mode mixities. *Acta Metall. Mater.* **43**, 3453-3458 (1995).
230. Mostovoy, S. & Ripling, E. J. Fracture toughness of an epoxy system. *J. Appl. Polym. Sci.* **10**, 1351-1371 (1966).
231. Herod, T. W., Chambers, N. C. & Veres, S. P. Collagen fibrils in functionally distinct tendons have differing structural responses to tendon rupture and fatigue loading. *Acta Biomater.* **42**, 296-307 (2016).
232. Chen, C., Wang, Z. & Suo, Z. Flaw sensitivity of highly stretchable materials. *Extreme Mech. Lett.* **10**, 50-57 (2017).
233. Long, R., Hui, C. Y., Gong, J. P. & Bouchbinder, E. The fracture of highly deformable soft materials: A tale of two length scales. *Annu. Rev. Condens. Matter Phys.* **12** (2020).
234. Wu, G., Krebs, C. R., Lin, F.-C., Wolberg, A. S. & Oldenburg, A. L. High sensitivity

- micro-elastometry: Applications in blood coagulopathy. *Ann. Biomed. Eng.* **41**, 2120-2129 (2013).
235. Khamdaeng, T., Luo, J., Vappou, J., Terdtoon, P. & Konofagou, E. E. Arterial stiffness identification of the human carotid artery using the stress–strain relationship in vivo. *Ultrasonics* **52**, 402-411 (2012).
236. Purslow, P. P. Positional variations in fracture toughness, stiffness and strength of descending thoracic pig aorta. *J. Biomech.* **16**, 947-953 (1983).
237. Nakajima, T., Kurokawa, T., Ahmed, S., Wu, W.-L. & Gong, J. P. Characterization of internal fracture process of double network hydrogels under uniaxial elongation. *Soft Matter* **9**, 1955-1966 (2013).
238. Lefranc, M. & Bouchaud, E. Mode I fracture of a biopolymer gel: Rate-dependent dissipation and large deformations disentangled. *Extreme Mech. Lett.* **1**, 97-103 (2014).
239. Lin, S., Londono, C. D., Zheng, D. & Zhao, X. An extreme toughening mechanism for soft materials. *Soft Matter* **18**, 5742-5749 (2022).
240. Wang, Y. *et al.* Probing fibrin's molecular response to shear and tensile deformation with coherent Raman microscopy. *Acta Biomater.* **121**, 383-392 (2021).
241. Hudson, N. E. *et al.* Submillisecond elastic recoil reveals molecular origins of fibrin fiber mechanics. *Biophys. J.* **104**, 2671-2680 (2013).
242. Li, J., Suo, Z. & Vlassak, J. J. Stiff, strong, and tough hydrogels with good chemical stability. *J. Mater. Chem. B* **2**, 6708-6713 (2014).
243. Baumberger, T., Caroli, C. & Martina, D. Solvent control of crack dynamics in a reversible hydrogel. *Nat. Mater.* **5**, 552-555 (2006).
244. Zhang, T., Lin, S., Yuk, H. & Zhao, X. Predicting fracture energies and crack-tip fields of soft tough materials. *Extreme Mech. Lett.* **4**, 1-8 (2015).
245. Yang, J., Bai, R., Chen, B. & Suo, Z. Hydrogel Adhesion: A Supramolecular Synergy of Chemistry, Topology, and Mechanics. *Adv. Funct. Mater.* **30**, 1901693 (2020).
246. McSherry, B. J., Horney, F. D. & DeGroot, J. J. Plasma fibrinogen levels in normal and sick cows. *Can. J. Comp. Med.* **34**, 191-197 (1970).
247. Kohli, S. *et al.* Thrombosis and Inflammation—A Dynamic Interplay and the Role of Glycosaminoglycans and Activated Protein C. *Front. Cardiovasc. Med.* **9** (2022).
248. Eriksson, A. C. & Whiss, P. A. Measurement of adhesion of human platelets in plasma to

- protein surfaces in microplates. *J. Pharmacol. Toxicol. Methods* **52**, 356-365 (2005).
249. Sun, Y., Oshinowo, O., Myers, D. R., Lam, W. A. & Alexeev, A. Resolving the missing link between single platelet force and clot contractile force. *iScience* **25**, 103690 (2022).
250. Darcourt, J., Demchuk, A. M. & Olivot, J.-M. Platelets and Clot Stiffness: A Challenge but Also an Opportunity Toward Achieving Consistent Complete Reperfusion. *Stroke* **52**, 2518-2520 (2021).
251. Johnson, S. *et al.* Mechanical behavior of in vitro blood clots and the implications for acute ischemic stroke treatment. *J. Neurointerv. Surg.* **12**, 853-857 (2020).
252. Fu, C.-H. *et al.* Fibrin and Platelet-Rich Composition in Retrieved Thrombi Hallmarks Stroke With Active Cancer. *Stroke* **51**, 3723-3727 (2020).
253. Neeves, K., Illing, D. & Diamond, S. Thrombin flux and wall shear rate regulate fibrin fiber deposition state during polymerization under flow. *Biophys. J.* **98**, 1344-1352 (2010).
254. Niessen, F., Hilger, T., Hoehn, M. & Hossmann, K.-A. Differences in Clot Preparation Determine Outcome of Recombinant Tissue Plasminogen Activator Treatment in Experimental Thromboembolic Stroke. *Stroke* **34**, 2019-2024 (2003).
255. Josefsson, E. C. *et al.* Platelet production proceeds independently of the intrinsic and extrinsic apoptosis pathways. *Nat. Commun.* **5** (2014).
256. Egidi, M. G., D'Alessandro, A., Mandarello, G. & Zolla, L. Troubleshooting in platelet storage temperature and new perspectives through proteomics. *Blood Transfus.* **8 Suppl 3**, s73-81 (2010).
257. Fereidoonzhad, B. & McGarry, P. A new constitutive model for permanent deformation of blood clots with application to simulation of aspiration thrombectomy. *J. Biomech.* **130**, 110865 (2022).
258. Furie, B. & Furie, B. C. Thrombus formation in vivo. *J. Clin. Invest.* **115**, 3355-3362 (2005).
259. Govindarajan, V. *et al.* Impact of Tissue Factor Localization on Blood Clot Structure and Resistance under Venous Shear. *Biophys. J.* **114**, 978-991 (2018).
260. Ruggeri, Z. Von Willebrand factor, platelets and endothelial cell interactions. *J. Thromb. Haemost.* **1**, 1335-1342 (2003).